Numerical modeling of impacts at high velocities by a meshfree method Smoothed particles Hydrodynamics. Application to micro-impacts in soft tissues

Shuangshuang Meng

THESE DE DOCTORAT DE L'ETABLISSEMENT UNIVERSITE BOURGOGNE FRANCHE-COMTE

PREPAREE A L'UNIVERSITE DE TECHNOLOGIE DE BELFORT-MONTBELIARD

Ecole doctorale n°

Sciences physiques pour l'ingénieur et microtechniques - SPIM

Doctorat de Mécanique

Par

Shuangshuang MENG

Numerical modeling of impacts at high velocities by a meshfree method Smoothed particles Hydrodynamics. Application to micro-impacts in soft tissues

Thèse présentée et soutenue à UTBM Site de Sévenans, le 12 Mars 2021.

Composition du Jury :

Mme Christine ESPINOSA	Professeur, ISAE-SUPEAERO,	Rapporteur
M. Raphael DUPUIS	Maitre de Conférences HDR, Université de Haute Alsace,	Rapporteur
M. Michel ARRIGONI	Professeur, ENSTA Bretagne,	Examinateur
M. Franz CHOULY	Professeur des Universités, Université de Bourgogne,	Examinateur
M. Lorenzo TADDEI	Enseignant-chercheur, UTBM,	Invité – encadrant
M. Nadhir LEBAAL	Maitre de Conférences HDR , UTBM,	Co-directeur de thèse
M. Sebastien ROTH	Professeur des UniversitésUTBM,	Directeur de thèse

ACKNOWLEDGEMENTS

I would like to particularly thank my supervisors, Prof.Sebastien Roth. This research could not have been accomplished without his sustaining support, guidance, patience and encouragement all the way. Especially the words 'step by step' give me much encourage when i hit a bottleneck in the research.

I would like to acknowledge my thesis committee, Mme Christine ESPINOSA, M. Raphael DUPUIS, M. Michel ARRIGONI, and M. Franz CHOULY for accepting and evaluating my thesis work.

I am also grateful to the China Scholarship Council (CSC) for putting faith in my studies and providing the financial support for this research at the Technological University of Belfort Montbéliard (UTBM) in France.

Besides, I would like sincerely to thank my co-supervisor Prof.Nadhir Lebaal and a number of colleagues: Mr.Monzer Al khalil, Mr.Lorenzo Taddei, Mr.Jianbo, Mr.Hassan Frissane, Mr.Marc Cescutti, and Mr.Germain SOSSOU for providing a welcoming and supportive community in this period of my PhD research. The support from friends is also important for me. I would like to convey my sincere appreciations to my friends: Xiao pan, Zhou yue, Chen kui, Liulin runjia, Zhuo shengrong, Xie shiming, Wu hongjian, Zhou yang, Chen xianlong, Liu rongrong, Zhao hui, Liu meimei, Zhu dan, Fan xiujuan, Li yizhuo, Wang zhoucheng, and many other friends in France and in China.

I strongly appreciate the beautiful encounters in Belfort, which make me fall in love with this place day by day. I am so lucky to meet warmhearted friends: Chantal, Marie, Glnette, Joc and Jean-paul, Nastasya, Felicie and her parents, my french teacher Annie, Helene and Sebastien family (of course with four lovely children), Guillaume, Adrien, as well as the friends in garden association and English club.

In the end, a biggest gratitude and love to my family.

CONTENTS

1

GENERAL INTRODUCTION

1.1/ BACKGROUND

The mechanical behavior of structures under high-speed loading is of main interest in vehicle engineering, military framework, and modern pharmaceuticals. Indeed, the material used in the design whatever is the context has to satisfy different requirements, especially specific criteria on manufacturing such as lightweight and high-strength, or similar properties as simulants of the biological body on medicine or pharmaceuticals. As an example of structures with these kinds of important requirements, body-armors can be cited with a primary need of human body protection and dissipation of energy when impacted by the projectiles, and also a need of lightweight and mobility for human ergonomic aspects. This balance between different development requirements for the designs of such protection devices needs a deep understanding of the behavior of the material under complex physical loading such as ballistic impacts.

The research to investigate the processes and behavior of various materials during the ballistic impacts can be categorized into three aspects: Experiments, theoretic analyses, and numerical simulations. The experiment is the most natural and essential way to observe and understand the physical world, which allows us gathering measurable or visual information via employing specific equipment. It is still one of the most important methods in scientific research. Analytical models consist of developing mathematical equations based on materials parameters allowing calculating physical parameters, such as penetration history, velocity history, deformation ranges in the target. The usages of analytical models require some supplements from experimental measurements and semi-empirical fits, which are developed and employed in a variety of fields because of

its simple and low-cost features. The numerical simulation is the calculation that is run on a computer following a program that implements a mathematical model for a physical system. Owing to the fast development of computer science in recent years, the third way is paid more and more attention. It has been developed and applied in various fields particularly for some complex and huge engineering problems.

The processes of high-velocity impacts often involve various damages and even severe destruction, thereby they have many high and strict requirements for experimental techniques and equipment. Particularly, for some research relevant to biological issues in the fields of medicine or pharmaceuticals, analytical and simulation methods demonstrate considerable significance because of the security and ethics problems in the experiments. The numerical method like the finite element method(FEM) based on element discretization was developed from the late eighteenth century. They integrate the engineering scientific methods and principles of calculus in mathematics, as well as modern computer science techniques. The CAE (computer aidered engineering) software developed based on these numerical methods such as FEM, CFD, and , has become the main tool to investigate complex physical problems in engineering.

1.2/ OBJECTIVES

Investigations on the ballistic behavior of soft tissue materials are significant research to the development of the medicine and pharmaceutical fields. They mainly involve the procedure about the particles or fragmentation penetrating or traveling into the soft materials. For instance, Fig.1.1 shows a needle-free drug delivery device, which is one of transdermal delivery technologies in the pharmaceutical industry. The micro-scale particles as drug powders are injected into skin with high velocity, and several factors should considered such as the particle diameters, trajectories, and momentum or velocities of projectile in this process. From the insight of mechanical investigation, the behavior of micro-particles is performed and observed by the experimental process like Fig.1.2. Fig.1.2 shows an example that a sphere with μm-size impacts into a soft tissue captured by some experimental equipment to understand the ballistics procedure. The size of projectile, the cavity deformation of soft tissue, as well as the trajectory of projectile fragments are important factors to design and evaluate the performance of the drug delivery device.

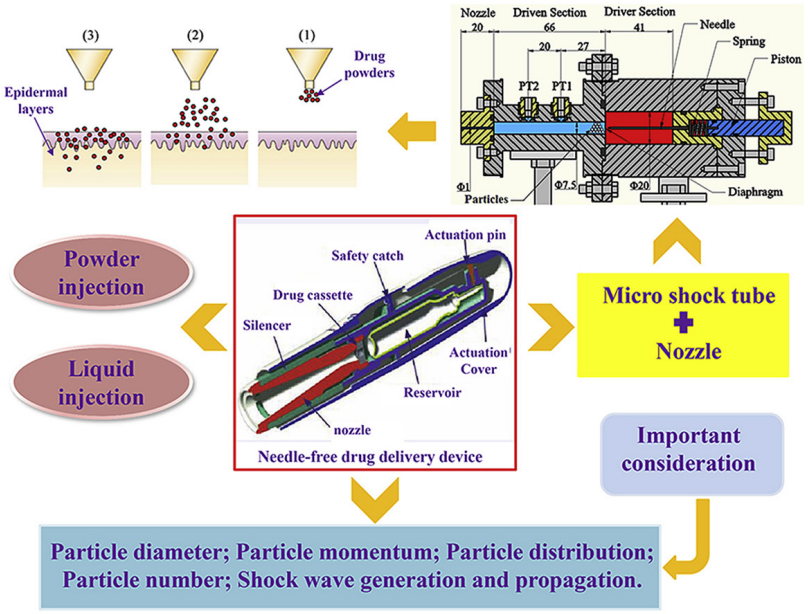

Figure 1.1: The system of needle-free drug delivery device provided in the [1].

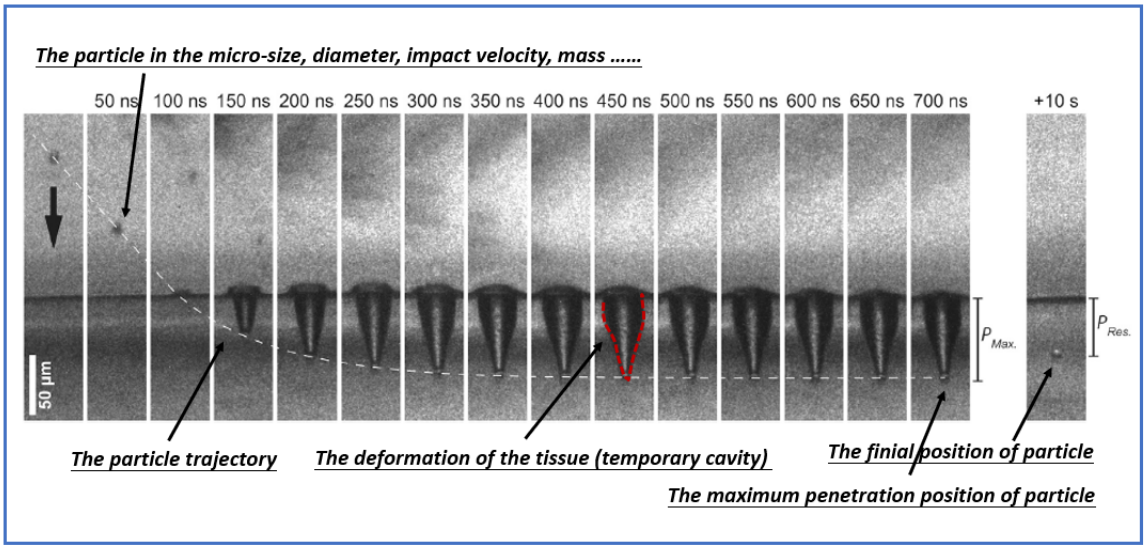

Figure 1.2: The process of a 13-μm steel sphere penetrating into a simulant of soft tissue called SEBS gel observed by the experiment [2].

The numerical methods are suitable approaches to study these kinds of processes. Although grid-based methods like FEM have been powerful tools in engineering, some numerical limitations still exist. One of the most severe problems is the large distortions of elements when solid structures are extremely deformed. The methods based on the meshing technique are not very suitable for simulating hydrodynamic phenom-

ena like the high velocity impacts which include large deformations, moving material interfaces, deformable boundaries as well as fragmentations, typically the process as shown in Fig.1.2. The mesh distortion can cause significant errors in these analyses. To avoid it, other numerical concepts have been developed, based on particle discretization, also called meshfree or meshless methods like The Smoothed Particle Hydrodynamics method (SPH).

SPH method is the earliest mehsfree method, proposed initially for the by Gingold & Monaghan in 1977. Compared to traditional grid-based numerical methods, some distinct benefits of the SPH method have been recognized during the various applications:

1. The particle modeling of Lagrangian nature in SPH can concern the time history of the material particles, which allows straightforward handling of very large deformations since the connectivity between particles are generated as part of the computation and can change with time.

2. The free surfaces, material interfaces, and moving boundaries can all be traced freely in the process of simulation, which is always challenging to many Eulerian methods.

3. The SPH method is a suitable alternative for non-continuum problems, typically examples involving bio- and nano- engineering at the micro and nanoscale, and astrophysics at astronomic scale, as well as the debris clouds phenomenon in HVIs.

4. SPH formulations are comparatively simple and easy to be developed or improved as 3D-codes by some algorithms or to be coupled with other numerical methods.

Owing to these advantages, the SPH has been extended to the solid mechanics in recent 30 years. Its potential in simulating extremely large deformations of materials has been identified, but the applications in micro-penetration are still not so much in the literature. Therefore, this thesis highlights the development of an SPH code and its applications on the soft materials penetrations, particularly, in the micro-scale. Various simulants as human body substitutes such as ballistic gelatin and polymers gels will be investigated under high-velocity impacts by SPH simulations.

1.3/ THESIS ORGANIZATION

The rest of this thesis is organized as follows:

Chapter 2: This chapter provides a state of the art for the advances in ballistic perforation impact on structures using the SPH method. Though the literature reviewing, the advantages and limitations of the SPH method applied in high-velocity impacts are recognized.

Chapter 3: Although the SPH method has been developed for the application in solid dynamics, the tensile instability is a main obstacle to simulate the material strength with a large deformations. Therefore, the first work is to investigate the stability and accuracy of SPH simulations for solid problem. A SPH code is programmed and implemented into the equations of elastic-plasticity for materials. Then, the influence on the stability and accuracy derived from the kernel functions is investigated. Combined with this analyses on the types of kernel functions, various problems such as vibrated beam and Taylor rod impacts are simulated by this SPH code.

Chapter 4: After programming a SPH code and validating it on several solid problems, a numerical model consisting of SPH and FEM is developed for the micro penetrations into soft materials. Gelatin is the most widely used soft material as a simulant of biological body, and its ballistic behavior under impact loading by micro-particles is investigated by this numerical model. A series of simulations involving the micro-particle (less than 10 μm) impact 10 % gelatin with a wide range of velocities from 200-1500 m/s are performed by this SPH model. The soft material SEBS gel as another simulant of biological body involves several benefits, but its ballistic behavior is paid less attention in the literature. The second highlight of this chapter is to investigate the responses of SEBS gel as a target in the micro-penetrations by the numerical simulations using SPH model. Also, the usability and university of several analytical models for penetrations is observed and discussed in the micro-scale.

Chapter 5: The work of this thesis is summarised and the future works are discussed in the last chapter.

2

A STATE OF THE ART ON IMPACTS TO STRUCTURES SIMULATED BY SPH METHOD

2.1/ INTRODUCTION

High velocity impacts (HVIs) are very important phenomenon in various fields such as vehicle engineering, military framework, medicine techniques, as well as manufacturing industry. The mechanical process of HVIs is complex and involves the extreme deformations on the materials. Penetration is a general description as to the sequence of impacts, which involves the perforation, embedment, ricochet, as well as the fragments and debris clouds with efficiently high velocity. Perforation means that the projectile passes through the target structure. Embedment means that the projectile is stopped in the target that appears generally in enough thick structures. Ricochet means that the projectile is deflected from the target without perforating. The fragments and debris clouds are the most comment damage in the target structures caused by the projectile which passes out the thin target with very high impact velocity. Therefore, the damage forms or material behavior during the HVIs depend on the configurations of projectile and target, impact conditions like initial velocity, as well as the material properties.

As the mentioned in the general introduction, the methods to investigate the process of HVIs can be categorized to three ways [3, 4]: experimental tests, analytical modeling involving semi-empirical data fits and numerical modeling. The numerical simulation is

widely developed in the literature since today's computational powers allow conducting high-performance calculations such as the finite element method (FEM) and finite difference method (FDM). Particularly, the FEM method as one of the typical grid-based methods is the main numerical tool for engineers because of its apparent advantages like (a) Lagrangian grid fixed on the moving material enables it easy to track and obtain the time history of any field variable; (b) irregular or complicated geometries can be modeled by using an irregular mesh; (c) it has been highly developed by academia and industry for a long time, and become a mature and comparatively commercialized approach. It also becomes a powerful predicting tool for the behavior of mechanical structures under HVI [5, 6, 7] in the past decades.

However, grid-based methods like FEM provide are suffering the mesh distortion problems when simulating hydrodynamic phenomena like explosion and HVIs which typically include large deformations, moving material interfaces, deformable boundaries as well as fragmentations. As an alternative, the mesh-free methods based on particle discretization, also called meshless methods like The Smoothed Particle Hydrodynamics method (SPH) [8, 9], Discrete Element Method (DEM) [10, 11], Dissipative Particle Dynamics (DPD) [12], Material Point Method (MPM) [13] etc, are developed. Some reviews on the mesh-free and particle methods and their differences can be found such as [14, 15, 16], but the SPH method as the earliest mesh-free method is the highlight in this thesis. It has been initially developed in the astrophysical field [8, 9]. Since the nineties, some researchers have adapted this method to solid mechanics in the framework of HVIs [17, 18]. This method has been widely improved during the 20 last years and appears to be very promising for solid mechanics for the understanding of large deformed mechanics.

Therefore, the objective of this chapter is to review the simulations for high-velocity impacts by the SPH method in the past 30 years. The structure of this chapter is organized by:

1. Firstly, an introduction about standard SPH and its improvements are represented, respectively.

2. Then, the application of SPH method in high velocity impacts (HVIs) problems is reviewed in the literature. This section focuses on the impacts consisting of the thin structures.

3. The limitations and improvements on impact problems by SPH simulations are reviewed based on the literature.

4. Following, the deep penetrations in various materials are represented, combined with the simulation approaches.

5. Finally, the deep penetrations in the biomaterials in the micro-scale is determined as the main investigation in this thesis by SPH simulations.

2.2/ SPH METHOD AND ITS DEVELOPMENTS

2.2.1/ THE ALGORITHM OF SPH METHOD

2.2.1.1/ APPROXIMATION OF VARIABLES

Standard SPH also called conventional SPH initially developed by Gingold et.al [8, 9] is regarded as a typical meshfree numerical method based on particle modeling, which mainly consists of two processes, kernel approximation, and particle discretization. The first major process in SPH formulation is the kernel approximation, which approximates the field variables. The nearby domain is determined by the kernel function W. The kernel approximation can be expressed by the following equations,

$$< f(\vec{x}) >= \int_{\Omega} f(\vec{x'}) W(\vec{x} - \vec{x'}, h) d\Omega \tag{2.1}$$

where, $\vec{x}$ is a parameter, and $\vec{x'}$ is a variable. The values of kernel function W depend on the distance of $\vec{x} - \vec{x'}$. Ω is the kernel support centred at a point $\vec{x}$. A function should satisfy several conditions like,

1) Normalization

$$\int W(\vec{x} - \vec{x'}, h) dx' = 1 \tag{2.2}$$

Obviously, SPH kernel function W is related with the distance between particles and parameter h. Because h determines the size of impact domain, its value directly influences the accuracy and computational quantity in particle approximation.

2) Compact supportness: this condition imposes the following equations,

$$if|\vec{x}-\vec{x'}| \leq \kappa h, \quad W(\vec{x}-\vec{x'}) \geq 0 \quad else \quad W(\vec{x}-\vec{x'}) = 0 \tag{2.3}$$

Where, the combination between smoothing length h and a scale factor κ determines the spread of the specified smoothing function. κ is one of properties of kernel function.

3) Dirac delta function condition when $h \to 0$,

$$\lim_{h\to 0} W(\vec{x}-\vec{x'},h) = \delta(\vec{x}-\vec{x'}) \tag{2.4}$$

Except for above mathematically obligatory conditions, some properties of kernel function are found to have a considerable weight in this algorithm like smoothness, the position of peak of kernel's shape as well as the features of its derivatives. Otherwise, kernel function also should be dimension-independent concerning its practicability for different problems, which means it can be written by the below form ,

$$W(\vec{x}-\vec{x'},h) = \alpha_d K(q), \quad q = |\vec{x}-\vec{x'}|/h, \quad d = 1,2,3 \tag{2.5}$$

Where, α_d is the dimension-dependent normalization constant for particular kernel functions.

Based on above conditions, the kernel function in SPH algorithm can be built systematically, as a study by Liu and his co-workers in [19].

Then, particle discretization process convert the kernel integral of Eq. (2.1) into a volume weighted sum, following by:

$$< f(\vec{x_i}) >= \sum_{j=1}^{N} \frac{m_j}{\rho_j} f(\vec{x_j}) W(\vec{x_i}-\vec{x_j},h) \tag{2.6}$$

In this summation, the subscript i and j denote particle number, m_j and ρ_j the mass and the density of particle j respectively. N is the total number of the neighbouring particles of particle i in its compact support which is determined by h. This implies that a summation is carried out over the the domain which depends on the types of kernel function.

2.2.1.2/ APPROXIMATION OF DERIVATIVES

Taking the derivative of Eq. (2.1) to approximate the derivative of $f(\vec{x})$,

$$< \nabla \cdot f(\vec{x}) >= \int_{\Omega} [\nabla \cdot f(\vec{x})] \quad W(\vec{x} - \vec{x'}, h) d\vec{x'} \tag{2.7}$$

the right hand side of above equation can be written as:

$$\int_{\Omega} [\nabla \cdot f(\vec{x})] W(\vec{x} - \vec{x'}, h) d\vec{x'} = \int_{\Omega} \nabla \cdot [f(\vec{x'}) W(\vec{x} - \vec{x'}, h)] d\vec{x'} - \int_{\Omega} f(\vec{x'}) \cdot \nabla W(\vec{x} - \vec{x'}, h) d\vec{x'} \tag{2.8}$$

Through the Green-Gauss theorem, the first term on the right hand side can be transferred into the form over its boundary,

$$\int_{\Omega} \nabla \cdot [f(\vec{x'}) W(\vec{x} - \vec{x'}, h)] d\vec{x'} = \int_{\Sigma} f(\vec{x'}) W(\vec{x} - \vec{x'}, h) \cdot \vec{n} d\Sigma \tag{2.9}$$

At the boundary Σ with the unit vector normal , the values of $W(\vec{x} - \vec{x'}, h)$ decease to zero according to its characteristic in Eq. (2.3), then the term in above equation vanishes. Therefore, Eq. (2.8) become the form like,

$$\int_{\Omega} [\nabla \cdot f(\vec{x})] W(\vec{x} - \vec{x'}, h) d\vec{x'} = - \int_{\Omega} f(\vec{x'}) \cdot \nabla W(\vec{x} - \vec{x'}, h) d\vec{x'} \tag{2.10}$$

Following the same step with Eq. (2.6), the above equation can be discretized by a number of particles to obtain its summation,

$$- \int_{\Omega} f(\vec{x'}) \cdot \nabla W(\vec{x} - \vec{x'}, h) d\vec{x'} \approx \sum_{j=1}^{N} \frac{m_j}{\rho_j} f(\vec{x}_j) \frac{\partial W(\vec{x}_i - \vec{x}_j, h)}{\partial x'} \tag{2.11}$$

With the symmetric nature of the smoothing functions, the approximation of the derivative $f(\vec{x})$ at particle i with the position vector $\vec{x}_i$ has the form like,

$$< \nabla \cdot f(\vec{x}) >= \sum_{j=1}^{N} \frac{m_j}{\rho_j} f(\vec{x}_j) \frac{\partial W(\vec{x}_i - \vec{x}_j, h)}{\partial x'} \tag{2.12}$$

2.2.1.3/ TECHNIQUES IN DERIVING SPH FORMULATIONS

To summary and reorganize the SPH formulation for approximating the function and its derivative, according to last section, for a given particle i , its any variable and derivative can be written as the summation as,

$$< f(\vec{x}_i) >= \sum_{j=1}^{N} \frac{m_j}{\rho_j} f(\vec{x}_j) W_{ij} \tag{2.13}$$

$$< \nabla \cdot f(\vec{x}_i) >= \sum_{j=1}^{N} \frac{m_j}{\rho_j} f(\vec{x}_j) \cdot \Delta_i W_{ij} \tag{2.14}$$

$$W_{ij} = W(\vec{x}_i - \vec{x}_j, h) = W(|\vec{x}_i - \vec{x}_j|, h) \tag{2.15}$$

$$\nabla_i W_{ij} = \frac{\vec{x}_i - \vec{x}_j}{r_{ij}} \frac{\partial W_{ij}}{\partial r_{ij}} \tag{2.16}$$

Based on [20] which used a technique to derive these SPH formulations, the following two formats are employed to involve the density inside the gradient operation,

$$\nabla \cdot f(\vec{x}) = \frac{1}{\rho}[\Delta \cdot (\rho f(\vec{x})) - f(\vec{x}) \cdot \Delta\rho] \tag{2.17}$$

$$\nabla \cdot f(\vec{x}) = \rho[\Delta \cdot (\frac{f(\vec{x})}{\rho}) + \frac{f(\vec{x})}{\rho^2} \cdot \Delta\rho] \tag{2.18}$$

Linked with above formats, Eq.(2.14) can be expressed as,

$$< \nabla \cdot f(\vec{x}_i) >= \frac{1}{\rho_i} \left[\sum_{j=1}^{N} m_j [f(\vec{x}_j) - f(\vec{x}_i)] \cdot \Delta_i W_{ij} \right] \tag{2.19}$$

$$< \nabla \cdot f(\vec{x}_i) >= \rho_i \left[\sum_{j=1}^{N} m_j [\frac{f(\vec{x}_j)}{\rho_j^2} + \frac{f(\vec{x}_i)}{\rho_i^2}] \cdot \Delta_i W_{ij} \right] \tag{2.20}$$

2.2.2/ THE IMPROVEMENTS BASED ON TRADITIONAL SPH

Firstly, as one of the most common and earliest techniques to reduce the numerical oscillation, artificial viscosity (AV) term is added to momentum and energy conservation equations in SPH formulations [8, 21, 22], given by:

$$\prod_{ij} = \frac{-qa\bar{c}_{ij}\mu_{ij} + qb\mu_{ij}^2}{\bar{\rho}_{ij}}, \qquad \vec{v}_{ij} \cdot \vec{x}_{ij} < 0 \tag{2.21}$$

$$\mu_{ij} = \frac{\bar{h}_{ij}\vec{v}_{ij} \cdot \vec{x}_{ij}}{|\vec{x}_{ij}|^2 + (\kappa\bar{h}_{ij})^2} \tag{2.22}$$

where qa and qb are constants. The notations $\bar{c}_{ij}$, $\bar{\rho}_{ij}$ and $\bar{h}_{ij}$ are the quantities average of particle i and j. When $\vec{v}_{ij} \cdot \vec{x}_{ij}$ is positive, $\mu_{ij} = 0$. Although artificial viscosity has been improved in several modified versions, it is still limited to ensure stability during SPH simulations, especially, during the material with large tension.

Artificial stress term was developed to specifically remove tensile instability in elastic dynamics [23, 24]. It is implemented by adding a strong repulsive force only when particles become too close to each other, resulting in a more stable simulation for elastic problems by SPH, but just for 2D problems. The artificial stress term has the following form,

$$\mathbf{R}_{ij}^{\alpha\beta} = (R_i^{\alpha\beta} + R_j^{\alpha\beta}) \cdot f_{ij}^n \tag{2.23}$$

Here, in 2-D problems, for example, when $\alpha = x$ and $\beta = x$, the term R_i^{xx} has the following form

$$R_i^{xx} = c^2\bar{R}_i^{xx} + s^2\bar{R}_i^{yy} \tag{2.24}$$

$$\bar{R}_i^{xx} = \begin{cases} -\zeta\frac{\bar{\sigma}_i^{xx}}{\rho^2} & \bar{\sigma}_i^{xx} > 0, \\ 0 & \bar{\sigma}_i^{xx} < 0. \end{cases} \tag{2.25}$$

In above equations, $R_i^{\alpha\beta}$ is the component of the artificial stress in the original coordinates, $\bar{R}_i^{\alpha\beta}$ is new component of the stress tensor in a rotated frame. c denotes $\cos\theta_i$ and s denotes $\sin\theta_i$ (θ_i being the rotation angle which makes the stress tensor diagonal). ζ is a constant that controls the weight of artificial stress. In addition, in Eq. (2.23), f_{ij}^n is related kernel function, presented by $W(r_{ij})/W(\Delta x)$ and the optimum value of n is given 4 by Monaghan in [24].

The artificial viscosity term Eq.(2.21) and artificial stress terms Eq.(2.23) are added into stress terms in order to improve SPH numerical stability, as following

$$\frac{\sigma_i^{\alpha\beta}}{\rho_i^2} + \frac{\sigma_j^{\alpha\beta}}{\rho_j^2} - \prod_{ij} \delta^{\alpha\beta} + \mathbf{R}_{ij}^{\alpha\beta} \tag{2.26}$$

In addition, XSPH also called conservation smoothing updates the velocity by an average of the particle velocities in every time step [22], which is suggested to be applied in tension problems simulated by SPH method to remit particles clumping in the study of [25]. It is following the form like,

$$\hat{v}_i = v_i + \alpha_{cs} \sum_j \frac{2m_j}{\rho_i + \rho_j}(v_j - v_i)W_{ij} \tag{2.27}$$

where $\hat{v}_i$ is the smoothed velocity modified by an average of the particle velocities in the neighbourhood of particle i.

Corrective SPH (CSPH) proposed by Chen also targeted to address the tensile instability [26]. The idea of this corrective method is to transfer the kernel estimate concept to the Taylor series expansion. Sugiura and Inutsuka [27] mitigate the tensile instability using the Godunov SPH method [28] that utilizes a Riemann solver and achieves the second-order accuracy in space. They conducted the linear stability analysis for the equations of the Godunov SPH method, and find that the tensile instability can be suppressed by selecting appropriate interpolation for density distribution in the equation of motion for the Godunov SPH method even in the case of elastic dynamics.

Above several improvements are completely based on the formulations of standard SPH where particles interact through a kernel function defined on the current configuration. According to the study in [29], it means that particles can enter or exit each other's support domains as the material deforms, which is maybe one of the reasons leading to tensile instability. Total lagrangian SPH developed recently calculated the kernel function on the reference configuration, which appears a good performance in removing tensile instability [30, 31]. The doctoral thesis of Reveles [30] developed a total Lagrangian SPH code for solid dynamics and it seems at present one of the most promising approaches to keep the numerical stability when applied SPH to HVI problems with quickly extreme deformations. Then, the pseudo-spring technique was developed particularly for modeling

crack growth in impact problems [32, 33, 34], combined with SPH formulation (so-called Pseudo-spring SPH). An efficient immediate neighbor interaction was formulated by connecting neighbors through pseudo-springs in this technique. The damage of material is evaluated by the behavior of pseudo-springs, which seems a very interesting approach to investigate the crake propagation during impacts. There are also other forms of SPH improvements such as MLSPH [35, 36], Godunov SPH [28, 27], δ-SPH [37], and Gamma-SPH [38] et.al., all of which are developed under the motivation to different SPH applications. Tab.2.1 lists the developments of SPHs in the past forty years, not involving all but including the most several important formats. More detailed reviews about developments of SPH formulations can be found in [39, 40, 14].

Table 2.1: The improvements and developments of SPH method

Name of methods	Year	Authors and references
Standard SPH	1977	Gingold and Lucy [8, 9]
Artificial viscosity	1989	Monaghan[22]
Axis-symmetry SPH	1996	Johnson etc. [41, 42]
CSPM	1999	Chen etc. [43, 44]
MLSPH	1999	Dilts etc. [35, 36]
Artificial stress	2000	Monaghan and Gray [23, 24]
Godunov SPH	2002	Inutsuka etc.[28, 27]
MSPH	2004	Batra etc. [45]
Total Lagrangian SPH	2006	Vignjevic, Reveles etc. [19, 30]
FPM	2006	Liu etc. [46]
δ-SPH	2009	Molteni etc. [37]
Pseudo-spring SPH	2013	Chakraborty, Amit etc. [32]
Hourglass for TL SPH formulation	2015	Ganzenmulle etc. [31]
JST SPH	2016	Lee etc. [47]
Gamma-SPH	2017	Limido etc. [38]

2.3/ HVIS ON THIN STRUCTURES

2.3.1/ HVI PROBLEM DESCRIPTIONS

The response of structures under high-velocity impact loading is complicated and uncertain, which depends on the material properties and impact conditions including projectile shapes, deformable or rigid projectile, impact velocity, target configuration particularly the

thickness, and target materials.

Backman et al. in [48] classified the most frequent types of damages during HVI for thin or intermediate targets, as shown in Fig.2.1. All of these damages result from the initial compression wave and they often happen with more than one single form in specific impacts, which often involve the elastic-plastic deformation, shear deformation, hydrodynamic process, phase transition, etc. The definition of the thin target means the stress and deformation gradients throughout its thickness do not exist. The mechanical problems like perforation, fragments, and debris clouds principally happen on the thin plates impacted by the high velocities. For example, the perforations accompanying plugging a), ductile hole enlargement b), radial fracture c), as well as fragmentation and debris cloud phenomenons d), as shown in Fig.2.2, have been observed in many experiments about impact thin structures.

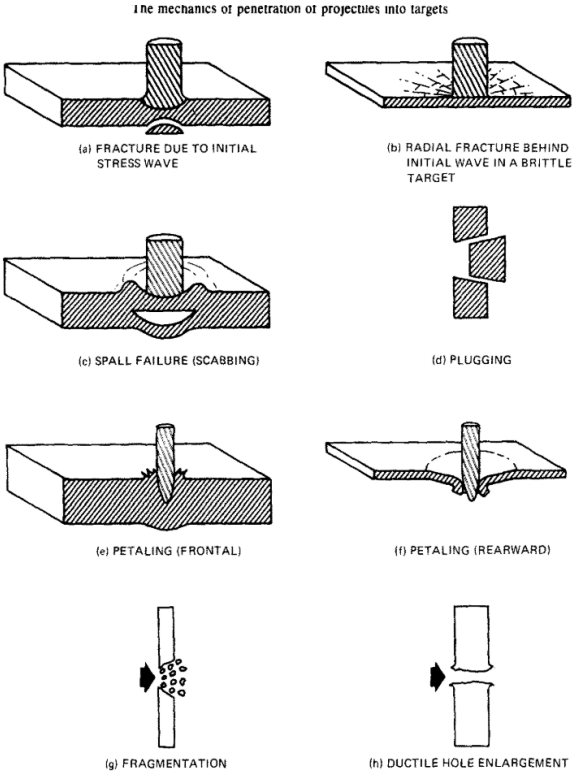

Figure 2.1: The types of damages in HVI from [48].

At the same time, the shapes of projectiles also determiner the mechanical damages during the HVIs, for example, the research in [34] which studied the influences on the

perforation of metal targets impacted by different types of bullets, the simulation carried out by SPH framework.

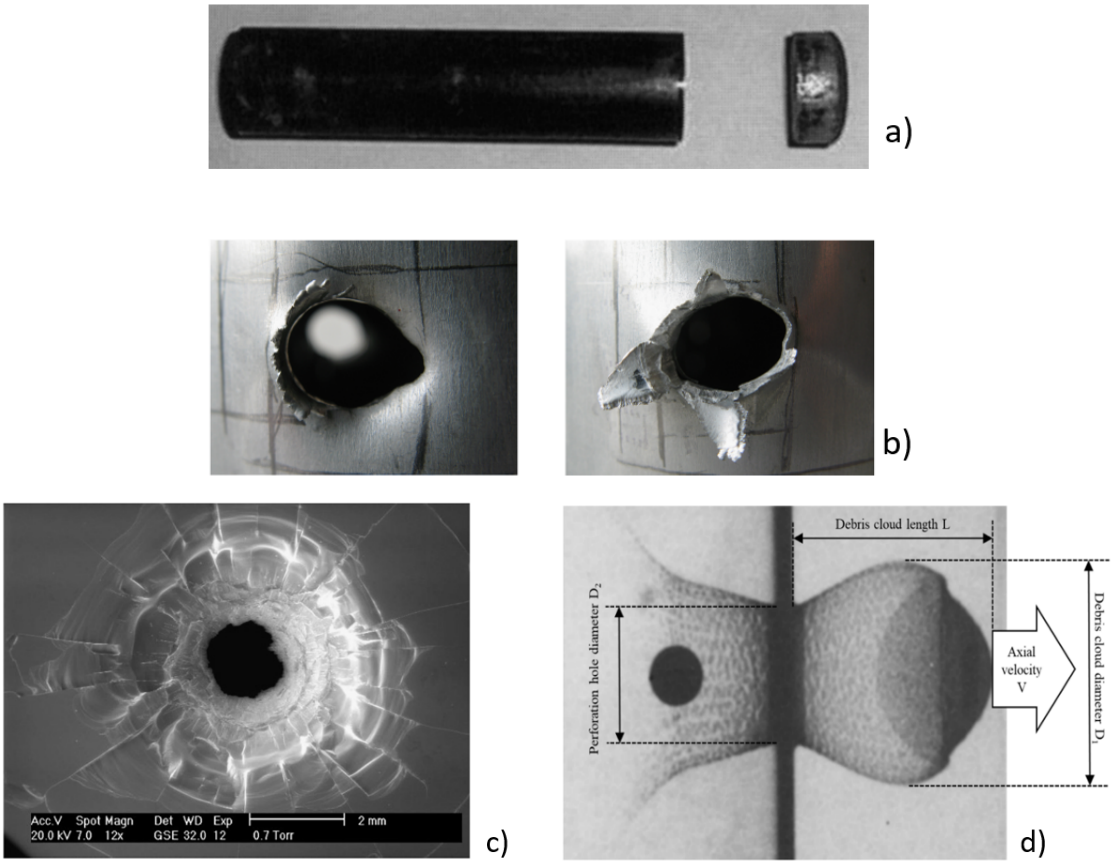

Figure 2.2: The types of damages observed by HVI experiments: a) shows the plugging situation after perforation by [49]; b) shows the petaling and ductile hole enlargement after perforation in [50]; c) shows the perforation accompanying with radial fracture in [51]; d) shows the debris could during the impact in [52].

More importantly, the damage types considerably rely on the target properties like ductile plates, brittle plates, soft structures as well as advanced composite plates [53, 54, 55, 56, 57, 58]. Particularly, for the brittle thin plates like the study [51], the ejecta and debris environment was emphasized to be investigated during HVIs. Ceramic as a typical brittle material has been widely used as a target material in the various engineering environment. It also motivates that lots of research are developed to study the ceramic damage with fragmentation during the HVIs by SPH method [59, 60, 61, 62].

2.3.2/ SPH APPLIED IN HVIS

2.3.2.1/ FIRST PROPOSAL - 1990

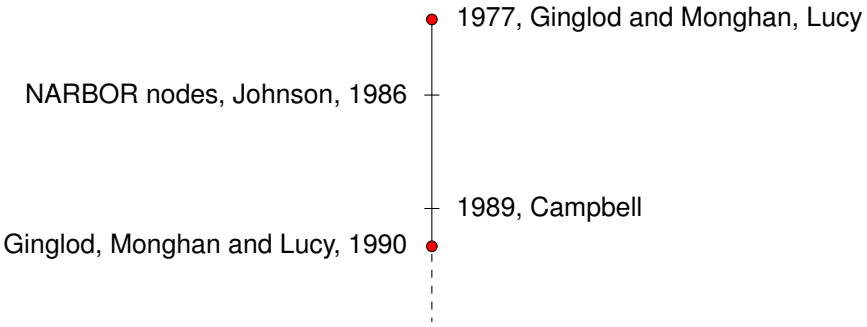

The first application dedicated to Hight Velocity Impacts on structures by the use of the SPH method seems to appear in the early 90s from one side in [63] and from the other side in [64]. A few years earlier, Johnson et al. [65] had introduced a particle method named NARBOR nodes to model violent impacts. This grid-less method uses the idea of neighbor particle interactions to define simplified strain and stress fields in a Lagrangian frame. This procedure based on free-nodes allows variable nodes connectivities and thus to deal with severe distortions. This first approach had given the inspiration that particle methods can offer interesting tools to investigate such complex situations.

In 1990, at the Next Free-Lagrange Conference, both Stellingwerf [63] and Cloutman [64] had exhibited a very similar work. Cloutman [64] introduced a very common standard formulation based on the work in [21, 66], which discretized the Euler's equations associated with a Tillotson EOS to model shocks, expansion, and change of phase of metals, such as Iron in this case. As firstly introduced in [21], in the presence of shock waves to prevent inter-penetration and spurious oscillations, an artificial viscosity had been introduced in the momentum and energy equations. The numerical test introduced in this study corresponded to the case of an Iron disk of 0.6 cm thickness and a 2.1 cm radius impacted at 6 km/s by an Iron sphere. The radius of the projectile was not given but seemed to be very close to the target thickness of 0.6 cm. The two bodies were discretized with 1984 particles for the target and 192 particles for the projectiles, distributed randomly. This work did not show any strong validation, although it compared, without showing any support of this, the SPH result with a Finite Difference result. Only some shape differences and dimensions were displayed, which suggested that the SPH procedure could offer a "realistic" solution for HVI problems at that age.

Subsequently, the authors in [64] provided the encouraging results by the SPH method in applied impacts. And more worthy, this study pointed out the important limitations such as: running time where he suggested the use of parallel computation; reducing shocks smoothing and inter-penetration; the implementation of physical phenomena such as surface tension, viscosity, and material strength; treatment of boundary conditions; optimal kernel and h-value because he used a Gaussian kernel. On the other side, the authors in [63] presented the code-named SPHC which seemed to be very similar to the one proposed in [64] at the difference that the SPHC code used two-dimensional Cartesian modeling and employed a Mie-Gruneisen EOS. The validation test consisted of an aluminum cylinder impacting an Aluminum plate at a speed of 7 km/s. The dimensions of the projectile and the plate were not given but should be in the same order as the previous test. Very few information was given except for the fact that the whole model was discretized with 500 particles. Again, no validation was presented, only the shape of the deformed target was discussed. These two works are the very beginning of HVI SPH modeling and even if no true validation is presented, both could conclude that the SPH method is very appealing for its simplicity and its capability to model important material distortions.

In the SPH models provided by both Cloutman [64] and Stellingwerf [63] at that time, they used the same standard formulation by considering only the Euler's equations with symmetric SPH discretization including an artificial viscosity. Particularly, at that age, the density evolution was not governed by the continuity equation but instead by the density summation:

$$\rho^h = \sum_j W_{ij}^h m_j. \tag{2.28}$$

Such a model provided a quite stable way to model perforation of structures for very high-velocity impacts as it can be observed with the Fig.2.3. It involved symmetrical SPH discretization of the linear momentum and energy conservation equations in the Euler's equations, employing linear and quadratic artificial viscosity, performed with the density summation procedure, and using an adapted time step. Nevertheless, at that stage the estimation of the method efficiency was not clearly revealed since no strong comparisons with experiments or other data have been brought.

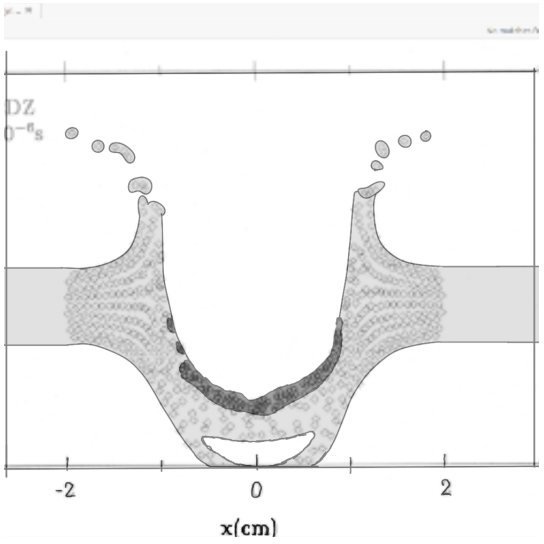

Figure 2.3: Illustration of the Stellingwerf's test [63].

2.3.2.2/ DEVELOPMENTS OF SPH CODES IN HVIS

As one of the pioneers in developing the SPH modeling impact problems, Petschek et al.[67] developed a 3D standard SPH code involving the artificial viscosity by Monaghan [22] and simulated a 3-g copper disk (11.18 mm diameter x 3.45 mm thick) impact on a 2.87 mm thick aluminum bumper plate at 5.55 km/s. Although a predetermined fixed value was given to describe the plastic flow regime during this high impact process, an encouraging result obtained by this code was that the maximum width and length of the debris clouds after impact were in agreement with experiments. Also, Stellingwerf is one of the pioneers in this field. At the beginning of the use of SPH method, Stellingwerf and his co-workers made a review of this computational technique in [68], and illustrated the great potential of this SPH method by the number of different simulations: a spherical aluminum projectile with radius 0.475 cm impacting a thin aluminum sheet with thickness 0.0381 cm at a velocity of 6.75 km/s, and including a series of impact simulations with disk projectiles radius of 0.95 cm impacting a 0.127 thick target at 10 km/s. The same group of researchers studied the variations in crater volume caused in the copper sphere impacts copper target with 4.0/3.0 cm thick at initial velocities from 6.0 km/s to 24.5 km/s using four numerical codes including SPH, MESA, EPIC and CALE codes in [69]. The investigation on the effect of a change in the yield strength in the material model was done and good agreement was found between these codes. In 1993, Johnson et.al incorporated SPH algorithm into a standard Lagrangian code such as EPIC in [70]. It

modeled the copper rod impact steel plate with 2.6 cm thick at 2 km/s and 4 km/s, and copper rod impact aluminum plate with 12.7 cm thick at 5 km/s. These studies involving the validations between SPH code simulations and experimental or other existing codes results made more and more researchers pay attention to the advantages of the SPH method in the application of HVI problems.

Except for EPIC software, SPH method was also incorporated into the other public numerical codes like AUTODYN-2D hydrocode and PAM-SHOCK 3D computer code. Some researchers employed these codes to study the impacting process on the thin structures [71, 72]. For example, in 1999, Faraud et al. investigated the debris cloud of the projectile impact on an all-aluminum triple wall system by the SPH method in [72]. The authors mainly compared the performances of two SPH formulations which had been incorporated into the PAM-SHOCK 3D computer code and the AUTODYN 2D hydrocode. Different constitutive laws were tested (Johnson-cook, Steinberg-Guinan), as well as different equations of states (Tillotson, Shock, Sesame). This study showed that both the SPH codes achieved a good representation of the debris cloud expansion before the impact on the 2nd BS, but the simulations of the impact on the 2nd BS and BW could not agree with the experimental observations. Both the PAM-SHOCK 3D computer code and the AUTODYN 2D hydrocode existed severe problems in energy and momentum conservation. Therefore, this study showed that at that age, the SPH technique was not sufficiently mature to support the development of complex debris shielding systems. At same time, Hiermaier et al. [73] and Groenenboom et al [74] also developed SPH codes and applied it to simulate HVI problem on thin structures. The simulations concluded a 0.5 cm diameters Al projectiles impact 0.15 to 0.4 cm thick plates at 5.75 to 6.85 km/s in [73]. Groenenboom et al. [74] conducted HVI both in 3D and 2D plane strain, investigating the role of a constant or variable smoothing length in SPH kernels, as well as the type of equation of state.

Actually, the SPH method obtained less interest and attention in the application of solid dynamics until the 21st century. The incorporation of SPH formulations to LS-DYNA commercial software provides much convenience to simulate HVI problems using this approach. For example, Michel et al. [51] used the SPH model in LS-DYNA to study the damaging and fragmenting processes during HVI on thin brittle targets. The simulation by the SPH model consisted of the steel projectiles on brittle targets (fused silica plates)

of 2 mm thickness with velocity impact ranging from 1 to 4 km/s. The Johnson Holmquist material model and pressure cut-off criteria were chosen for target material. This SPH model successfully predicted the fragments clouds geometries and velocities. Besides, the perforation hole and spallation zones in the target were obtained in the simulation results, being in a good agreement with experimental observations. The influence of target thickness on damages and matter ejection was also investigated numerically in this study. Fig.2.4 is the simulation result from [51], showing the spalling phenomenon, the particle clustering representing the macro and micro spalls naturally.

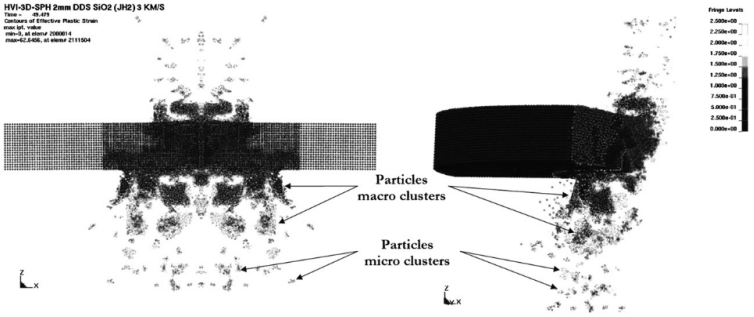

Figure 2.4: Illustration of SPH simulation in [51]: two types of spalls can be identified (macro and micro spalls) represented by SPH particles clusters as fragments.

Kilicc et.al. performed perforation tests on 9 and 20 mm thickness armor by both Lagrange and SPH methods in LS-DYNA in order to determine the ballistic limit of 500 HB armor steel against 7.62 mm 54R B32 API hardened steel core ammunition [75]. Johnson-Cook constitutive relations for both strength and failure models were developed in these tests. It is worthy to notice that, as concluded by authors in this study, the use of SPH formulation did not predict spall and fragmentation behavior more accurately as expected, even involving a finer particle size in the SPH discretization. What is worse, even a hybrid SPH modeling used to decrease numerical cost, still, SPH is too costly when compared with the Lagrangian formulation.

A series of experiments about cylindrical Lexan projectiles impact on steel target plates with a velocity range of 4.5-6.0 km/s were performed in the study of [76]. The authors also develped numerical models to these impact by SPH in LS-DYNA and the Eulerian-based hydrocode CTH, involving that a 2-D axisymmetric SPH model for both projectiles (5.58 mm diameter and 8.61 mm length) and target plates (12.7 mm thick) using a 0.05 mm distance between each particles. A combination of Mie-Grüneisen EOS and Johnson-

Cook relationship was chosen for material modelling. The study compared numerical results to experimental data in terms of impact cratering and bulge, and demonstrated that both simulation models were in general agreement with the experiments capturing all the major features observed experimentally. As a further research by this same group, Roy et al. [77] mainly optimized the numercal settings in these two simultion models, including determining SPH particle sensitivity, and identifing the best meshing strategy in CTH. The Hugoniot elastic limit and spall strength of A36 steel was mainly investiged combined the experimental and numerical results. Consequently, both simulation approaches SPH and CTH were proved to be able to accurately match he physical measurements of impact cratering, as well as predicting the velocity profiles in the PDV experiments.

Also, Xiao et al. studied SPH simulations by LS-DYNA of the normal perforation of monolithic and layered Weldox 460 E steel targets with impact velocity in the range of 80–405.7 m/s and target thickness in the range of 2–12 mm in [78] . A coupled constitutive model of viscoplasticity and ductile damage developed in [79] was used to model the dynamic behaviors of the target material Weldox 460 E steel. The model defines a damage evolution based on a constitutive relation considering stain hardening, strain-rate hardening and temperature softening. This work mianly studied the effects of target thickness or number of layers for the ballistic resistance of monolithic targets and layered targets based on a series of simulation results. By employing the SPH formulation in LS-DYNA, Thurber et al. [80] performed the simulations of 9.53 mm diameter aluminum spheres, impacting 2.33 mm thick aluminum plates. They mainly investigated the assumption that the responses of materials under severe loadings like HVI involve the principal fluid-like behavior of solids. Different material parameters were implemented in the Johnson-Cook model, as well as Mie-Grüneisen EOS to simulate different shades of aluminum targets.

In addition, Sakong et al. [81] also used the SPH method in LS-DYNA to simulate HVI problems with different projectiles and thin plates (steel and aluminum), but the main contribution in this study is that the fragment distribution from the particle dispersion during the impacts was analyzed by using a clustering algorithm. The authors firstly represented the possibility of applying the machine learning algorithm on the result analysis of high-velocity impact. In this study, the simulations involving cylindrical or sphere projectiles impact to aluminum plates with mm-scale thickness at 2.15 or 6.64 km/s velocities were performed. This simulation predicted well the HVI process involving the residual veloc-

ity, hole diameter, and spalling diameter, debris clouds in the target plates. Besides, the threat of the fragment to a certain structure can be evaluated quantitatively, by employing the machine learning algorithm to analyze the trajectory similarity of the particles.

2.3.2.3/ NEW SPH FRAMEWORKS

Although some commercial software like LS-DYNA, Abaqus, as well as Hyperworks have included SPH solvers, most of them implemented the standard SPH formulations, a few coupled with some improved techniques like artificial viscosity, artificial stress or conservation smoothing approaches. Several new frameworks based on the SPH algorithm are still developed aiming to get more stable and accurate simulations for HVI problems, such as pseudo-spring SPH, KGC-SPH, Gamma-SPH, γ-SPH-ALE, and decoupled finite particle method (DFPM).

Pseudo-spring SPH was developed initially by Amit and chakraborty et al. in [32, 82]. The main concept of the pseudo spring strategy can be represented by Fig. 2.5, in which SPH interaction is restricted only to the nearest neighboring particles through connecting pseudo-springs. This network of springs is supposed between all the interacting particles, and they do not provide any extra stiffness to the system. The function of these springs is to collect all the information about damage state of the material and hence a damage evolution law defines degradation of the inter-neighbor spring forces. The interactions between particles are dominated by a parameter f, defined as $f_{ij} = 1 - D_{ij}$, where D_{ij} is the accumulated damage in the pseudo-spring between the $i - j$ particles pair. D_{ij} is defined as $D_{ij} = 0.5(D_i + D_j)$, where D_i and D_j are the damage parameters at the ith and jth particles respectively. Therefore, by evaluating the interaction factor f_{ij} when it reaches the critical value, this spring breaks. The breaking of spring denotes the formation of a crack and the corresponding disconnected particles represent the material body on either side of this newly formed crack surfaces. Therefore, this pseudo spring technique has a fundamental strength in modeling crack propagation. The same group of researchers furtherly applied this model to study crack propagation in the bi-material interface in [82], and to study ballistic sensitivity of pre-notch in the metallic beam in [83].

In 2017, Islam et al. used this pseudo spring strategy combined with SPH to study the failure of ductile material under impact loading in [33]. A series of impacts of a cylindrical

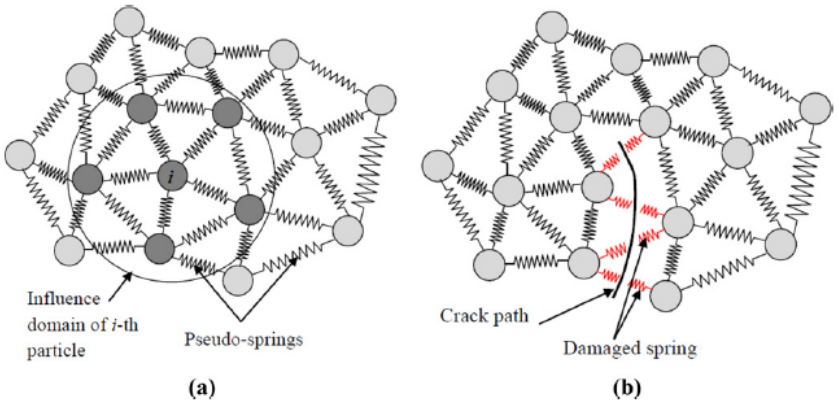

Figure 2.5: The pseudo-spring model (a) undamaged configuration (b) cracked configuration from [32].

projectile on plates with 8 mm and 10 mm were simulated in this study, the material both of projectiles and targets being Weldox 460 E steel. As well known, ductile material failure is much more complex including large plastic deformation, heat generation due to plastic work, material instability due to localization of plastic deformation, and the growth of microvoids leading to damage. The attempt of this study implied that this SPH based on the pseudo spring method is a very promising approach to model the complex damages in impacts. In the same year, Islam et.al. employed the pseudo-spring SPH to investigate the damage in ceramic and ceramic-metal composite structures under high impacts in [84]. The ceramics are typically brittle materials that involve abrupt failure and cracks, which is easier to be captured and modeled by use of the pseudo spring concept. Afterward, A Total Lagrangian SPH method was improved combined with Pseudo-spring contact in [85] to model crack initiation, propagation, and material failure of notched beams under the impact. This study provided several impact examples of notched beams, but no HVI simulations. Recently, Islam et al. in [34] used Pseudo-Spring SPH again modeling the projectiles impact metal target with a range of 6mm-16mm thick plates. The projectile was modeled as a perfectly plastic material with very high yield stress (1900 MPa). The target was modeled by JC constitutive law, including usages of six damage models. This work mainly focused to investigate the effect of damage model on the computed ballistic response of metal plates (Weldox 460E steel and 2024-T351 aluminum alloy plates). The effects of the projectile geometry and hardening were also investigated in impact response. It can be concluded that the pseudo-spring SPH framework equipped with a suitable damage model can predict the plate perforation for different thick plates at differ-

ent velocities. Moreover, in the same year, the authors in [61] used Pseudo-spring SPH to model ceramic and ceramic-metal composite plates including 30 mm deep target, 9 mm thin target, and deformed projectile. Three constitutive models JH1, JH2, and JHB were used in this study. Effects of interparticle spacing, the compact support of a kernel function, and types of kernel functions like the Wendland and the cubic B-spline kernels, as well as the projectile nose shapes (blunt, hemispherical and conical) on computed results have been described.

zhang et al. developed an improved SPH called KGC-SPH (kernel gradient correction (KGC)) to model the impacts of an aluminum sphere penetrating an aluminum plate in two- and three-dimensional spaces [86]. The KGC technique can mathematically improve the accuracy of the gradient of the kernel functions, which has been implemented to the SPH schemes both of 2D and 3D but only modeling the incompressible fluid flows. The authors firstly extended it to investigate the HVI process. In the KGC technique, a modified or corrected kernel gradient is obtained by multiplying the original kernel gradient with a local reversible matrix, and the detailed formulations can be found in [87, 86]. The Johnson-Cook model and the Mie–Gruneisen eos were applied in the simulations. The simulations for 2D and 3D HVIs of 1.0 cm diameter aluminum cylinder onto a 0.4 cm thick aluminum plate at 6180 m/s and 4119 m/s were carried out. All the simulation results illustrated that the SPH method with KGC can be effective in modeling HVI problems and can produce more accurate results than the conventional SPH methods without kernel gradient correction. The followed work about the application of the SPH-KGC coupled method was provided in [88]. They mainly investigated the sizes of the craters produced by HVI at different initial impact velocities and the variation of the crater size over the impact velocity. A series of 3D HVIs in which the aluminum sphere impacts the aluminum plate with a thickness of 0.4 cm at different velocities from 2 to 11 km/s (with an interval of 0.5 km/s) were performed and observed in this study. The two-stage phenomenon (the varying stage and steady stage during the increase of the crater size versus impact velocity) was accurately predicted by this new formula.

Limido et al. [38] proposed an improved SPH called Gamma-SPH to reduce standard SPH drawbacks like lack of interpolation completeness, tensile instability, and the existence of spurious pressure, as well as high computational time. The main concept of this improvement is based on a centered formulation for the pressure gradient term in

the momentum equation and on the introduction of a stabilization term proportional to the pressure difference between two neighbor particles. The stability of this new formulation is ensured and theoretically proved under a CFL-like condition. The simulations of 9.53mm diameter aluminum sphere impact aluminum plates with 0.8 mm and 4.039 mm thick at 6.7 km/s velocity were conducted. Oblique impact consisting of a 3 mm aluminum sphere against to 2mm thick aluminum plate at 32° tilted and 4059 m/s velocity was also simulated by this Gamma-SPH. The debris clouds for both normal and oblique impacts observed in simulation and experimental results were in good agreement.

An alternative scheme called γ-SPH-ALE was deveoped to model the HVI cases and investigate the debris clouds in [89]. Indeed, γ-SPH-ALE is the combination of SPH-ALE formulation [90] and FV low-Mach scheme [91]. The simulations of aluminum spheres impact aluminum plates with different thick at 6.7 km/s were performed by this SPH scheme. An oblique impact with a 3 mm-diameter sphere to the plate with 2 mm thick at velocity 4050 m/s was also deducted by γ-SPH-AL method. An elastic perfectly plastic material model combined with the Mie-Grüneisen equation of state was applied to the material of both projectiles and targets. The simulation results revealed that the proposed scheme increases both stability and accuracy and reduces the computation time compared to classical solvers.

Zhang et al. also investigated the damaging effect of target plates induced by high-velocity impact using a decoupled finite particle method (DFPM) in [92]. DFPM was a recently developed corrective SPH method by Liu and his co-workers in [46, 93]. DFPM does not need to solve redundant and challenging pointwise corrective matrix equations when approximating a field variable and its derivatives. The authors made a comparison on the formulations of different SPH improvements like FPM [93], CSPM [44] and KGC [86], and the point can be concluded that DFPM indeed has its advantages on mathematical accuracy and implementations. Different from these formulations of SPH versions like FPM, CSPM, and KGC all of them involving the corrective matrices which can be ill-conditioned in extremely deformed domains, DFPM can obtain a more stable calculation especially for cases with highly disordered particle distribution. Lots of 2D and 3D HVI examples including less than 5mm thick metallic plates impacted by 2-13 km/s velocities were performed by both conventional SPH and DFPM in this study. The numerical results demonstrated that the DFPM can achieve a more accurate computation on the boundary

than using conventional SPH, as well as have the capability to alleviate tensile instability. The hole size and damage in HVIs were also predicted and agreed with experimental data.

2.3.2.4/ NON-METALLIC PROJECTILE-TARGET SYSTEMS

Nowadays, environmental protection and safety standards in the modern industry make the materials of structures involving higher requirements, traditional metallic structures have been not enough. Some advanced structures like laminated composite structures are used in various engineering areas, involving aerospace, automotive, marine, civil, sport, etc. The study of the dynamic response of impact laminated composite plates was also performed by the SPH method in recent years [53, 54, 55, 56].

The differences in SPH modeling the targets with different materials can be shortened into two parts: one is the specific constitutive laws implemented into SPH formulations; the other is the modeling process by particles, particularly for laminated structures. The different constitutive laws for metals, various types of composite materials, as well as ceramics, have been developed and can be found in the literature. The challenging work is to integrate them into the SPH algorithms.

About modeling the laminated structures by SPH particles, Shintate et al.[54] introduced its details, as shown in Fig.2.6. In this study, the authors used the improved SPH method to simulate an aluminum projectile striking to laminated graphite/ epoxy (Gr/Ep) composite plate targets with several different layup configurations. Every single layer was modeled macroscopically as a uniform medium, and then the numerical laminated plate model for the SPH method realized the discontinuity of stresses between neighboring layers of the laminated composite plate targets. Fig.2.6 illustrates this concept that the layers A and B are assumed to be arranged without bonding. Then the model is based on the assumption that only positive pressure acts between the particles P_A and P_B which belong to layers A and B, respectively, when the two particles are approaching each other. The inner product of the relative velocity vector and the relative position vector of two particles is utilized to determine whether the two particles are approaching each other or not. Fig.2.8 is the numerical model of the target in this SPH simulation. Back in the 1990s, the SPH method combined with the macro-homogeneous, anisotropic material concept for

fiber composites was already developed for HVI problems by[53]. In recent years, some studies [55, 56] also employed a similar conception to model the laminated structures as the target in impacts.

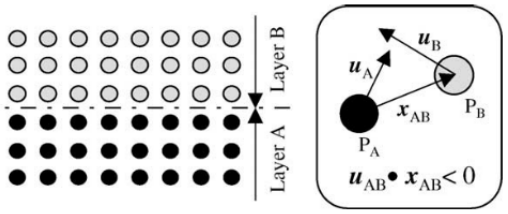

Figure 2.6: Numerical laminated plate model by SPH particle from [54].

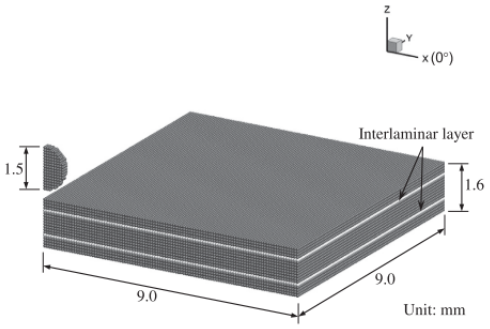

Figure 2.7: The SPH model for CFRP laminate from [55].

Except for developing the SPH model for laminated structures, the main contribution in [54] is to develop an improved SPH method with new particle generation and particle merger techniques. The new particle generation technique means generating new particles if the area with no particles exceeds a certain value or the distance between the adjacent particles exceeds a certain value, following two rules. Because the new particle generation technique to prevent the numerical fractures causes the overabundance of particles. Another particle merger technique was presented in simulation in which two close particles of a triangular element are merged into one particle if the distance between the two particles attains a certain value. Fig.2.9 displays a comparison with an HVI example between the results by standard SPH and this improved SPH. This improved SPH was proved not only a promising approach to decrease the numerical fracture during HVI problems involving the deformation with a large tensile strain by a conventional SPH, but also a robust and effective way to model the laminated plates.

Carbon fiber reinforced plastics (CFRPs) have good specific strength, specific modulus, and fatigue properties compared with conventional metals, so they have been applied to primary load-bearing structures such as wings and a fuselage in the latest airplanes.

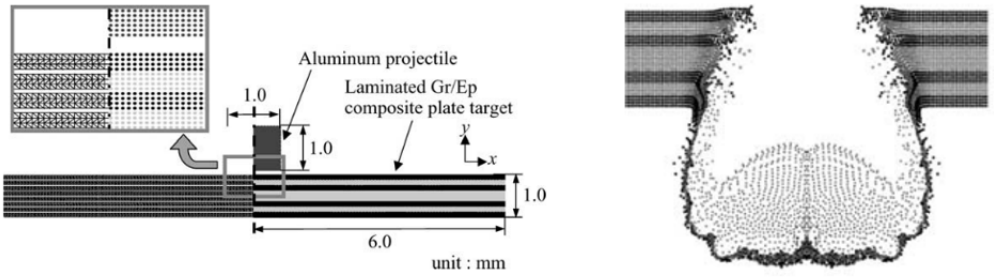

Figure 2.8: The SPH model of the laminated Gr/Ep composite plate (left); debris cloud produced by impact at 4.0 km/s (right) provided in [54].

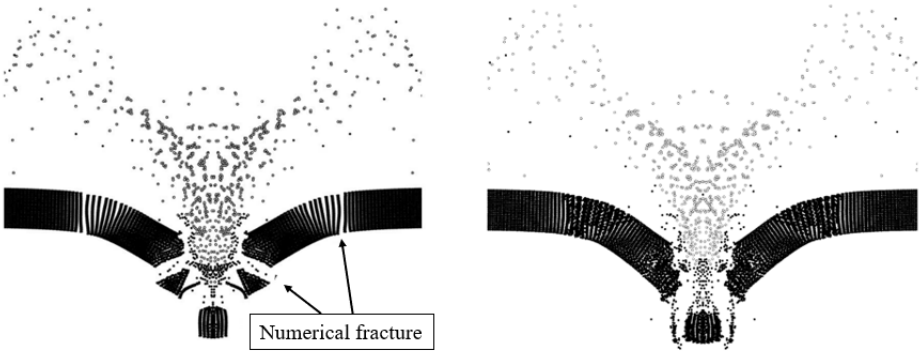

Figure 2.9: The unphyscial fractures during standard SPH model (left) and improved SPH model (right) in [54].

Yashiro et.al investigated mechanisms of the extension of high-velocity impact damage in CFRP laminates by experiments in [94] and numerical simulations with the SPH method in [55]. Fig.2.7 shows the SPH model for a CFRP laminate, and the simulation in this study consisted of 1.5 mm diameter steel balls impact CRFP laminate with 1.6 mm thickness at 200 to 1200 m/s. 0° and 90° layers for cross-ply laminate were modeled, as well as interlayer particles were inserted into the ply interface to represent delamination. Damage in a particle was judged by modified Chang–Chang criteria, and a material degradation rule was applied to the stiffness and stress in the damaged particle. This SPH model succesfully predicted the high-velocity impact damage including a crater and matrix cracking/crushing in the top ply, catastrophic failure of the middle plies, and fiber breaks and matrix cracking in the bottom ply. In 2019, Giannaros et.al. performed the simulations of carbon fiber reinforced polymer composites (CFRP) material behavior to hypervelocity impact using the SPH model in LS-DYNA in [95]. The numerical examples

consisted of the sphere projectiles with different diameters impact to 2.3 mm thick CFRP plates at the velocities ranging from 1.93 to 4.96 km/s. The simulation results including shapes of debris clouds, ballistic limit, and the crater diameters were in good agreement with experimental observations. It showed that the SPH method and MAT_59 material model provided in LS-DYNA can predict the behavior of CFRP plates under the impact loading. However, the authors claimed that the numerical failures before material failure still should be alleviated by additional solutions. And a strain rate dependent and experimentally calibrated orthotropic material model should also be further developed to simulate CFRP behavior, which at the same time, should be compatible with the SPH code of LS-DYNA.

High-strength cementitious (HSC) materials also have been paid more attention in the application of passive protection from weapon effects recently, because of its properties involving comparatively low cost, ease of rapid on-site manufacture, and high early strength. Nordendale et.al. studied the responses of the high-velocity projectile impact on HSC materials by both Traditional Lagrangian finite element analysis (FEA) and SPH in [56], and they mainly focused on a comparison of the simulation performances between FEA and SPH models. The projectile used was a MIL-P-46593A Standard fragment simulating projectile (FSP), and the HSC plates were modeled by a modified Advanced Fundamental Concrete (AFC) constitutive model in both FEA and SPH methods. Multiple impact simulations were performed with velocities varying from 1067 m/s to 1097 m/s. The authors concluded that the ability of the SPH model to capture residual velocity proved to be just as accurate as traditional FEA models, but they are significantly more time-consuming. However, SPH has a great advantage to model debris field compared to traditional FEM; and modeling the high-rate impact of a brittle target is the issue of spalling and fragmentation.

Ceramics as a typical brittle material are often used in protective structures. The difference of SPH modeling ceramics target and metallic target in HVIs is mainly on the usage the suitable constitutive laws. In 2020, a recent study was provided by Xiao et.al that SPH models were established to simulate fracture and fragmentation of the projectile and the target during the impact process of a ceramic tile by a projectile in [59]. The case of an Al_2o_3 ceramic plate with 12.7 mm thickness impacted by a deformed cylinder with a diameter of 6.14 mm and a length of 20.86 mm at 903.9 m/s was conducted by SPH model

in LS-DYNA. JH-2 model (Johnson and Holmquist (1994)) was used to describe material behaviors of Al2O3 ceramic, which includes pressure, strain rate, damage, and bulking effects. The simulation results showed that the JH-2 model is suitable and attractive for modeling the high-velocity impact of ceramic-type materials. In this study, two methods including a penalty contact method (PCM) and particle approximate method (PAM) were employed to handle interactions between the projectile and the target. The simulation results illustrated that PCM and PAM induced insignificant differences in modeling the high-velocity impact of the deformable projectile on the ceramic tile. The sensitivity of SPH numerical parameters like artificial viscosity, smoothing length, and particle spacing on simulation results was also investigated.

Another new study in [62] is to develop an FE-SPH coupled model to investigate the responses of HVIs with the Al_2o_3 tiles target and multi-layered targets with Al2O3 front layer and AA6061- T6 backing layer. In this model, the FE belonging to the ceramic part was converted into SPH particles when the element conversion criterion was met. Two projectiles were used: 7.62x51 P80 and 12.7x99 AP in the simulations. This study concluded that the FE model can not obtain accurately simulating the transmission of the projectile decelerating force to the rear plate with a consequently incorrect prediction of the residual velocity and damage morphology in multi-layered targets. In contrast, the SPH model combined with FEM elements is more suited for the simulation of the response of ceramic materials. Fig.2.10 is the numerical result of impact multi-layered target, from which it can be seen that the crack is the principal damage for brittle ceramic plate. Indeed, as the above description of the new types of SPH schemes, 'pseudo-spring' SPH seems the most promising approach to simulate the ceramic damages under impact conditions because of its natural property to capture the crack transmission by the behavior of pseudo-spring [61].

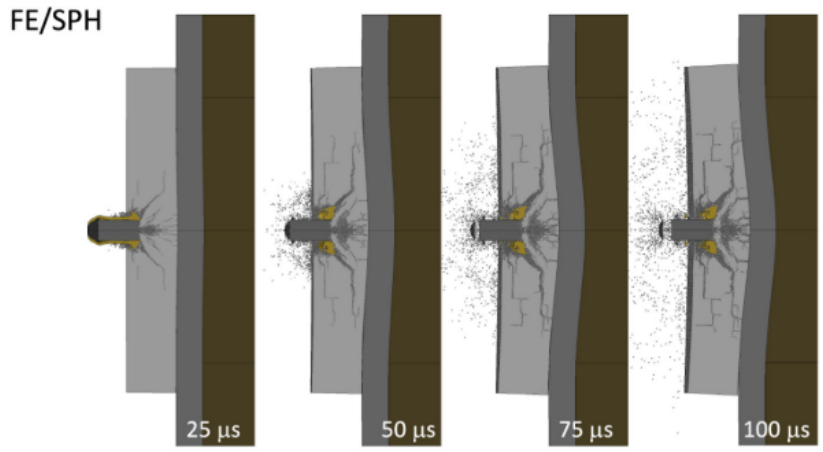

Figure 2.10: Impact sequence of 7.62x51 P80 against multi-layered target simulated by the numerical models from [62].

2.4/ LIMITATIONS AND IMPROVEMENTS

Some advantages of the SPH method applied to simulate the dynamic solids have been well recognized, and from the literature review in the last section, it can be seen that the SPH method also has become one of the most important approaches to investigate the responses of high-velocity impacts. However, the pioneers warned about numerical weaknesses in the use of this mathematical formulation for solid mechanics. The shortcomings of SPH algorithm like estimated accuracy of neighbors, interfaces for large density discontinuity, high time-consuming, and the particles instabilities become more visible in modeling large solid structures. Particularly, the instabilities due to tensile behavior are inevitable in simulating solid dynamic problems like HVIs.

In the earlier 1990s, some techniques including conservation smoothing in [96] in 1994, implementation of kernel renormalization in [42, 97] in 1996, more accurate computation on the boundary in [98, 99] had been developed to improve the SPH performances. The details are provided by the earlier review articles in [17, 100]. With the motivation of simulating HVI problems that involve more complicated and uncertain physical phenomenon, some improvements for SPH formulations are still under research combined with the mechanical properties in HVIs. Besides, the fracture models merged into SPH formulas also should be developed to improve the realism of complete fragmentation during HVI, as claimed in [100]. This section would show some limitations and improvement of SPH

method applied in simulating HVI problems.

2.4.1/ ACCURACY, INSTABILITY

Firstly, numerical accuracy is the primary consideration that relays on numerical stability to some degree, but numerical instability is still the inevitable problem for most numerical algorithms. In terms of SPH simulating HVI problems, the particles often suffer the severe clumping phenomenon when the materials are under extremely large deformations. Some analyses for the stability of the SPH method has been done by Belytschko and his co-workers based on the features of the particle method with Eulerian and Lagrangian kernels in [101, 29, 102]. Several types of instabilities including tensile instability were identified, and they claimed that tensile instability is a severe limitation to the SPH application in solid dynamics.

2.4.1.1/ ARTIFICIAL VISCOSITY

Artificial viscosity is the most common technique to mitigate the numerical oscillations, also to reduce tensile instability for some problems. The earliest standard SPH also involves an artificial viscosity proposed by Monaghan et al. [21, 22]. Nevertheless, the performances of this artificial viscosity depend on the choice of parameters (α, β), and it easily makes the system over-dissipative if unsuitable parameters are used. Shaw et al.[103] discussed this point in detail and introduced a modified method to avoid choosing unsuitable parameters. There are also some studies focusing on the effects of artificial viscosity on the simulation results for impact problems.

Back in 1996, Johnson et.al. studied the effects of different artificial viscosities for the SPH method in [41]. The types of artificial viscosity developed by different authors are listed in Fig.2.2. Johnson et.al. used five examples elected to describe a wide range of physical problems including plastic flow, wave propagation, erosion, rigid projector impact, and localized shear in this study. They were simulated by standard SPH formulations with six schemes of artificial viscosities, involving MAV by Monaghan al.et. in [8, 21, 22], BAL by Balsara et al. [104], node and bond viscosity [105], as well as three different combinations of parameters in MAV viscosity. By analyzing the simulation results, the authors declared that only changing the coefficients of MAV-type artificial viscosity can

not provide improved results. Additionally, the types of artificial viscosity illustrated different performances for different problems. For example, the MAV-type viscosity showed generally good results in plastic flow, rigid projector impact, and wave propagation problems but appeared severe numerical instability in the other two examples. It is difficult to find that a certain existing artificial viscosity algorithm or set of coefficients was clearly superior for the range of problems. The conclusion of this study was only to remind users should pay much caution when performing SPH computations for specific problems. At the same time, more work was required to develop artificial viscosity algorithms (or other algorithms) to improve the SPH instability problem.

Table 2.2: The types of artificial viscosity incorporated to SPH formulations

Ref	Abbreviation	Parameters	description
[8, 21, 22]	MAV	α, β	The most common type, not stable
[104]	BAL	α, β	capable for High-velocity impact
[105]	NBAV	α, β	not stable
[106]	MON	α^*	capable for High-velocity impact

The smoothing length (h) of kernel function and distance (d) between particles are also important parameters that can significantly affect the stability of simulation results. The study by Mehra et al. in [107] considered this point and also investigated the influence of four SPH schemes including three types of artificial viscosity (MAV, BAL, and MON in Tab.2.2) and a contact SPH scheme (CON) for the simulations of impact problems. They conducted a series of simulations on HVIs with variable values of the ratio h/d. The diameters of craters and shapes of the debris clouds during the impacts achieved in the simulations were observed and compared with experiments. The authors discovered that both BAL and MON viscosities had a good performance for hypervelocity impacts, but the MAV viscosity and CON scheme can not obtain the correct debris cloud shape as measured even adjusted a wide range of h/d. However, it is worthy to notice that the CON algorithm (also called the Godunov-type scheme) with its attractive quality of being free from arbitrary parameters, performed well at moderate impact velocities, not suffering from the numerical fracture. So, there is still no existing artificial viscosity term which is capable to keep generalized stability for SPH simulations, especially for the HVI problems with complex physical responses.

2.4.1.2/ TENSILE INSTABILITY

Actually, in the SPH method, tensile instability is still the most unmanageable problem. When particles are under tensile stress state or sufficiently close to one another, the motion of the particles becomes unstable, which may lead to particle clumpings representing as large tension exhibit 'numerical fracture' or artificial void in structure. This situation becomes a more significant concern in impact and penetration problems since the elastic dynamics involve considerable attractive forces. In 2012, Liu and his co-workers in [108] used the coupled SPH-FEM (SFM) to simulate high velocity perforation of steel and aluminum alloy plates of different thicknesses impacted by steel projectiles with various geometries, such as blunt, conical and ogival noses. The main contribution in this study is that a modified Johnson–Cook (MJC) model focusing on strain rate and adiabatic heating effects was adopted for metals, and material properties for Weldox 460E steel and AA5083-H116 aluminum plates were determined in the simulations. The authors claimed that for thin plates, due to the inherent tensile instability problem associated with the SFM approach, the agreement between numerial and experimental results was not obtained. Therefore, as introduced in section 2.2, most of the attention to improve the SPH application in sold dynamics is paid on the tensile instability problem.

Artificial stress also called Monaghan stress was the earliest technique to be particularized for solving tensile problems in solid dynamics in [23, 24]. A strong repulsive force is added to momentum and energy conservation equations, only when particles become too close to each other. It has been validated in impact problems by Monaghan's research, but only performed for low-velocity impact problems. According to the study by Mehra et al. [109], artificial stress could reduce the void size caused by particle tensile instability but unable to completely remove it when the impact velocity is high. Mehra et al. deducted simulations consisting of a steel sphere impact a 2 mm thick Aluminium plate at 3.1 km/s by SPH code combined with artificial stress and Godunov-type scheme (CON) in [109]. The numerical results showed that the Godunov-type scheme (CON) performed better than artificial stress in terms of mitigating tensile instability. But this observation is only by one impact. As the authors claimed, more studies with different impact scenarios should be considered to identify the presence or absence of tensile instability in the Godunov-type SPH. In fact, Godunov SPH method was developed to remove the tensile instability initially applied in fluid dynamics, which uses a Riemann solver and achieves

the second-order accuracy in space in [28, 27]. In 2017, Sugiura et al. [110] extended the Godunov SPH method to elastic dynamics by incorporating deviatoric stress tensor that represents the stress for shear deformation or anisotropic compression. The authors validated this algorithm in several classic examples such as the collision of rubber rings, oscillation of plate, as well as the impact problems. But, the impact example was still at moderate impact velocities (3.1 km/s), and its performance is still unknown at high-velocity impacts.

There are also some new SPH schemes developed recently involving removing the tensible instability such as Total Lagrangian SPH [30, 31], decoupled finite particle method (DFPM) [46, 93], and Gamma-SPH [38], etc, but no adequate examples applied in HVI problems, Tab.2.3 showing these several approaches corresponded to impacts.

Table 2.3: The techniques incorporated to SPH formulations to mitigate tensile instability.

Ref	Name	Description
[23, 24]	Artificial stress	Capable for 2D and low-velocity impact in [23]
[111, 112, 28]	Godunov-type scheme (CON)	Capable for moderate/high-velocity impact (up to 3.1 km/s) in [107, 109, 110]
[30, 31]	Total Lagrangian SPH	No much application in HVIs
[46, 93]	(DFPM)	Capable for High-velocity impact (up to 6 km/s) in [92]

2.4.2/ TIME-CONSUMING, COUPLED SPH AND CONTACT ALGORITHMS

Essentially, in SPH formulas, the approximation process is determined based on a contemporary domain of arbitrarily distributed particles, so neighbor searching is one of the most important steps in SPH to seek the nearest neighbor particles of a particle to define nodal connectivity. This directly leads to the SPH process time-consuming, especially for larger-scale and 3D problems requiring tremendous particles. To address this problem, two ways have been considered in the literature. One is employing the CPU/GPU computer algorithms, and the other is by coupling the FEM element model. A few studies like [113, 114, 115] have achieved the SPH formulation incorporated with GPU algorithms. Particularly, one work by Frissane et al. in [115] deserving to be mentioned is that a 3D

SPH code linked with the GPU algorithm was developed to model the process of high-velocity impacts of thin metal plates struck by a blunt projectile. The simulation results showed that this 3D SPH GPU numerical code was able to accurately predict the response of HVI problems, more importantly, costing a restrained amount on calculating memory and time.

The SPH has a strong ability to solve dynamic problems with large deformations without mesh distortions while it is not as good as the FEM in terms of computational time and boundary conditions. Besides, FEM has been developed for many years and has been a very mature technique involved in different commercial software. With this concern, the coupled SPH-FEM method can effectively use the strengths of these two methods for the simulations of large deformation problems. Some studies focusing on the coupling algorithms also have been developed in the past years [111, 116, 112, 117, 118, 119]. The coupled ways between SPH and FEM methods are mainly identified into two kinds: one way is converting techniques from FE elements to the SPH particles depending on the physical states of materials; the other is modeling different domains of the structure with SPH and FE respectively based on the interface contact algorithms. Fig.2.11 shows these interactions between SPH particles and FEM elements. The left one is from the study of [120], which displays that all the structure is modeled by FEM elements at the beginning and then the elements convert to SPH particles as the material deforms increasingly. The right form is provided in [121], where the center part of the target plate existing large deformation is modeled with SPH particles and the other part with finite elements. Also, if the projectiles are deformed largely such as using brittle materials, they are modeled using SPH particles while elements for rigid or small performed projectiles.

An approach to couple FE-SPH methods is based on a Lagrangian mesh whose elements are converted into SPH particles when a conversion variable (strain, stress, or any state variable) reaches a critical value. This idea was proposed and applied to simulate impact problems initially by Johnson et al. [122, 123, 120]. In the study of [122], two different converting schemes were used: SPH nodes sliding on a standard finite element mesh and SPH nodes automatically generated from a standard FE mesh. The simulations were carried out by this coupled method involving rigidly pointed and rounded nose projectile impacting aluminum targets, as well as, tungsten penetrator impacting steel target. The same researcher group improved the converting technique based on setting mass nodes

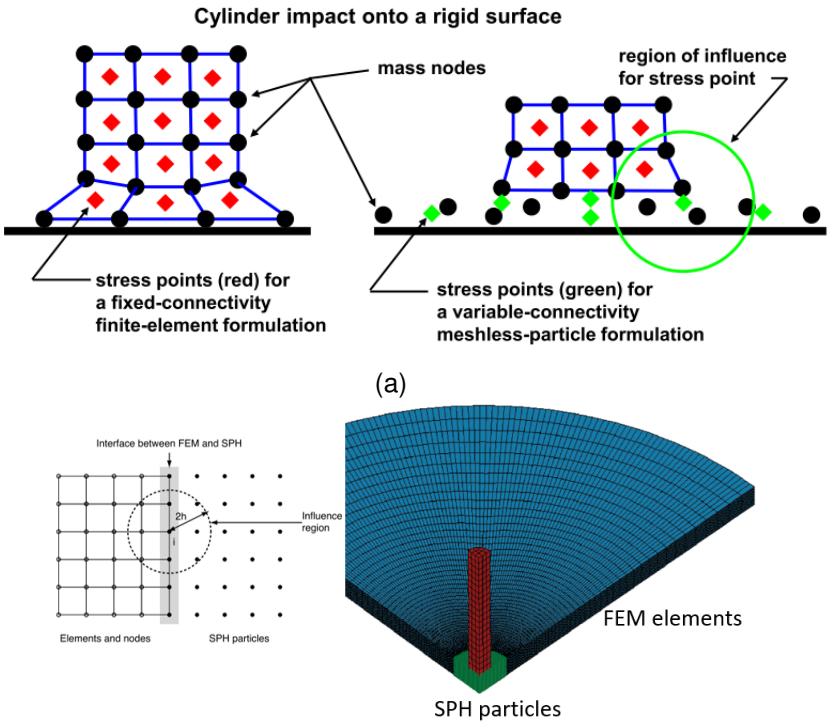

Figure 2.11: The FE-SPH coupled models: Left is the elements converting to SPH particles as the material deforms increasingly from [120] and Right is modeling different domains of the structure with SPH and FE, respectively, from[121].

and stress points in [120]. A new coupled FE-SPH method called combined particle-element method (CPEM) was developed to model the process of HVI examples in this study. The oblique impact consisting of a steel rod impact 4340 steel plate at 2 km/s was conducted by this CPEM. Subsequently, Rodriguez et.al. also applied this CPEM method modeling 4mm-thick plate of aluminum impacted by the projectiles with different nose shapes (conical, hemispherical, blunt) in [124]. It is proved that the coupled method can reduce the time-consuming compared single SPH modeling, as well as using the advantages of both FEM and SPH, but the implementation seems complex.

On the other hand, various contact algorithms are developed for calculating the contact interactions between SPH particles and FEM elements on the interfaces of FE-SPH domains. A contact algorithm based on a contact potential to link the SPH codes and FEM solver in DYNA3D (developed at Lawrence Livermore National Laboratories) is proposed in [125]. In this algorithm, FE nodes were treated as particles, then a particle to particle contact approach was applied, allowing frictionless sliding between FE and particles.

The authors validated this FE-SPH coupled method by the simulations for three different impact problems: a plate impact, water impact, and rod penetration. The case of an ogive–nose high strength steel projectile impacting an aluminum plate under an angle of 30° was simulated, illustrating interesting results. As another example, an SPH–FEM coupling algorithm also was developed by Zhang et al. [126], which adopts background particles in the position of FE nodes, considering the attachment and contact between SPH particles and finite elements. The perforation of a cylindrical Arne tool steel projectile impacting a plate Weldox 460 E steel target was simulated in 3D at a series of impact velocities. The coupled computational model of viscoplasticity and ductile damage, combined with Gruneisen EOS was used for the target plate. Considering the comparatively small deformation that happened in the projectile, an elastic material model was used for the projectile material. All the simulation results were agreed with experiments with acceptable accuracy in terms of ballistic limit velocity. Besides, the numerical results of coupling the SPH–FEM method demonstrated higher spatial accuracy and efficiency than that of SPH only and LS-DYNA. What is worthy to notice that the plastic deformation of the projectile may become severe with higher impact velocity, and this absorbs a lot of the initial kinetic energy. More suitable constitutive models should be chosen for the projectile material with a higher velocity impact, as proposed in [126].

The benefits of the coupled FE-SPH method applied to impact problems are obviously recognized. Numbers of simulations have been implemented in this way such as [127, 121, 128, 129]. A hybrid method composed of FE analysis and SPH is used to analyze the perforation of steel material and aluminum plates with varying thickness by different projectiles in [121]. However, the authors claimed that at a lower range of impact velocities, failure behavior in a thin target was not observed correctly mainly due to the tensile instability problem inherent in the SPH method. FE solutions are in better agreement and may be adopted for this range of impact velocities. Zhang and co-workers applied a FEM-SPH-FEM technique in LS-DYNA combined with fragment identification and statistics methods to investigate the debris cloud in HVI [128]. The case of d=9.52 mm sphere impact plate with 2.2mm thickness at 6640m/s was simulated in this study. The quantity, the size, the mass, and the velocity of a specific fragment were computed and investigated with these statistics on the binary graph, obtaining good simulation results. A coupled SPH-FE model is also used to simulate a metal-jet penetration into a double hull made of different materials – steel and SPS (Sandwich Plate System) in [129]. The

shaped charge was modeled with SPH and the double-hull structure was modeled with FEM; A penalty method was used to treat the interaction between metal-jet particles and target elements during the entire process. The simulation results were compared with experiments and analyzed to acquire a better understanding of the process of a metal-jet penetration into a double-hull structure. More applications of coupled FE-SPH simulations for HVI problems can be found in the appendix table.

2.5/ MECHANICAL CHARACTERIZATION OF SOFT MATERIALS UNDER IMPACT

A considerable advance on the application of SPH simulating HVIs problems on thin structures has been achieved in the past decades. The research to investigate the behavior of soft materials or bio-materials under impact loading is also paid more and more attention because of the requirements and developments in the fields such as protections on wound ballistics, traumatic injuries, and some pharmaceutical techniques [130, 131].

Fig.2.12 is a typical result of soft materials penetrated by the projectile with high velocity. The obvious difference between the biomaterials and metallic materials as an impact target is that the soft and large elastic properties of biomaterials can lead to a deep penetration and a temporary cavity phenomenon in the target materials. The hydrodynamic process involving the extreme deformations and the behavior like fluid is also characterized in biomaterials under impacts in the literature like [132, 133, 57].

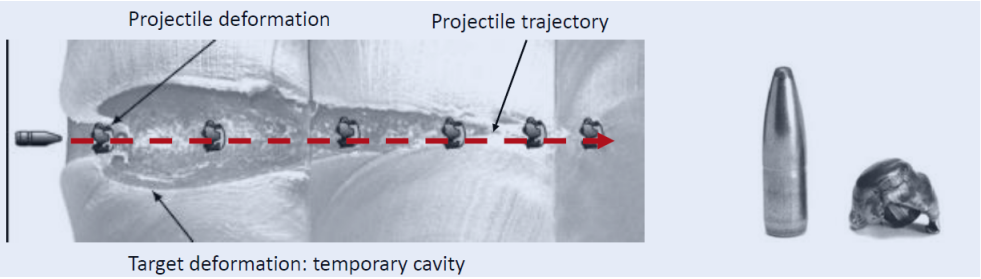

Figure 2.12: The process of a bullet penetrating into soft tissue observed by the experiment [134].

2.5.1/ BALLISTIC PENETRATIONS IN THE MACRO-SCALE

2.5.1.1/ BALLISTIC EXPERIMENTS AND SOFT MATERIALS

Numerous research, particularly the experiments, can be found to investigate these similar behaviors of Fig.2.12 for human parts and organs under dynamic loading and impacted by bullets [135, 136]. The experiments on some live tissues were carried out to observe and understand the ballistic wounds and their bio-mechanical properties. For instance, organs and tissues from fresh human cadavers have been used [137, 138], and some animals including horses, cattle, goats, sheep, dogs, and pigs also have been used extensively to conduct trauma studies [139]. However, they are being less used today because of the serious ethical issues [140].

Some soft materials as biofidelic human tissue simulants are developed in recent years such as epoxy resin [141], synthetic gel [142] or ballistic gelatin [143, 144]. Particularly, ballistic gelatin has been regarded as one of the most important simulants as real biological tissues. Gelatin blocks are prepared by dissolving the calibrated amount of usually 250A bloom gelatin powder into warm water, possibly adding preservative and pouring the solution into molds where it first cools off and then solidifies. It was firstly used in the ballistic experiment in [145] and was found that similar penetration depths were produced in gelatin compared to those measured in soft tissue. At present, two common gelatin formulations (10% and 20% Ballistic Gelatin) are employed in many experiments to understand the behaviors of soft tissues such as [146, 147, 148, 149], which proved that the gelatin simulated close enough soft tissues by comparing the behaviors between gelatin and porcine or chicken meats by experimental tests.

In order to observe the ballistic behavior of gelatin for the understanding of the live tissues, various tests have been carried out to characterize its mechanical properties. Compression tests at different loadings and strain rates up to $1/s$ using a Polymer Split Hopkinson Pressure Bar (PSHPB) have been conducted by Cronin et al. [150, 151]. The mechanical properties of 10% ballistic gelatin were calibrated using a compression test apparatus with temperature-controlled platens to maintain the sample temperature at a fixed level. Penetration testing was carried out using a standard impact test to assess the effect of aging. The primary conclusion of this study was to show the importance of temperature and aging time to achieve a suitable and consistent response from ballistic gelatin. The

material properties were estimated using the stress at failure, strain at failure, and material stiffness as characterized by the Neo-Hookean constitutive model. Further research was predicted by authors that a strain-rate dependence and a hyperelastic behavior law should be developed for gelatin material. Ravikumar et.al conducted mechanical compression experiments on gelatin specimens at strain rates spanning two orders of magnitude (0.001-0.1s^{-1}) and observed a nonlinear load-displacement history and strong strain rate-dependence [152].

Therefore, the mechanical responses of ballistic gelatin are quite different associated with the loading speeds and impact conditions. While the quasi-static and low-velocity behavior (less than 30 m/s) can be described through some hyperelastic models [153, 152]. As far, the hyperelastic Mooney-Rivlin model is regarded as the most promising constitutive law for the gelatin deformations [154, 155]. In the study of [155], the wave propagation behavior in ballistic gelatin was investigated by imparting an impulse motion into a long cylindrical gelatin specimen and then capturing the transient deformation using a high-speed digital camera. The high strain rate behavior of gelatin was considered in the experiments using a polymer split Hopkinson pressure bar (PSHPB). The hyperelastic Mooney-Rivlin model was employed to analyze the responses of gelatin. Kwon and Subhash investigated the mechanical behavior of ballistic gelatin under quasi-static and dynamic compressive loading [156]. The dramatic increase in the strength of gelatin at high rates was discovered in these experiments. The compressive strength increased from 3kPa at a strain rate of around 0.0013/s to 6MPa at a strain rate of around 3200/s. This phenomenon was discussed and a conclusion that ballistic gelatin is highly sensitive to the strain rate was provided in this study. According to the literature [157, 2], the ballistic gelatin behaviors under high-velocity loading also should be described through hydrodynamic theory, as explained for Fig.2.12. Therefore, the mechanical process of penetrating soft materials is complex and not easy to be understood only by experimental observations.

Gelatin has been widely used in experiments and numerical simulations to understand the ballistic response of soft tissues. At the same time, new homogeneous synthetic simulants are also being developed in order to avoid the instabilities of material properties of gelatin caused by the environments and aging [158]. Some alternative tissue simulants like Perma-Gel, Associ-ating Gelatine's (PAG), or transparent gel candleis (a clear syn-

thetic medium) can be found in the literature [159, 160, 158]. Particularly, the synthetic polymer SEBS gel (styrene-ethylene-butylene-styrene) has been recognized its practical advantages recently as a sutiable simulant. According to the experimental observations in [161, 142, 162], synthetic SEBS gel involves environmental stability, reproducibility, mechanical consistency, and transparency. In the study of Mrozek et al. (2015) [161], the authors investigated the mechanical properties of SEBS gels by using tensile, compression, and rheological tests. The conclusions of this study were that the projectile penetration during SEBS gel impacts could be accurately described using mechanical properties like modulus and toughness measured in the quasi-statics strain rate regime. The group of Bracq et al. highlights the development of constitutive modeling for the synthetic polymer SEBS gel. According to their experimental studies like tensile and compressive tests at diverse strain rates [142, 162], a novel strain-rate-dependent hyper-viscoelastic law for the SEBS gel was developed first. This constitutive law was validated by implementing it in a FEM model and acquired an agreement with experimental data. In recent work by Shen et al. (2020) [132], an elastohydrodynamic constitutive law of SEBS gel combined with the effect of the strain rate was also proposed. The related experiments were conducted with both targets and projectiles of several centimeters dimension. This research demonstrates that the elasticity of SEBS gel material is non-linear and depending on the strain rate. Actually, the synthetic polymer SEBS gel is paid not enough attention at present. Considering it involves the similar mechanical properties with ballistic gelatin but better practical performances, this thesis will provide an investigation for this material in following chapter.

2.5.1.2/ ANALYTICAL INVESTIGATIONS

In the field of penetrations in soft tissues, the factors to be investigated include the various material properties, the trajectory of the projectile, the pressure wave in the soft material, the temporary and permanent cavities, as well as the yawing, tumbling and fragmenting depending on the states of projectiles. Fig.2.13 shows a general flow about this. The experiments can provide the most direct observations for the penetrating process like Fig.2.12 involving the trajectory, time history of cavity size etc.

Analytical models are developed by the mathematical formulations incorporating some essential and relevant physical and mechanical theories and parameters. The various

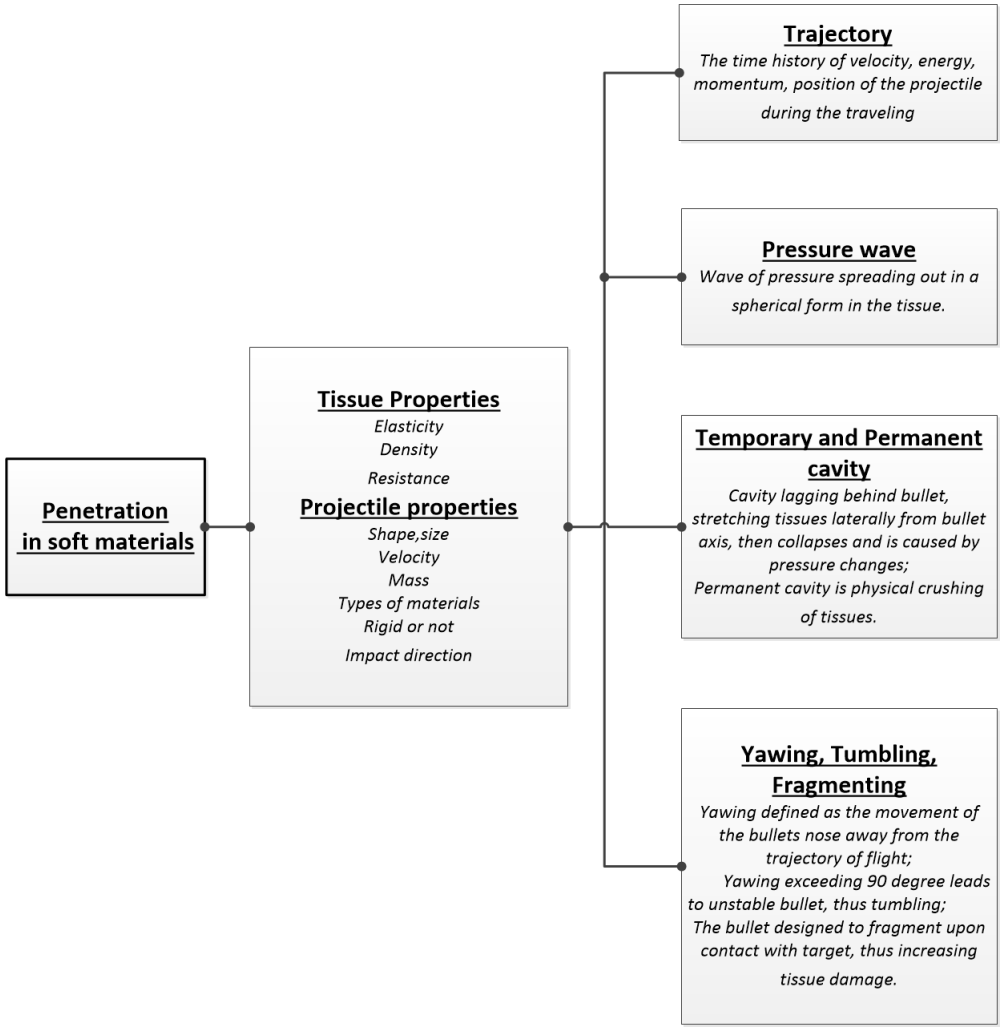

Figure 2.13: The process of a bullet penetrating into soft tissue observed by the experiment [134].

models that describe the behavior of a spherical fragment penetrating soft materials have been developed and employed in the literature such as [163, 164, 165, 166, 57]. The Poncelet model is still the most widely used to model the projectile trajectories as a validation to some experiments [166, 167]. In the Poncelet equation, the retardation force of the projectile during the impact into soft materials consists of a constant strength term C and a term proportional to the square of the instant penetration velocity BV^2, where the strength resistance R, related to the apparent yield stress σ_t, is a material-specific constant. This analytical model was initially validated by Sturdivan's experiments in 1978 [163] for a 20wt% gelatin target. In 2014, Liu et al. developed another analytical model involving the dependent-strain-rate resistance and a viscous term to investigate the trajectory of a projectile in 20 wt % gelatin [168]. Based on a general penetration model

composing of an inertia component, a viscous component and the natural strength component of the target material proposed by Allen et al.[169], a new motion model of rifle bullet was established in the penetration of gelatin by S.Liu et al. [170]. The change of the effective wetted area of the bullet was studied well with the increase of angle of yaw in the penetration process. By introducing an area detached ratio and the influence of slenderness, drag and lift coefficients were deducted for a new motion model. The penetration depth, deflection path, yaw angle, velocity, lift force and drag force at different initial conditions are calculated by this model.

Except for modeling the trajectory of the projectile in the penetration by analytical formulations, some research also develop the analytical model to study the cavity phenomenon caused by the deformation of target materials like [171]. Liu proposed a quasi-static expansion model of spherical cavity in the 10 wt% ballistic gelatin via modeling the large elastic deformation by the Mooney-Rivlin constitutive equation and the failure behavior by elastic-fracture [171]. The maximum cavity volumes in 10 wt% ballistic gelatin penetrated by fragments of various shapes and a bullet were observed by this model. Fig.2.14 shows the shapes of cavities during the penetrations by different projectiles and impact velocities analyzed by the model in [171]. The research investigated the cavity expansion in the soft material called Polyvinyl Alcohol Hydrogels by elastic solution and experiments in [172]. In 2018, by combination with parameters obtained from the motion model of rifle bullet in [170], cavity dynamics in gelatin was studied and a motion model of temporary cavity in gelatin penetrations of rifle bullets was proposed by Liu et al.[173]. The maximum cavity wall radius, radial movement along the penetration trajectory and temporary cavity profiles were investigated by this analytical model. It is significant for the trauma assessment to develop an appropriate cavitation model in gelatin for penetrations of rifle bullet.

2.5.1.3/ NUMERICAL INVESTIGATIONS

Numerical simulations are developed to investigate the penetration process that happened in soft materials or some simulants of soft tissues in recent years. At an earlier time, An et al. [174] performed a series of simulations for the evolution of a temporary cavity and the pressure in a body of water under high-velocity impacts by a rigid sphere using the commercial finite element (FE) software LS-DYNA. The commercial software AUTODYN was employed to simulate the behaviors of ballistic soap impacted by steel spheres

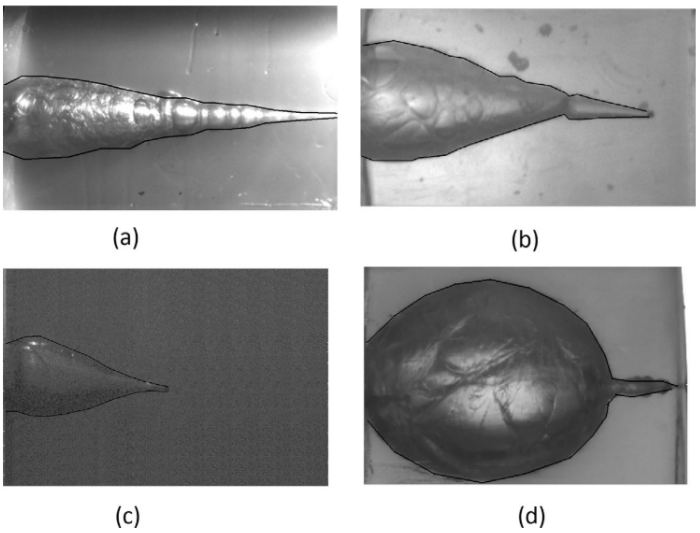

Figure 2.14: The shapes the temporary cavity caused by (a) steel sphere of 0.45 g (856 m/s); (b) steel cylinder of 0.9 g (1032 m/s); (c) steel rhombus of 0.25 g (651 m/s) and (d) bullet of 4.15 g (738 m/s). The black lines in the figure are used to calculate the cavity volume. where[171].

[175], and also to study deformations induced by the penetrations of ABS (Acrylonitrile-Butadiene-Styrene) plastic spheres into gelatin at velocities up to 160 m/s [176].

In the investigation of ballistic responses in the soft tissues, the simulations are carried out predominately based on the gelatin and validated also by existing experiments related to gelatin blocks such as [177, 176, 178, 179]. Most of these simulations were performed by the numerical methods based on meshing. Minisi et al. [177] simulated the projectile-gelatin interaction at high impact velocities with the 10% gelatin modeled as a hydrodynamic material with the Mie-Grüneisen equation of state at high strain rates and a Mooney-Rivlin material at lows train rates. Worthy to be noticed, a study in 2013 by Wen et al.[178] successfully simulated the trajectory of projectiles, the time history of the temporary cavity, and the pressure in the 10% gelatin by LS-DYNA software with finite element method. The authors studied experimentally and computationally the penetrations of a steel sphere into ballistic gelatin at a moderately high speed (up to 1630 m/s). They modeled the gelatin materials using an isotropic and homogeneous elastic-plastic constitutive law combined with a polynomial equation of state, which provided good results compared with experiments. The same research group also performed the simulations using FE method to study the penetration of a rifle bullet into a block of ballistic gelatin [180]. The effect of the angle of attack of the rifle bullet for

the penetration process were highlighted in these simulations. Fig.2.15 shows the FEM model for this soft penetration by Wen et al. in [178, 180].

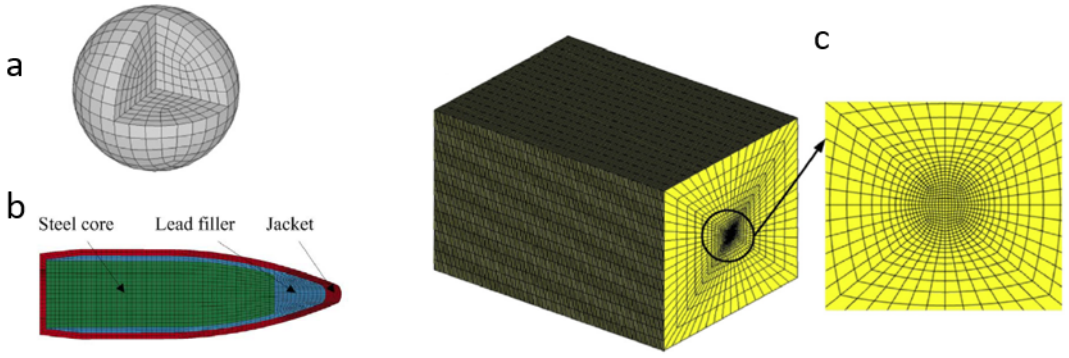

Figure 2.15: (a) is the sphere projectile in [178]; (b) is the rifle bullet projectile in [180]. (c) is the FE model for gelatin block in both of [178] and [180].

Also, in 2014, a FE model was developed to investigate the ballistic behavior of 20% gelatin under high-velocity impacts [179]. The gelatin was modeled using an elasto-plastic hydrodynamic constitutive law, similar to the one used in the study of Wen et al.[178]. A series of simulations were performed by this model for the penetrations involving different sphere projectiles of (2.38, 4.76, 6.3 mm diameters) impacting with a large range of velocities from 230 to 2229 m/s. The penetrating histories were simulated and validated by experimental and analytical results. Zhang et al. [181] also used a FEM model to investigate the process of a 56-type 7.62-mm rifle bullet penetrating the gelatin-bone composite target. In recent, Chen et al. [182] developed an adaptive finite element material point method (AFEMP) that includes the advantages of both the finite element method (FEM) and the material point method (MPM) to model the penetrations into ballistic gelatin. By the comparisons with the experimental results, the accuracy of the AFEMP program was verified, and the temporary cavity phenomenon in the gelatin target can be better described than the finite element method according to this study.

Although the numerical methods based on meshing techniques have been used to simulate the penetrations in the soft materials by a few research, the mesh distortion problem is still risque and requires extra work when simulating the extremely large deformations that happened in the deep penetrations. As introduced previously, the particle numerical

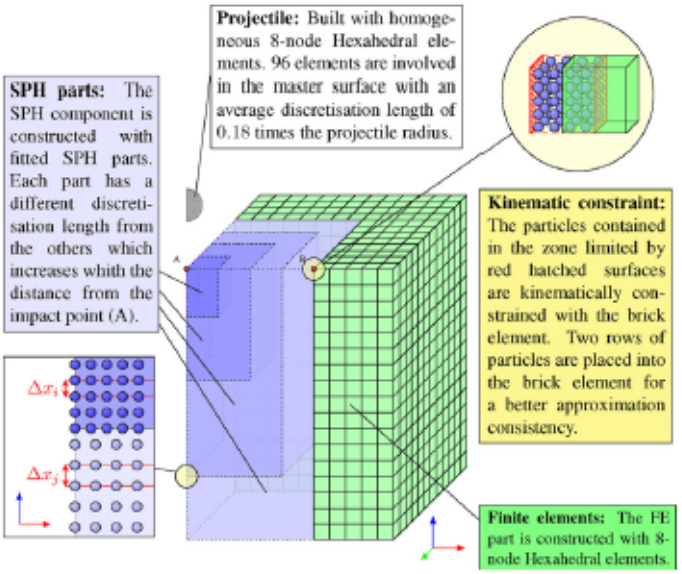

Figure 2.16: The SPH model combined with FE elements for soft penetration in [133].

methods like the SPH method is more suitable to simulate this kind of problems. The previous review on the advance of HVIs on thin structures simulated by the SPH method proves this point. However, for the soft penetrations that happened in the thick structure, there is less research on the applications of particle methods.

In 2015, Taddei et al. [133] developed an original numerical model combined SPH particles and FE elements by software HyperWorks with Radioss to investigate the ballistic response of 20% gelatin under high-velocity impacts. The configuration of this model is shown in Fig.2.16, in which the domain of impact center is discretized by SPH particles and the far domain is by elements. This SPH model simulated a series of penetrations in the gelatin impacted by rigid projectiles and achieved a good agreement with experimental observations. Then, this numerical model was used to simulate the penetrations into 10% gelatin under high-velocity impacts [57]. In this study, the multi-layered gelatin was the target block impacted by a rigid sphere, which was also stimulated by this numerical model. A good agreement was obtained between SPH simulation and analytical results. Frissane et.al developed an axisymmetrical SPH code to simulate the penetration process into gelatin [58]. The same penetration cases with the study of [133] were simulated by this code and a better accuracy between the numerical and experimental results was achieved.

Compared with the wide usage of the SPH method in simulating perforation on thin structures, there are only a few studies on the application of the SPH method to simulate the deep penetrations into soft materials in the literature. To the author's knowledge, except for ballistic gelatin, there is almost no numerical investigation of another simulant of soft tissues called polymer gels under high-velocity impacts. Therefore, expanding the application of the SPH method to the investigations on deep penetrations is an interesting and original work.

2.5.2/ BALLISTIC PENETRATIONS IN THE MICRO-SCALE

To understand the penetration process in the soft materials is significant work, which has been paid attention via experimental, analytical, and various numerical methods. However, most of them are investigated under the macro-scale. During the past few years, interest in the development of transdermal delivery technologies of pharmaceuticals has been renewed by the promise of needle-free drug delivery via penetration of high-speed drug-carrying projectiles into the viable epidermis and dermis [183, 184]. This kind of technique involves a similar penetration process that happened in the soft tissues but in the micro-scale. The sizes of the transdermal powders are on the μm-scale or smaller. The physical process and mechanical behavior show completely different properties when the penetrations transmit from the macro-scale to the micro-scale. This trend has been validated in the observations via several experiments and analyses [185, 167].

In terms of the experiments, the investigation of the deformation of soft materials in extreme dynamic environments is achieved by a novel laser-induced particle impact platform (LIPIT) in recent years, which was developed by a research group including J.-H. Lee and D. Veysset et al. [186, 187, 188, 189, 2]. In the LIPIT platform shown in 2.17, an intense short laser pulse is used to accelerate microparticles to supersonic velocities, and individual particle impact events are observed with a high-frame-rate camera. It can capture real-time in-situ visualization of the deformation response with high accuracy. Fig.1.2 is one of the results obtained by this experimental technique, which provided an observation of the response and deformation of ballistic SEBS gel with various concentrations (10vol%,20vol%,30vol% and 30vol%) [2]. Veysset et.al. used this experimental platform to investigate the ballistic behaviors of gelatin and elastomers under high-velocity impacts in [167]. The authors conducted a considerable increase of resistance in the target ma-

terials in the micro-scale penetrations via combining with the analytical model. Thanks to these experimental observations, the performance of soft materials under micro-impact loading can be observed and evaluated, but the quantified mechanical properties are still required to be further researched.

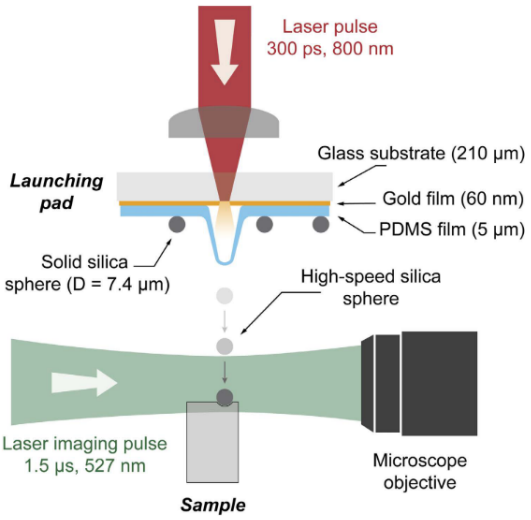

Figure 2.17: Particle launch and imaging configuration in the LIPIT platform provided in [188].

Numerical simulation is an efficient alternative to investigate the complex physical problem of high-velocity microparticle penetration in soft tissue, and very few work seems to exist in the literature on this specific point. Among those works, Guha and Shear in [190] developed a finite element model of the impact and penetration of a 2 m gold particle into the human dermis. They validated this numerical model with macro-scale steel ball-gelatin system by using a dimensional analysis and then investigated the performance of transdermal power injection technology. They found an elastic modulus of 2.25 MPa for skin stimulants, which is one of the key material parameters for impact in soft tissue studies. However, this model is based on a scaled-up system, which means the numerical computation is not directly used on the micro-scale structure.

As the author's knowledge, there is no more study to investigate the penetrations of soft materials in the micro-scale by the simulation approaches. The main limits in simulating such phenomena research lie in two points: one is the complex properties of soft tissues, which are still under the developments. As known for several simulants of the soft tissues such gelatin and SEBS gel, their mechanical properties involve hyper-elasticity,

viscous-elasticity, the high sensitivity to the strain rate, as well as high depending on the loading types. What's more, when the deformation of the soft materials happens in the micro-scale, the mechanical behavior becomes more questionable; The other is that the large deformations under quick and extreme impact loading make the simulation methods based on the meshing techniques no longer sufficient. The micro-scale condition also requires some specific treatments from the numerical models. Taking into account the successful attempts of the SPH method to model the deep penetrations in the gelatin materials [133, 58], this thesis provides an original investigation about the ballistic behaviors of soft materials under micro impact loading by developing the numerical model using the SPH method. Two different simulant materials involving 10% gelatin and 40 vol % SEBS gel are simulated as the target materials and their mechanical properties under micro impacts are observed and discussed.

2.6/ CONCLUSION

This chapter reviews the developments of SPH method and its application in the field of HVIs problems. Although SPH method is known to involve some numerical drawbacks like numerical instabilities, boundary inaccuracy, and time-consuming, particularly in solid impact problems, a state of the art in this chapter witnessed the great success of the SPH method applied to diverse impact problems, mainly showing as:

1. As far, different versions of SPH formulations have been developed to improve the comprehensive performance of SPH simulations, like CSPM, Godunov SPH, total Lagrangian SPH, and pseudo-springs SPH, etc. Besides, most of them have been applied to impact problems.

2. The SPH formulation involves great compatibility with other different algorithms and then is developed to some coupled numerical methods like Gamma-SPH, FE-SPH, γ-SPH-ALE, etc.

3. The most of fragmentation and debris clouds phenomenons in HVIs on thin structures are predicted well by the SPH method thanks to its natural particle property.

4. The application of the SPH method has been extended to a diversity of HVI problems, not limited to metallic projectile-target systems. It comes from the develop-

ments of constitutive laws for different materials, and also the good compatibility of SPH schemes.

During the literature review, a trend is found that the target materials in impact systems at present demonstrates a large variety on types of materials such as various composite laminates, brittle materials like ceramics, advanced high-strength cementitious materials, as well as multilayered structures consisting of completely different materials except for the metallic materials. Moreover, the SPH method has also been extended to simulate the ballistic response of soft tissue materials in recent years like [57, 58], particularly, to the bird-strick problem involving the SPH modeling of birds body [191, 192, 193]. This trend can be foretold with the high requirements of the modern industry. Therefore, to investigate the HVIs by SPH method in further work still should pay many effects like,

1. Tensile instability is still an important factor to affect the simulation accuracy. Although lots of improvements have been developed, the performance of them still depends on the impact conditions like low or high impact velocity, the types of materials. Total Lagrangian SPH seems a comparatively stable scheme, but it needs more applications to different HVI systems to validate its performance.

2. The behavior of crack propagation as one of the most important damages during impacts, very depends on the types of materials and target structures, particularly for some multilayered structures or laminated composites. There is no much simulation in this situation. To the best of the authors ' knowledge, Pseudo-spring SPH seems the most promising scheme for this.

3. The investigations to fragmentation and debris clouds during HVIs are still on the qualitative analysis. The quantitative analysis is necessary, but it is a challenging work for SPH application.

4. The other important further work is HVIs problems happened in the soft tissues. Developing the SPH model with material constitutive law to investigate the responses of soft tissues, esoterically in the micro-scale, is a interesting work. This study is also the main contribution of this thesis.

To sum up, the strong capability of the SPH simulating high-speed velocity impacts has been witnessed in the literature reading. The study to the ballistic behaviors of soft tissues

under micro-impacts is an significant work, but no much simulating investigations. Therefore, this thesis focuses on the application of the SPH method modeling the penetrating process in the soft materials such as gelatin and polymer gels in the micro-scale.

3

THEORETICAL POINTS: DEVELOPMENT OF A SPH CODE TO DYNAMIC SOLIDS

3.1/ INTRODUCTION

By reviewing the application of the SPH method in the literature, it can be seen that the SPH has become one of most important simulation approaches in solid dynamics because of its great potentials in simulating extremely large deformations. In terms of the essence of the SPH, it uses a kernel function for numerical approximations. Some literature demonstrate mathematically that the types of the kernel function directly influence the stability and overall accuracy of SPH simulation. However, less attention is paid to the influences derived from kernels particularly on simulating dynamic solids problems by SPH. In addition, some research introduce that there are strong relations between SPH kernels and tensile instability which is one of shortcomings in SPH method, a kind of particles clumping phenomenon probably leading to some nonphysical cracks when the solid material is largely stretched or compressed. At present, no method exists to completely avoid these instabilities, although a few corrections like Artificial Viscosity, Artificial Stress, Corrective SPH (CSPH) or the Godunov-type SPH have been proposed. Therefore, the objective in this chapter is that the performances of SPH method with different kernels is studied, including classical types and several new ones proposed recently. Combined with some corrected techniques,a 2D SPH code is developed and introduced in this chapter, and the suitability of these kernels in SPH method is discussed in solid dynamic problems like bending deformation of elastic beam and some tests about elastic-plastic deformation in impact problems. The structure of this chapter is organized by:

1. Introduce the role of kernel function in SPH algorithm, involving the relations between the different types of kernel function and numerical instability and accuracy.

2. The formulation of Corrective SPH method (SPM) is represented, which is a technique to correct the calculation of kernel function and also is implemented in the SPH code.

3. The procedure of implementation the SPH code for solids is introduced.

4. The validation to the SPH code is carried out by numerical examples like bending deformation of elastic beam and elastic-plastic deformation in rod impacts.

5. The discussion to the numerical results and different performances of different types of kernel function in solid problems.

3.2/ THE ROLE OF KERNEL FUNCTION

3.2.1/ THE TYPES OF KERNEL FUNCTION

At present, series of B-spline functions are classical and traditional SPH kernels in most applications [194, 195], for examples cubic spline and quintic functions shown in Fig.3.1. It also lists several existing SPH kernels, like the Gaussian function, Wendland fucntion and some new types (Double cosine function and Hyperbolic shaped). Fig.3.2 shows the shapes of these six kernel functions and their derivatives. Gingold and Monaghan in their original paper [8] firstly used the Gaussian function as a SPH kernel because it is sufficiently smooth even for high orders of derivatives. However, the Gaussian function doesn't exactly satisfy the compactness condition, as it never goes to zero theoretically with the variable $|r|$ increasing. As a study by Liu and his co-workers in [196], the kernel function in SPH algorithm can be built systematically. For instance, type-5 kernel in Fig.3.1 is constructed based on the $cosine$ functions which is characterized by having enough smoothness in any order of derivatives, thereby a better accuracy can be acquired as SPH kernel [197]. In addition, a hyperbolic shaped kernel function (type-6 kernel in Fig.3.1) is also constructed and used in the SPH formulas to simulate viscous liquid drop problems in [198]. This function possesses non-negative second derivatives which is regarded to remove the pairing instability in compressive regimes.

Index	Name of Kernel	Function (α^d is the dimension-dependent)
Type-1	Cubic spline [19]	$W(r,h)=\alpha^d\begin{cases}1-\frac{3}{2}q^2+\frac{3}{4}q^3 & q<1\\ (2-q)^3/4 & 1\le q<2\end{cases}$ Or $W(r,h)=\alpha^d\left((1-q)^3-4(\frac{1}{2}-q)^3\right)\quad 0<q\le 1$
Type-2	Gauss [19]	$W(r,h)=\alpha^d e^{-q^2}\quad 0<q\le 3$
Type-3	Quintic [19]	$W(r,h)=\alpha^d\begin{cases}(3-q)^5-6(2-q)^5+15(1-q)^5 & q<1\\ (3-q)^5-6(2-q)^5 & 1\le q<2\\ (3-q)^5 & 2\le q\le 3\end{cases}$ Or $W(r,h)=\alpha^d\left((1-q)^5-6(\frac{2}{3}-q)^5+15(\frac{1}{3}-q)^5\right)\quad 0<q\le 1$
Type-4	Wendland [32]	$W(r,h)=\alpha^d(1-\frac{1}{2}q)^4(2q+1)\quad 0\le q<2$ Or $W(r,h)=\alpha^d(1-q)^4(1+4q)\quad 0<q\le 1$
Type-5	Double cosine [34]	$W(r,h)=\alpha^d\left(4\cos(\frac{\pi}{k}q)+\cos(\frac{2\pi}{k}q)+3\right)\quad 0<q\le k$
Type-6	Hyperbolic shaped [33]	$W(r,h)=\alpha^d\begin{cases}q^3-6q+6 & 0<q\le 1\\ (2-q)^3 & 1<q\le 2\end{cases}$

Figure 3.1: A list for six types of SPH kernels.

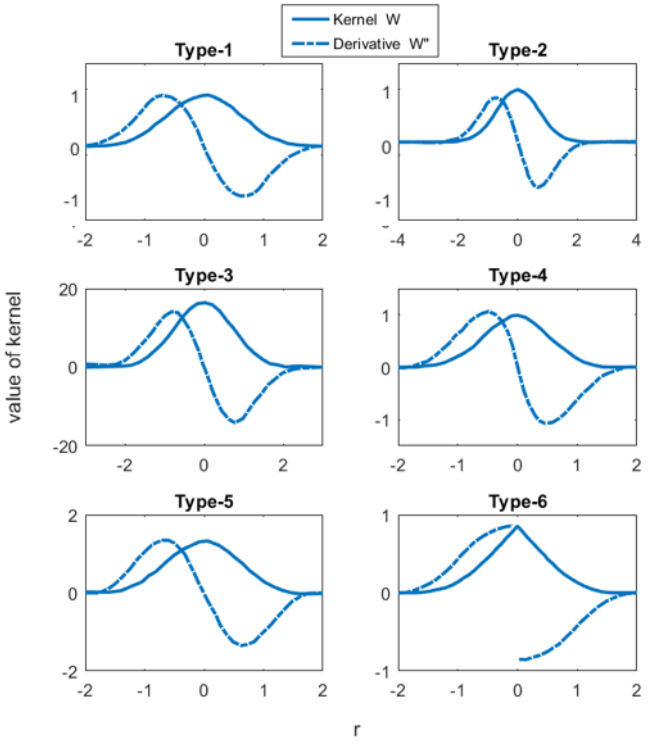

Figure 3.2: The shapes of kernel functions and their derivatives.

3.2.2/ NUMERICAL INSTABILITY VIA KERNEL TYPES

Although SPH has been applied to different engineering problems, it still suffers some drawbacks like inconsistency on the boundary, zero-mode problems, and various numerical instabilities. Particularly, in solid dynamics with large deformations, the numerical instabilities involving tensile instability and pairing instability are considerable problems that can lead to nonphysical fractures.

As a classical research discussing the numerical instability when applied SPH method in solids, Swegle [199] proposed an unstable growth condition by analyzing the particles clumping phenomenon in stretched material (so called tensile instability or pairing instability) when using B-spline kernel in SPH algorithm. This condition can be written as following,

$$W^{"}T \geq 0 \tag{3.1}$$

where, $W^{"}$ is the second derivative of the kernel W and T is stress state, which is negative in compression and positive in tension. This condition means that the instability of SPH algorithm depends on the sign of the product of the total stress and the second derivative of the kernel function. Fig.3.3 shows the the regions of stability and instability of a cubic B-spline kernel.

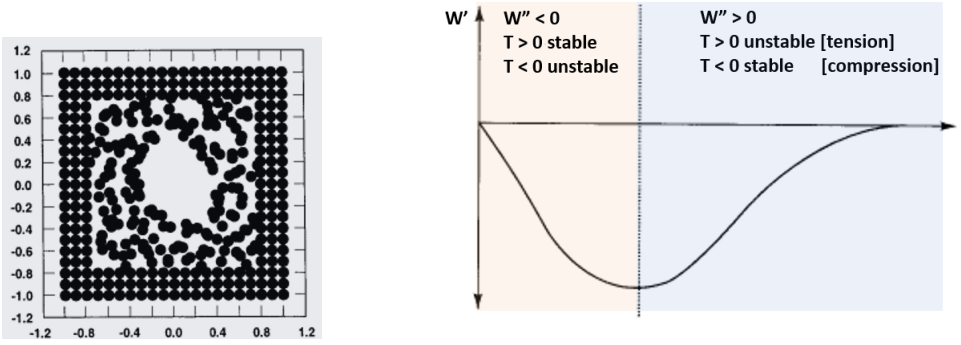

Figure 3.3: The stability analysis from the research of Swegle et.al [199]: (a) The particle clumping phenomena in the SPH simulation. (b) The regions of instability and stability of a cubic B-spline kernel.

In 2012, Dehnen in [200] discovered that the Wendland kernels have the similar shapes for derivatives with traditional B-spline kernels, but without providing pairing instability even with a large number of neighbour particles. By linear stability analysis, they concluded that non-negativity of the Fourier transform of SPH kernel functions is a necessary

condition for stability against particles pairing, which is a different insight with Swegle's analysis. Besides, they proved theoretically that Wendland kernel has this property and can keep stable in all the numbers of neighbour particles.

Thanks to these analyses, the influences from kernel types are paid attentions in research how to decrease the instability in SPH applications. Yang in [198] proposed the new types of kernels (type-6 kernel in Fig.3.1) in order to remove the tensile instability and proved these ones can achieve more stable simulations in flow problems, but for solid dynamic problems where exists more severe particles disordering, there is no much particularly practical investigation from the view on kernels.

3.2.3/ THE ACCURACY VIA KERNEL TYPES

It is difficult to estimate the numerical errors of SPH algorithm just from kernels properties, since the algorithm accuracy depends on a number of factors, and also is influenced by the types of problems. Sigalotti (2019) in [201] developed a general error analysis to simultaneous treatment of both the kernel and particle approximation errors for arbitrary particle distributions. This error analysis using the Poisson summation formula can achieve a functional dependence of the error bounds on SPH interpolation parameters, like the types of kernels, smoothing length h, and the number of neighbours. A term A_w is derived in this research as an estimate which involves the parameters from particular kernels as following,

$$A_w^n = \frac{2^n \alpha_d B_n k^n}{n} \tag{3.2}$$

in which, α_d and k, respectively, is the dimension-dependent constant like Fig.3.1 and scale factor of smoothing length. n is the dimension and $B_n = 2\pi^{n/2}/\Gamma(n/2)$, in which Γ is the Gamma function. According to Di G.Sigalotti, a bigger value of A_w means a lower accuracy in SPH particle approximation. They also validated this estimate means by discretizing a simple analytical problem and deducted that Lucy's kernel is a better choice in 2D whereas Wendland C2 is the better one in 3D problems.

Tab.3.1 shows the values of A_w for 4 different kernel functions from Fig.3.1. The values of A_w from type-4 kernel is the smallest, which implies that it is able to obtain a better accuracy in SPH particle approximation. The satisfied accuracy in particle approximation which is the major step in SPH formulation can ensure a good simulating result.

Table 3.1: Numerical values of A_w

types of kernels	a_α 2D	a_α 3D	k	2D	3D
type-1	$80/(7\pi)$	$16/\pi$	1	45.7	170
type-2	$1/\pi$	$1/\pi^{3/2}$	3	36	162.7
type-3	$3^7 \cdot 7/(478\pi)$	$3^7/(40\pi)$	1	128.1	583.2
type-4	$7/\pi$	$21/(2\pi)$	1	28	112

Both Sigolotti's errors estimation and Walter Dehnen's instability analysis show that Wendland function seems a promising alternative as SPH kernel, but it is not often used in some practical simulations. This chapter is intended to highlight how these kinds of kernels in list of Fig.3.1 influence the instability and accuracy and look for the most suitable kernel when SPH simulating solid dynamics.

3.2.4/ CORRECTIVE KERNEL PROCESS

Based on the formulation of Standard SPH, corrective SPH (CSPH) proposed by Chen in [26, 44] is implemented in this code. The idea of this corrective method is to transfer the kernel estimate concept to the Taylor series expansion, which has been proved that this transposition is very effective addressing tensile instability. Besides, it also helps to improve boundary deficiency problems which is an another major obstacle for the standard SPH.

Here, the formulation of CSPH is represented in 2D directly. The Taylor series expansion for a 2D function is employed and it is cut after the linear element.

$$f(x', y') = f(x_i, y_i) + (x' - x_i)\frac{\partial f}{\partial x}|(x_i, y_i) + (y' - y_i)\frac{\partial f}{\partial y}|(x_i, y_i) \tag{3.3}$$

based on above format, the expansion is multiplied by $\frac{\partial}{\partial x}W$, $\frac{\partial}{\partial y}W$, then integrated over the whole domain,following as,

$$\int \frac{\partial W}{\partial x} f(x', y')dx' = \int \frac{\partial W}{\partial x} f(x_i, y_i)dx + \int (x' - x_i)\frac{\partial W}{\partial x}\frac{\partial f}{\partial x}|(x_i, y_i)dx' + \int (y' - y_i)\frac{\partial W}{\partial x}\frac{\partial f}{\partial y}|(x_i, y_i)dx \tag{3.4}$$

$$\int \frac{\partial W}{\partial y} f(x', y')dx' = \int \frac{\partial W}{\partial y} f(x_i, y_i)dx + \int (x' - x_i)\frac{\partial W}{\partial y}\frac{\partial f}{\partial x}|(x_i, y_i)dx' + \int (y' - y_i)\frac{\partial W}{\partial y}\frac{\partial f}{\partial y}|(x_i, y_i)dx \tag{3.5}$$

Reorganizing these terms,

$$\int \frac{\partial W}{\partial x}(f(x', y') - f(x_i, y_i))dx' = \frac{\partial f}{\partial x}|(x_i, y_i) \int (x' - x_i)\frac{\partial W}{\partial x}dx' + \frac{\partial f}{\partial y}|(x_i, y_i) \int (y' - y_i)\frac{\partial W}{\partial x}dx \tag{3.6}$$

$$\int \frac{\partial W}{\partial y}(f(x', y') - f(x_i, y_i))dx' = \frac{\partial f}{\partial x}|(x_i, y_i) \int (x' - x_i)\frac{\partial W}{\partial y}dx' + \frac{\partial f}{\partial y}|(x_i, y_i) \int (y' - y_i)\frac{\partial W}{\partial y}dx \tag{3.7}$$

Discretizing employing the usual nodal integration,

$$\sum_{j=1}^{N} \frac{\partial W}{\partial x}(f(x_j, y_j) - f(x_i, y_i))\frac{m_j}{\rho_j} = \frac{\partial f}{\partial x}|(x_i, y_i) \sum_{j=1}^{N} (x_j - x_i)\frac{\partial W}{\partial x}\frac{m_j}{\rho_j} + \frac{\partial f}{\partial y}|(x_i, y_i) \sum_{j=1}^{N} (y_j - y_i)\frac{\partial W}{\partial x}\frac{m_j}{\rho_j} \tag{3.8}$$

$$\sum_{j=1}^{N} \frac{\partial W}{\partial y}(f(x_j, y_j) - f(x_i, y_i))\frac{m_j}{\rho_j} = \frac{\partial f}{\partial x}|(x_i, y_i) \sum_{j=1}^{N} (x_j - x_i)\frac{\partial W}{\partial y}\frac{m_j}{\rho_j} + \frac{\partial f}{\partial y}|(x_i, y_i) \sum_{j=1}^{N} (y_j - y_i)\frac{\partial W}{\partial y}\frac{m_j}{\rho_j} \tag{3.9}$$

Writing this in compact matrix form reveals that the CSPM corrector,

$$< \nabla \cdot f(x_i, y_i) >_i = \frac{\left[\sum_{j=1}^{N} (f_j - f_i)\nabla W_{ij}\frac{m_j}{\rho_j}\right]}{B} \tag{3.10}$$

$$B = \left[\sum_{j=1}^{N} (x_j - x_i) \bigotimes \nabla W_{ij}\frac{m_j}{\rho_j}\right] \tag{3.11}$$

3.3/ THE PROCEDURE OF SPH CODE IMPLEMENTATION

This section mainly introduces the programming implementation of a SPH code, which is based on the standard SPH scheme combined with some techniques involving CSPH, artificial viscosity and stress, as well as XSPH.

3.3.1/ THE SPH FORMULATIONS FOR SOLIDS

3.3.1.1/ SPH FORMULATIONS FOR NAVIER-STOKES EQUATIONS

Firstly, the procedure of deriving conversation equations in solids into SPH formulations is presented. In an Eulerian referential, the conversation laws take the following form:

1. Conservation of mass:
$$\frac{D\rho}{Dt} = -\rho\Delta \cdot \vec{v} \tag{3.12}$$

2. Conservation of momentum:
$$\rho\frac{D\vec{v}}{Dt} = -\Delta \cdot \bar{\sigma} \tag{3.13}$$

3. Conservation of energy:
$$\frac{De)}{Dt} = -\frac{\bar{\sigma}}{\rho} : \Delta \otimes \vec{v} \tag{3.14}$$

The density ρ, specific internal energy e, the velocity $\vec{v}$, and the stress tensor component $\bar{\sigma}$ are the function of the spatial coordinates $\vec{x}$ and time t. Here, $\bar{\sigma}$ is the Cauchy stress tensor.

The summation for density can be written by,

$$\rho(\vec{x_i}) = \sum_{j=1}^{N} m_j W(\vec{x_i} - \vec{x_j}, h) \tag{3.15}$$

The above expression is simple and used at the initial development of SPH method, but it is not able to ensure the correct calculation at the free boundary. Therefore, the approximation for the rate of change of density is carried out to instead of Eq.(3.15). To approximate the equation of Conservation of mass (Eq.(3.12)) by using the formulas of SPH discretization processes, Eq.(3.12) can be written as,

$$\int_{\Omega} \frac{D\rho}{Dt} W(\vec{x}-\vec{x'},h)d\Omega = -\int_{\Omega} \rho \frac{\partial \vec{v}}{\partial x'} W(\vec{x}-\vec{x'},h)d\Omega \tag{3.16}$$

According to the formats in chapter 2, the derivative of a vector field $\vec{v}$ can be approximated as,

$$< \frac{\partial \vec{v}}{\partial x'} >= \sum_{j=1}^{N} \frac{m_j}{\rho_j} \vec{v}_j \cdot \frac{\partial W(\vec{x}_i - \vec{x}_j, h)}{\partial x'_i} \tag{3.17}$$

Then, the conservation of mass equation can be discretized by,

$$< \frac{D\rho_i}{Dt} >= \rho_i \sum_{j=1}^{N} \frac{m_j}{\rho_j} (v_i^{\alpha} - v_j^{\alpha}) \frac{\partial W(\vec{x}_i - \vec{x}_j, h)}{\partial x_i^{\alpha}} \tag{3.18}$$

To approximate the equation of Conservation of mass (Eq.(3.13)) by using the formulas of SPH discretization processes, Eq.(3.13) can be written as,

$$\int_{\Omega} \frac{D\vec{v}}{Dt} W(\vec{x}-\vec{x'},h)d\Omega = -\int_{\Omega} \frac{1}{\rho} \frac{\partial \vec{\sigma}}{\partial x'} W(\vec{x}-\vec{x'},h)d\Omega \tag{3.19}$$

The following expression can be obtained to the SPH discritized forms on the equations on conversation of momentum and energy,

$$< \frac{Dv_i^{\alpha}}{Dt} >= -\sum_{j=1}^{N} m_j \left(\frac{\sigma_i^{\alpha\beta}}{\rho_i^2} + \frac{\sigma_j^{\alpha\beta}}{\rho_j^2}\right) \frac{\partial W(\vec{x}_i - \vec{x}_j, h)}{\partial x_i^{\beta}} \tag{3.20}$$

$$\frac{\mathrm{d}e_i^{\alpha}}{\mathrm{d}t} = -\frac{\sigma_i^{\alpha\beta}}{\rho} \frac{\partial v_i^{\alpha}}{\partial x_i^{\beta}} = -\frac{1}{2} \sum_{j=1}^{N} m_j (v_i^{\alpha} - v_j^{\alpha}) \left(\frac{\sigma_i^{\alpha\beta}}{\rho_i^2} + \frac{\sigma_j^{\alpha\beta}}{\rho_j^2}\right) \cdot \frac{\partial W_{ij}}{\partial x_i^{\beta}} \tag{3.21}$$

3.3.1.2/ THE FORMULATIONS ON ELASTIC-PLASTICITY

In solids, the stress tensor in Eq.(3.20) and Eq.(3.20) can be written as following,

$$\sigma^{\alpha\beta} = -P\delta^{\alpha\beta} + S^{\alpha\beta} \tag{3.22}$$

where, P is pressure and $S^{\alpha\beta}$ is the deviatoric stress tensor. In this paper, for elastic problem, the pressure is computed using a simple Equation of State (EoS):

$$P = K(\frac{\rho}{\rho_0} - 1) \tag{3.23}$$

where, K is the bulk modulus. For the elastic-plastic problem, the Mie-Gruneisen EOS [18] is used,

$$P = (1 - \frac{1}{2}\Gamma\eta)P_H + \Gamma\rho e \tag{3.24}$$

where,

$$P_H = \begin{cases} a_0\eta + b_0\eta^2 + c_0\eta^3 & \eta > 0, \\ a_0\eta^3 & \eta < 0. \end{cases} \tag{3.25}$$

$$\eta = \frac{\rho}{\rho_0} - 1 \tag{3.26}$$

$$a_0 = \rho_0 C^2, \quad b_0 = a_0[1 + 2(S - 1)], \quad c_0 = a_0[2(S - 1) + 3(S - 1)^2] \tag{3.27}$$

Here, S and C are respectively the linear shock-velocity and the particle-velocity parameters to describe the Hugoniot fit and Γ is the Gruneisen parameter.

The deviatoric stress tensor $S^{\alpha\beta}$ can be calculated by its derivative,

$$\frac{\mathrm{d}S^{\alpha\beta}}{\mathrm{d}t} = 2\mu(\dot{\varepsilon}^{\alpha\beta} - \frac{1}{3}\delta^{\alpha\beta}\dot{\varepsilon}^{\gamma\gamma}) + S^{\alpha\gamma}R^{\beta\gamma} + S^{\beta\gamma}R^{\alpha\gamma} \tag{3.28}$$

$$\dot{\varepsilon}^{\alpha\beta} = \frac{1}{2}(\frac{\partial v^\alpha}{\partial x^\beta} + \frac{\partial v^\beta}{\partial x^\alpha}) \tag{3.29}$$

$$R^{\alpha\beta} = \frac{1}{2}(\frac{\partial v^\alpha}{\partial x^\beta} - \frac{\partial v^\beta}{\partial x^\alpha}) \tag{3.30}$$

Combined with the SPH formulations, the equations (3.28)-(3.30) can be described as summation forms of particles by following formula:

$$(\frac{\partial v^\alpha}{\partial x^\beta})_i = -\sum_{j=1}^{N} \frac{m_j}{\rho_j}(v_i^\alpha - v_j^\alpha)\frac{\partial W_{ij}}{\partial x_i^\beta} \tag{3.31}$$

For plastic problems, the yield stress σ_y is constant in perfectly-plastic behavior law while in Johnson-Cook law, the yield stress should be updated by following equation:

$$\sigma_y = (a + b\varepsilon_p^n)(1 + c\mathrm{lin}(\frac{\dot{\varepsilon}}{\dot{\varepsilon}_0}))(1 - T^{*m}) \tag{3.32}$$

where, the parameters a, b, c, n are constants related to material properties. ε_p is the plastic strain and $\dot{\varepsilon}$ is plastic strain rate. $T^* = \frac{T-T_{room}}{T_M-T_{room}}$, where T_M is the fictitious melting temperature of the material, T being the current temperature, T_{room} being the room temperature and m being the thermal softening exponent.

In the case study of this work, Von Mises yield criterion is applied. The second stress invariant $J_2 = 0.5 S^{\alpha\beta} S^{\alpha\beta}$ is checked in every time step. If $\sqrt{J_2}$ exceeds the yield stress $\sigma_y/\sqrt{3}$, the individual stress components are given new values $S^{\alpha\beta}_{new} = fS^{\alpha\beta}$, where the value of f is defined by

$$f = \min(\frac{\sigma_y}{\sqrt{3J_2}}, \quad 1) \tag{3.33}$$

The plastic strain $\varepsilon_p^{\alpha\beta}$ can be calculated by the increment form,

$$\triangle\varepsilon_p^{\alpha\beta} = \frac{1-f}{2\mu} S^{\alpha\beta} \tag{3.34}$$

The equivalent strain ε_e is defined as $\varepsilon_e = \sqrt{0.5\varepsilon^{\alpha\beta}\varepsilon^{\alpha\beta}}$, which includs both elastic and plastic deformation.

3.3.2/ THE STRUCTURE OF SPH CODE

Fig.3.4 is the flow diagram of a standard SPH combined with these modifications mentioned in above sections. It is applied in elastic-plastic formulations. The SPH method is the typical Lagrangian particle method, which approximates a function and its spatial derivatives through averaging or summation over neighboring particles. Therefore, a step called Nearest neighboring particle searching (NNPS) is one of main calculated modules. During it, the types of kernel function is a key which has an important influence for the instability and accuracy of numerical results. In my code, six different types of kernel function are included in order to investigate their different performances in solid dynamic problems.

The basic SPH methodology and the accompanied algorithms in the SPH coding are generally involved under the main loop of time integration process. As shown in the flow diagram (Fig.3.4), the time integration consists of smoothing function and derivative estimation, NNPS, the derivative estimation for physical variables, boundary treatment, artificial viscosity or stress, etc. The typical procedure for implementing a SPH code

includes:

1. Initialization. This part includes the input of the initial configuration of the problem geometry, total number information of the discretized particles, particle distance, boundary conditions, material properties, time step and other simulation control parameters.

2. Discretization. This setup process can be implemented in some commercial tools like CAD/CAE when the geometry is complex.

3. Time integration. The loop time integration algorithms like Leapfrog, Predictor-corrector and Runge-kutta are some common used methods, which may have different advantages and disadvantages. The loop contains the major modules in SPH simulation, consisting of:

   1) Nearest neighboring particle searching (NNPS), which also can be achieved by several different algorithms. Because this step is very time-consuming when the problem includes a large number of particles, and it should be calculated in every time step. So, The efficiency of the specific approach often determiner the time-consuming of the whole simulation.

   2) Calculating the smoothing function.

   3) Density estimation. Here, there are two ways for estimation, one using summation density approach, the other calculating density change rate (P124 book liu).

   4) Calculating the internal forces arising from the particle interactions. The pressure is obtained from the density and energy through the equation of state depending on the physical problem.

   5) Calculating the external forces if necessary.

   6) Corrective kernel function

   7) Calculating the artificial viscosity and stress terms.

   8) Updating the particle momentum, energy and density; updating the particle position and velocity;

   9) Averaging the velocity if using conservative smoothing.

4. Output results. When the time step reaches to a prescribed one or at some interval, the resultant information for a computational state is saved to external files for later analyses or post-processing.

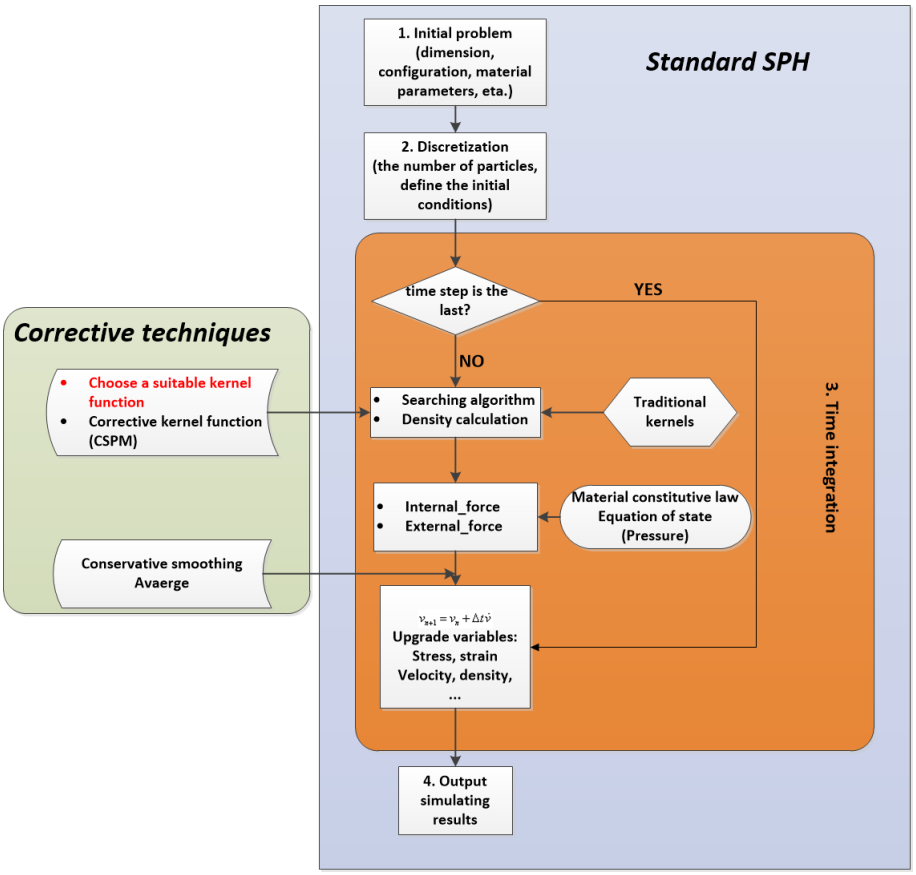

Figure 3.4: The flow diagram of SPH code implementation.

3.3.3/ THE TIME INTEGRATION

In this code, the predictor-corrector Leap-Frog (LF) scheme is applied in SPH time integration. Denoted the time step $\triangle t$, and the predictor step is

$$v_{n+1/2} = v_n + \triangle t \cdot \dot{v}_n \tag{3.35}$$

$$r_{n+1/2} = r_n + \triangle t \cdot v_n + 0.5(\triangle t)^2 \cdot \dot{v}_n \tag{3.36}$$

where, r presents the position of the particle. For velocity v, $\dot{v}$ is acceleration and the corrector step is calculated as following:

$$v_{n+1} = v_{n+1/2} + 0.5\triangle t \cdot (\dot{v}_{n+1/2} - \dot{v}_n) \tag{3.37}$$

here, $\dot{v}_{n+1/2}$ is calculated using the predicted values. The density ρ, energy e and deviatoric stress S are calculated by the same steps with velocity v. In this scheme, the time step is evaluated using the following equation

$$\triangle t = c_s \frac{h}{c_i + |v_i|} \tag{3.38}$$

where c_i is the elastic wave speed. c_i can be valued as $c_i = \sqrt{E/\rho}$, where E is Young's modulus of the material. c_s is a coefficient, taken as $0.1 \sim 0.3$.

3.4/ THE APPLICATION OF SPH CODE IN SOLIDS

3.4.1/ ELASTIC BEAM EXAMPLE

In this sample, the plane stress assumption is applied for the slender beam, therefore a two-dimensional bending problem is simulated by SPH method with kernels listed in Fig.3.1. The geometrical dimensions of the beam structure are shown in Fig.3.5, where the length $L = 100$mm, the width $t = 10$mm and the beam thickness is fixed to 1mm. As illustrated in Fig.3.5, the left edge of the beam is fixed and the other edge is free and has a concentrated load F. The value of the load is a quadratic function of time, starting from 0 to the maximum value F_{max} at time $t = 1.5$ms. F_{max} is kept constant until to the end of simulation $t = 3.0$ms (Fig.3.6). All the material parameters are provided in Tab.3.2 and the related parameters in CSPH are given in Tab. 3.3.

Figure 3.5: The beam model and the left is fixed.

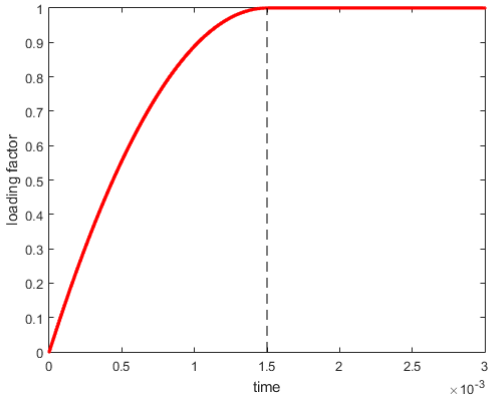

Figure 3.6: The dynamical loading.

Table 3.2: Material parameters

Material	Young's modulus	Poisson's ratio	Density	Sound speed
Steel	210GPa	0.3	7800kg/m^3	5960m/s

Table 3.3: The parameters in CSPH: dx is the initial distance between two particles; $\triangle t$ is the time step; AV and AS, respectively, is the artificial viscosity and artificial stress; XSPH is from the literature [201].

F_{max} kN	dx mm	$\triangle t$ s	h mm	AV α,β	AS ζ	XSPH $\bar{\zeta}$
1.75	1	1.0e-7	$1.2dx$	0.1,0.1	0.5	0.5
17.5	1	1.0e-7	$1.4dx$	0.5,0.8	0.9	0.5

According to [202], when the loading force $F_{max} = 1.75$kN, the maximum load is not very large and thereby the beam deflection can be considered as a linear change with load. The reference deflection can be estimated by the static solution reported by Timoshenko [203] with $W_{analytical} = FL^3/3EI + 6FL/5GA = 33.59$mm. The average errors e_{av} with different kernels are listed in Tab.3.4, ranging from 17.62% to 2.25%. Fig.3.7 shows the distributions of beam deflection and the simulation (a) by our codes (CSPH with type-1 kernel) is very close to the one obtained by Lin et al.in[202] (figure (b)). Although these six kernels have the different accuracy in terms of the final deflections, all of their distributions in the whole beam are smooth and close.

When loading force $F_{max} = 17.5$kN (the same loading process in Fig.3.6), the beam

Table 3.4: Errors e_{av} is calculated by $e_{av} = \frac{1}{T}\sum_{t=1.5ms}^{t=3.0ms}\frac{|W_t - W_{analytical}|}{W_{analytical}}$, where T is the number of time steps during the time $1.5ms \sim 3.0ms$

Types of kernel	Type-1	Type-2	Type-3	Type-4	Type-5	Type-6
Errors	2.55%	8.11%	7.96%	9.58%	17.62%	8.86%

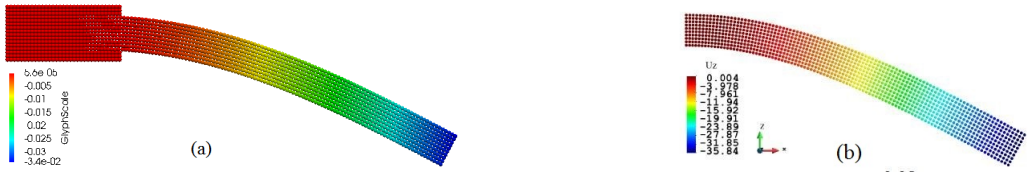

Figure 3.7: the deflection distributions: (a) is simulated by our code with type-1 kernel (m) and (b) is simulated by Lin et al. [202] (mm).

deflection W_c is non-linear related with loading force, and its analytical deflection is $W_{analysical} = 81.1$mm at the end of time according to Timoshenko [203] and Lin [202].

Different numerical phenomenon with above case $F_{max} = 1.75$kN, when the beam bends to nearly maximum deflection $W_{analytical} = 81.1$mm with a large loading force, numerical instabilities with varying degrees happen when using different kernels, as shown in Fig.3.8. Obviously, when using the type-2 and type-3 kernel, the non-physical cracks emerge even increasing the coefficient of artificial stress to 0.9 (Tab.3.3), which directly lead to wrong simulations. When applying type-5 kernel, the particles clump severely and cause the pairing instability in compressed part of the beam. The pairing instability also occurs in the case with type-1 kernel. Although the slightly tensile instability still exists in the fixed end of the beam with type-4 and type-6 kernel, it is not very severe, especially the average errors e_{av} is 4.89% using type-4 kernel.

Fig.3.9 and 3.10 illustrate the energy time history for the 6 different kernel functions. Because the external force is loaded during the whole of beam deformation with the form in Fig.3.5, the total energy consisting of kinetic and strain energy continue to increase with time. Then the free end of beam tends to keep swing at the point of the maximum deformation, which means the kinetic energy should gradually decrease to zero and deformed energy to the maximum. As shown in energy plots, the oscillation of the curves in kinetic energy and total strain energy tend to weaken except for the cases in type-3 and type-2 kernels. It is remarkable that kinetic energy increases rapidly and strain energy is opposite to decrease quickly at the end of calculating time when using type-3 and type-2 kernels. Additionally, it is worth noticing that the values of kinetic energy using

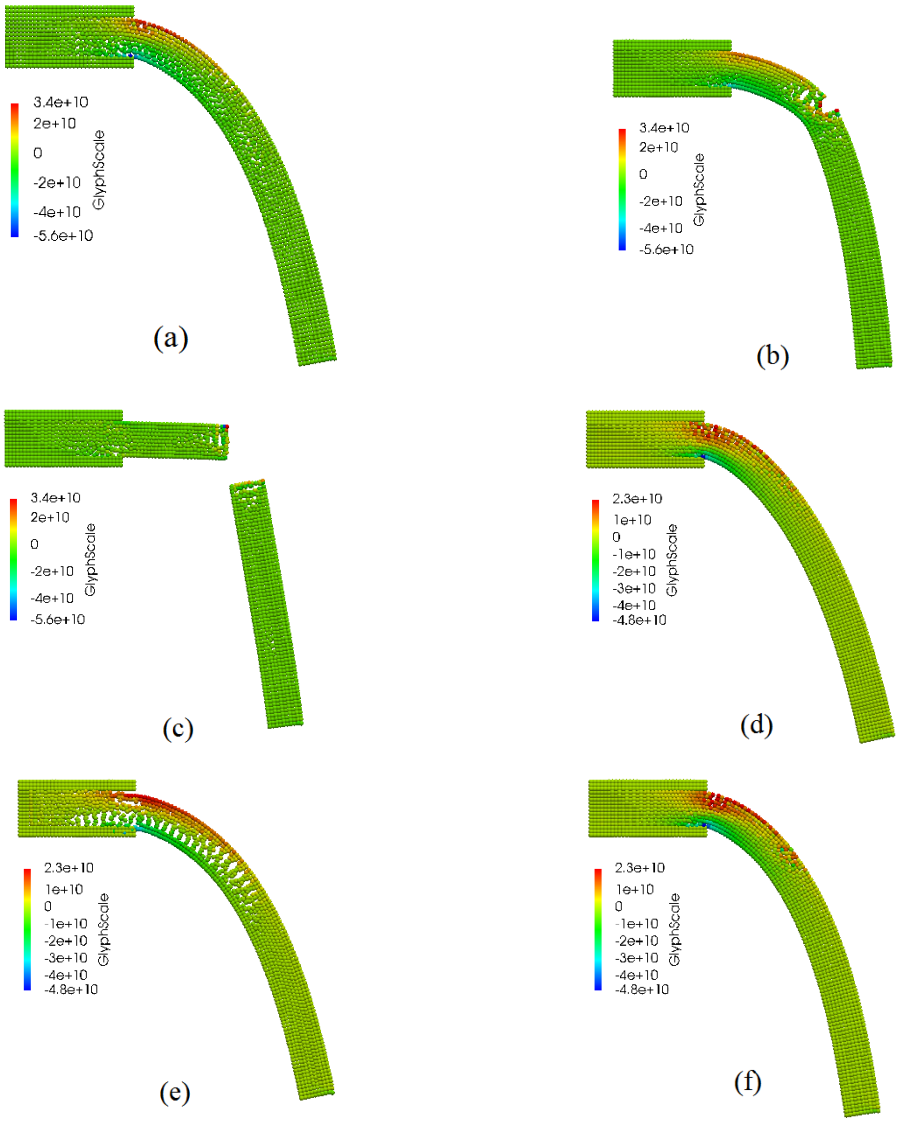

Figure 3.8: Distributions of σ_{xx} at the maximum deflection with 6 kernels, (a)-(f) matching with type-1 to type-6 kernel, respectively.

type-5 kernel are always smaller than using other kernels because of the severe pairing instability observed in Fig.3.8 (e). At the same time its strain energy stabilizes to higher values than others illustrated in Fig.3.10. The similar case is also found from blue curve in kinetic energy plots connecting with Fig.3.8 (a) when using type-1 kernel which shows slight particles disordering. There is no much difference between the cases of type-4 and type-6 kernels in Fig.3.8 (d) and (f) and their kinetic energy plots in Fig.3.9. But the lower strain energy in type-4 kernel case can be noticed than using kernel-6 in Fig.3.10. In addition, Fig.3.11 also shows that the simulation with type-4 kernel is in agreement with the results of both SPH code in [202] and FEM method in [202] in terms of the distribution

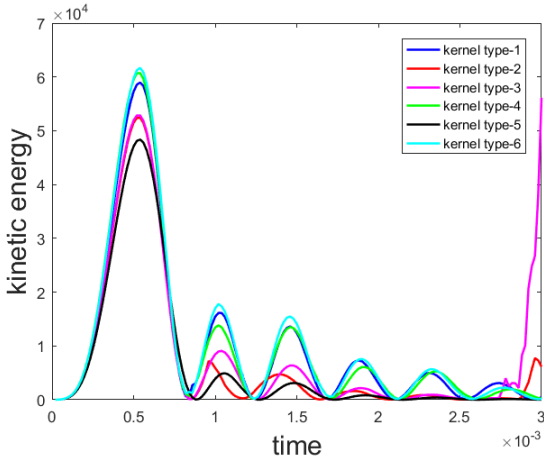

Figure 3.9: time history of total kinetic energy.

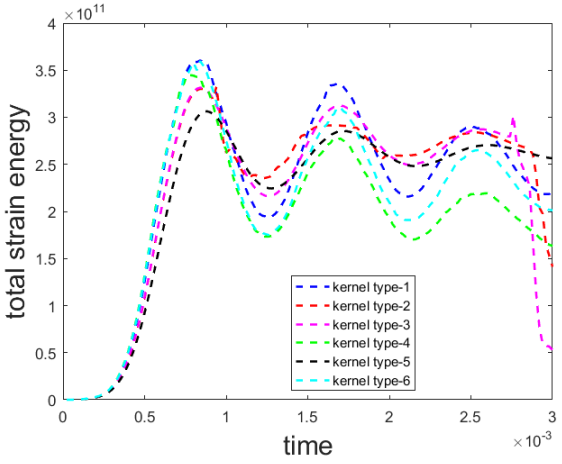

Figure 3.10: time history of total strain energy.

of the deflection.

3.4.2/ TAYLOR TEST EXAMPLE

Fig.3.12 illustrates the configuration of this test consisting in an iron rod impacting a rigid surface. The settings of the simulations are extracted from the study of Libersky and Petschek [204], using the same geometry and material parameters. The simulations are carried out in 2D. Perfectly-plastic behavior is applied coupled to the Mie-Gruneisen EoS. Material parameters are provided in Tab.3.5. Results of the simulations are compared with simulations conducted with the EPIC-2 code in [204].

Table 3.5: Material parameters in 2D rob impact.

Parameters	Young's modulus	Shear modukus	Yield stress	C	S	Γ
Values	208GPa	80GPa	600MPa	3630m/s	1.80	1.80

The rod is discretized by 2050 SPH particles with an initial space dx of 1.058mm and a smoothing length h of $1.5dx$. The computational total time is $50\mu s$, starting when the rod interacts with the rigid surface. Fig.3.13 compares the rod shapes at the end of the impact using different kernel functions, from which it is observed obviously that the simulation using kernel type-4 is the closest to the result by EPIC-2 code. The simulation using

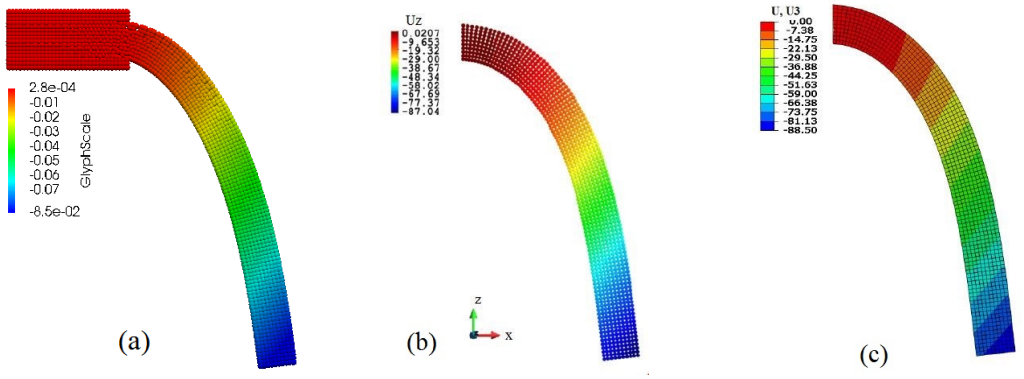

Figure 3.11: Distributions of deflections: (a) is simulated by our code using type-4 kernel (m), (b) is simulated by Lin's SPH code in [202] (mm) and (c) by FEM method in [202] (mm).

type-6 kernel function does not provide coherent result and shows severe numerical instability, comparison to the simulation with type-4 kernel. Fig.3.14 and 3.15, respectively, illustrates the distribution of equivalent strain with type-4 and type-6 kernel function.

The 3D Taylor impact test consists in a cylindrical rod of 37.97mm long and 7.595mm diameter impacting a rigid surface. The structure is made of 4340 steel material and with a velocity of 181 m/s. The Johnson-Cook constitutive law is applied to the rod. The same examples are also studied at an experimental level by House and his colleagues in [205] and at a numerical level by Batra in [206] The material parameters are listed in Tab.3.6. The values of parameters in SPH algorithm of our simulations are illustrated in Tab.3.7.

Table 3.6: Material parameters for Jonhnson-Cook law.

ρ kg/m^3	μ GPa	K GPa	C J/KgK	a GPa	b MPa	n	c	m	T_M K	T_{room} K	$\dot{\varepsilon}_0$ /s
7830	89.2	169.1	460	792	510	0.26	0.014	1.03	1293	293	1

Table 3.7: the SPH parameters in 3D rob impact.

dx	$\triangle t$	h	AV	XSPH
3.88mm	1.0e-8	$1.5dx$	1.5,1.5	0.1

Fig.3.16 demonstrates the time histories of the radius of impact mushroom simulated by SPH with six kernels listed in Tab.3.1, from which we can see that the result using type-4 kernel is the closest one to the result by MSPH [206], compared with simulations using other kernels. MSPH has been compared with existing commercial code LS-DYNA and corresponding experiments and been validated that it is a vary effective SPH algorithm

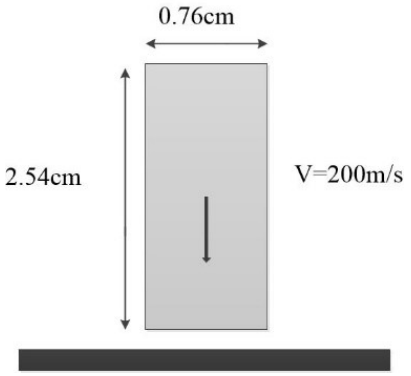

Figure 3.12: Model geometric of rob.

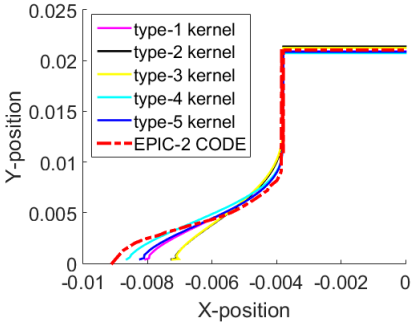

Figure 3.13: The shapes of rod at the impact end.

for simulating impact problems in literature [206]. Fig.3.17 also shows the comparison on time histories of rod length during the impact between our simulations and MSPH. In terms of this value, there is not much difference caused from variable kernels, and the final length at the end of impact is acquired with a value near 34.3mm using all of six kernels in our simulations, which is matched well with 34.7mm by MSPH and 34.5mm by LS-DYNA FE-code, respectively. All the errors of SPH numerical simulations compared with experimental datas are shown in Fig.3.18 and 3.19. Fig.3.18 shows using type-4 kernel the accuracy is the best (4.4%) while the traditional ones type-1 to type-3 (B-spline and Gaussian functions) result in more 10% errors. Although the error on the final length is the largest when using type-4 kernel shown in Fig.3.19, its value is only about 1.05% which is a vary satisfactory result.

3.5/ DISCUSSION

In this section, a discussion connecting the simulations in above section with some research on analysis for kernels' performances is conducted hereafter.

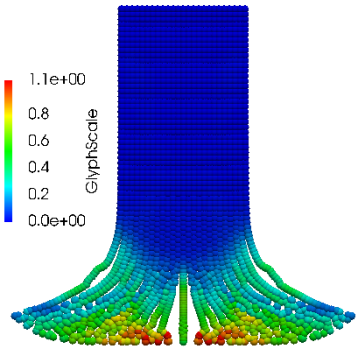

Figure 3.14: The distribution of equivalent strain with type-6 kernel.

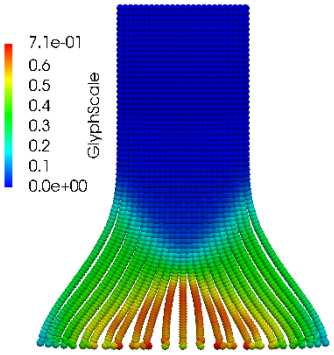

Figure 3.15: The distribution of equivalent strain with type-4 kernel.

3.5.1/ EFFECTS OF KERNEL TYPES ON THE INSTABILITY

Tests in last section show that with the deformation increasing, the severe particles clumping resulting from nonphysical cracks still emerges even using artificial stress combined with CSPH and XSPH. The results also demonstrate the distinguishing performances on particles instability influenced by kernel types. Section 3.2.2 has provided the instability analyses associated with kernel properties and this section would discuss again combining with the numerical results.

Swegle gave stability and instability regimes for B-spline kernel [199], which can be a reference for the situation in example 4.1. Using type-1 and type-3 kernel, both of them as one of B-spline kernel, shows the particle pairing in maximum deflection of beam in Fig.3.8, especially type-3 kernel causing severe nonphysical cracks. Fig.3.2 shows the shapes of type-3 kernel which can represent the common properties of B-spline function. According to the point from Eq.(3.1) , some researchers modify the shapes of kernel functions to avoid the particles dropping into the instability regimes of kernels. Yang X in [198] introduced that hyperbolic shaped kernel function (type-6 kernel in Tab.3.1) which possesses non-negative second derivatives can completely remove the pairing instability in compressed regimes. The curve of type-6 kernel has been tested and successfully achieved simulating results in viscous liquid drop problems in [198]. For solid problems, the beam deflection tests in Fig.3.8 illustrate that using hyperbolic shaped kernel function can indeed achieve more stable simulation in compressed part compared with other kernels. However, because of non-negativity in whole of kernel impact domain, this func-

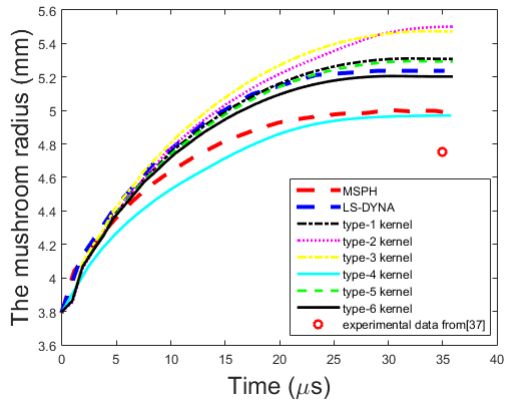

Figure 3.16: The time history of mushroom radius in our simulations using 6 types of kernels, and the simulations by MSPH and LS-DYNA in [206].

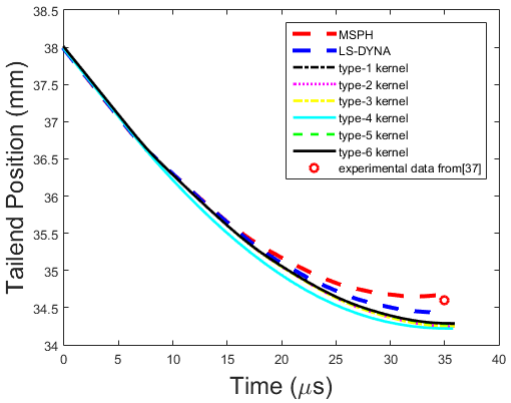

Figure 3.17: The time history of rod length in our simulations using 6 types of kernels, and the simulations by MSPH and LS-DYNA in [206].

tion is limited into compressed problems and can't ensure the stability for large stretched problems. Additionally, it can be noticed that the type-4 kernel named Wendland function involving similar second derivatives with B-spline kernel (seen Fig. 4.20) can also get smooth and stable results in large deformation both in compressed and stretched parts of bending beam, as shown in Fig.3.8 and 3.11.

Particles instability of course influences a lot in system energy shown in Fig.3.9 and 3.10. The nonphysical cracks due to severe pairing instability can lead to the beam cut and free at the maximum deformation and thereby release partial deformed energy such as Fig.3.8 (b) and (c). It results in the kinetic energy of free part of beam still increasing with the existing loading in Fig.3.9, and the total strain energy decreasing quickly in Fig.3.10. In the cases without obvious fracture, the values of kinetic energy using type-5 and type-1 kernels are smaller than the ones using kernels type-4 and type-6. At the same time, more pairing instability can be found in particles using type-5 and type-1 kernels and they also show higher strain energy compared to type-4 and type-6 kernels. This might be explained that pairing instability with disordering deformation among particles can consume higher deformed energy and thereby reduces the kinetic energy of whole system. This assumption is in accordance with the work of Maronne and Colagrossi [207], in which authors conclude that the numerical cavitation due to tensile instability affects the energy decay, the mechanical energy then remaining higher than other solvers. In addition, although there is no obvious difference between the cases using type-4 and type-6 kernels, illustrated in Fig.3.8 (d) and (f), the lower strain energy in type-4 kernel case in Fig.3.10

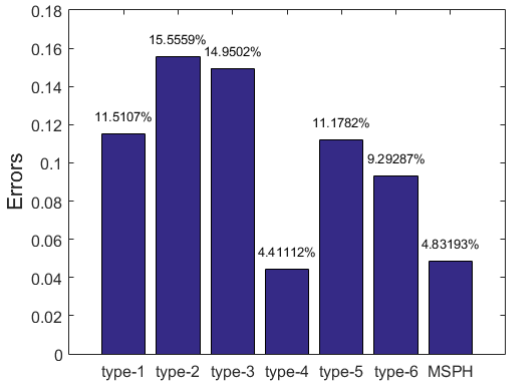

Figure 3.18: The errors of mushroom radius at impacted end compared with experimental data from[205].

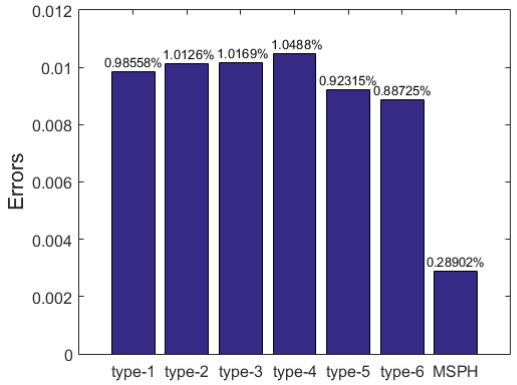

Figure 3.19: The errors of rod length at impacted end compared with experimental data from[205].

seems imply more smoothness among particles. Therefore, the same result by our simulating tests is obtained with Dehnen's analysis concluding that Wendland kernel can make the simulations more stable both in stretched and compressed sections.

3.5.2/ EFFECTS OF KERNEL TYPES ON THE ACCURACY

Section 2.4 illustrates an error estimation concerning the parameters of kernels proposed by Sigalotti in [201], which also demonstrates the positive view on SPH accuracy when using Wendland kernel. The simulations in Taylor tests in section 4 indeed show that using type-4 kernel can get more reliable accuracy.

Based on error estimation in [201], the values of A_w (Tab.3.1) for type-3 kernel is the largest both in 2D and 3D, which is possible to lead to a worse accuracy in SPH particle approximation and then influences the performance in SPH method. The phenomenon in numerical examples in section 4 is matched with this theory in some points: the most severe particles instability in bending beam test (Fig.3.8) and the largest errors in Taylor tests when using type-3 kernel (Fig.3.13 and 3.16). In addition, values of A_w from type-1 kernel are close to the values from type-2 kernel both in 2D and 3D, but these two kernels have different performances in instability and accuracy (type-1 seems better much than type-2 in section 4 examples), a possible reason is that the compactness of type-2 kernel is not strictly satisfied (Eq.(3.6)) in spite of its sufficiently smooth even for high orders of derivatives. This discussion doesn't include type-5 and type-6 kernels, because a limited understanding about the universality of this estimated means.

Type-5 and type-6 kernels are new types and constructed for specific problems having gotten good simulating results. It also noticed that in solid dynamics, using type-6 kernel has a very good stability like type-4 as illustrated in Fig.3.8 and a second accuracy only to the case using type-4 kernel in Fig.3.18, but it completely does not work for 2D Taylor impact problems shown in Fig.3.14. Concerning type-5 kernel which is characterized by having enough smoothness in any order of derivatives, it yet cannot satisfy the requirement in accuracy, the example shown in Tab.3.4, and still does not have a good performance in pairing instability in Fig.3.8. Therefore, it is difficult to find a kernel function perfectly fit to all situations. By observation and discussion, combined numerical examples with analysis research in literature, the conclusion is acquired that the Wendland function is a better and more reliable choose as SPH kernel in solid dynamic problems.

3.6/ CONCLUSION

Kernel function is one of the most important concepts in SPH algorithm and its properties cause unignorable influences for the results of simulations. In addition to some basic conditions linked to the definition of SPH formulations, like normalization, compactness and Dirac delta property et., other mathematical features like the shape of the second derivative of the kernel, the sign of its Fourier transform, as well as several constant parameters also play insignificant roles in SPH overall performances. This chapter compares a few kernels' performances with applications in dynamical solids problems, including several conventional kernels like B-splines function, Gauss function, Wendland functions and two new types (double cosine function and Hyperbolic shaped function).

It is well known that the pairing instability is a serious problem in developing SPH applications in simulating solids. Based on our numerical tests, the choice of suitable kernel function is able to improve the pairing instability in some degree, as well as obtains a better accuracy. Thus, Wendland function appeared to be a good candidate as SPH kernel in simulating elastic-plastic problems.

4

SPH APPLICATION: HIGH-VELOCITY IMPACTS INTO SOFT TISSUES BY MICRO-PARTICLES

4.1/ INTRODUCTION

Investigating high-speed microparticle impact responses into soft tissue is essential to several fields such as medicine and biology with technological applications like transdermal delivery of pharmaceuticals. The understanding of the physical process involved in such a phenomenon is complex and few experimental tools are available to study high-velocity microparticle penetration in soft tissues. Besides, considering the practical and ethical issues, various simulants of human tissues including skin, muscle, brain, and other internal organs have been developed and investigated, such as epoxy resin [141], ballistic gelatin [143, 144], and polymers [142, 208]. One way to overcome these issues is to use numerical simulation as an efficient way of investigations, but also include difficulties such as accurate models for materials properties, micro-scale computation, and mathematical formulations. Smoothed Particles Hydrodynamics (SPH) has been applied in solid dynamics to simulate extremely large deformation and perforation of targets by various projectiles, as reviewed in the state of the art in the chapter**??**. After the theoretic study in the code and its validations to several benchmark problems in the chapter 3, this part develops an original numerical model based on SPH to study the dynamical phenomena during micro-scale impact of spheres into soft materials including ballistic gelatin (BG) and SEBS gel. The structure of this chapter is organized by:

1. The analytical models for penetrations including the Poncelet equation, Liu's model and Modified-CG model are introduced firstly, which are often as the effective tools to validate the numerical results. The Poncelet model is represented and its coefficients are studied for the micro-penetrations. Then, the suitability and the fitting approaches of the analytical models based on a series of experiments on the micro-penetrations are discussed.

2. A 3D numerical model combined with SPH particles and FEM elements is developed using Hyperworks software. The material constitutive law for gelatin and SEBS gel is introduced.

3. Then, the simulations on ballistic behavior of 10 wt% BG impacted by a silica sphere with 7.38 μm diameter with 200-1290 m/s velocity are performed using this 3D numerical model. The perpetrating history of the projectile and the temporary cavity of the gelatin are investigated and validated by experimental results.

4. The second part of the simulations is on ballistic behavior of 40 vol% SEBS gel impacted by a steel sphere with a range of diameters like 10-25 μm diameters. The impact velocities are in a range of 20-1000 m/s. The trajectory of the projectile and the elasticity of the SEBS gel are investigated and discussed based on the comparisons between the numerical and experimental results.

5. A discussion about the suitability and limitations of this numerical model is provided.

4.2/ ANALYTICAL MODELS FOR PENETRATIONS

The analytical model is one of the most important approaches to understand the impact process. The formulations of analytical models incorporate some essential and relevant physical and mechanical theories and parameters. The various models that describe the behavior of a spherical fragment penetrating soft materials have been developed and employed in the literature such as [163, 164, 165, 166, 57]. Generally, the suitability of analytical models depends on the physical conditions, experimental fitting, as well as empirical data. Therefore, it is possible that the analytical models represent the different performances when the penetrations happened in the macro-scale and micro-scale. The Poncelet equation describing the complete trajectory of the projectile is the most widely

used in this field at present, thereby a study is firstly provided on the application of Poncelet model to micro-penetrations, particularly applied in the ballistic gelatin.

4.2.1/ PONCELET MODEL

4.2.1.1/ THE FORMULATION

the Poncelet model is regarded as a validation to some experiments [166, 167] and to some numerical simulations [57]. The equation is written in the [169] as,

$$-M\dot{V} = BV^2 + C \tag{4.1}$$

where, B and C are considered as the inertial drag and the strength resistance terms. Given a initial velocity v_0, the penetration depth P can be solved as a function of the instantaneous velocity v:

$$P(t) = \frac{M}{B}[\ln\cos(\frac{\sqrt{BC}}{M}(T_f - T)) - \ln\cos(\frac{\sqrt{BC}}{M}T_f)] \tag{4.2}$$

where T_f is the final time at which the velocity of the projectile decreases to zero, which can be calculated by,

$$T_f = \frac{M}{\sqrt{BC}}\tan^{-1}(v_0\sqrt{\frac{B}{C}}) \tag{4.3}$$

where M is the mass of the sphere projectile, and B and C defined as being two important material properties in [164] are defined as,

$$B = \frac{\rho_t \pi d^2 C_d}{8} \tag{4.4}$$

$$C = \frac{R\pi d^2}{4} \tag{4.5}$$

where ρ_t and R are, respectively, the density and the strength resistance of the gelatin. C_d is the inertial drag coefficient and d is the diameter of the projectile. Combined with the Eq. (4.3), the maximum penetration depth P_{max} can be obtained from the Eq. (4.2),

$$P_{max} = P(T_f) = \frac{2\rho_p d}{3\rho_t C_d} \ln\left(\frac{\rho_t C_d v_0^2}{2R} + 1\right) \tag{4.6}$$

4.2.1.2/ A DISCUSSION FOR THE PARAMETERS

In the Poncelet equation, the retardation force of the projectile during the impact consists of a constant strength term C and a term proportional to the square of the instant penetration velocity BV^2, where the strength resistance R, related to the apparent yield stress σ_t, is a material-specific constant. This analytical model was initially validated by Sturdivan's experiments in 1978 [163] for a 20wt% gelatin target. The explicit values of drag coefficient C_d and strength resistance R should be changed in specific penetrations. In the work by Wijk et al. [164], the strength resistance R was found to be 0.52 MPa for 10wt% gelatin and 3.5 MPa for 20wt% gelatin. Intuitively, the strength of gelatin material should increase with percentage. As for the drag coefficient C_d, its value is recommended to 0.35 at $24°$C and 0.375 at $10°$C in [164].

In the investigation of micro-particle (silica spheres with 7.38 μm diameter) impact 10wt% gelatin in [167], the the value for C_d = 0.4 was taken from [209] and the parameter R was obtained by fitting maximum penetration data. According to this study in [167], the strength resistance R was extracted by the following relation,

$$P_{max}^{Exp} = \frac{2\rho_p d}{3\rho_t C_d} \ln\left(\frac{\rho_t C_d v_0^2}{2R} + 1\right) + \frac{d}{2} \tag{4.7}$$

where the P_{max}^{Exp} is the experimental maximum penetration. It can be noticed that the above equation includes a term of $d/2$ compared with the Eq.(4.6), which takes into account the particle's 'nose' contribution. A value of R = 21 MPa was obtained by the way of Eq. (4.7) and in turn used to calculate the complete particle trajectory in Eq. (4.2).

It is worth noticing that, for the same target material, the value of strength resistance R = 21 MPa is more than 40 times on the macro scale (0.52 MPa), which could be explained by the sample strain rate sensitivity that is exhibited from the macro to the micro-scale. Generally, a higher strain rate (markedly more than 10^6 s^{-1}) can lead to higher hardness in impact [210], which manifests by a higher resistance. This observation is the most important result in the applications of analytical models for macro-penetrations and micro-penetrations.

Although the Poncelet model with the parameters (C_d = 0.4, R = 21 MPa) was validated by Veysset et al. [167] to model penetration of 7.38-μm diameter silica spheres into 10wt% gelatin. We found that a variation of drag coefficient C_d = 0.375 combined with R = 21 MPa shows that the curve by Poncelet equation is also in agreement with experimental result. Fig.4.1 illustrates that there is a small difference at the final penetration between the curves using C_d = 0.4 and C_d = 0.375 in Poncelet equation (Eq.(4.2)) to model the trajectory. The combination of (C_d = 0.375, R = 21 MPa) can achieve a better fitting than the other, because it keeps the consistency for the whole time history on penetration length.

Another point deserving to be discussed is the applicability of the Poncelet model with specific values of parameters (C_d, R) in micro-sized penetration. Although the parameters C_d = 0.375 or 0.4 and R = 21 MPa have demonstrated their ability to fit well with the impact trajectory of the microparticle (only for d = 7.38 μm) in Veysset's work [167], its generalization is still questionable. Indeed, the Poncelet equation involves a constant resistance R whose variation with strain rate is unknown. A review paper [211] claims that the Poncelet model is one of the most classic analytical models for penetration mechanics, but the authors confirmed that a better fit to the experimental data is achieved only if very high-velocity impacts are not included. The authors in [211] also explained that the Poncelet parameters should change during penetration when the very high-velocity impacts occur.

To confirm this point, Fig.4.2 shows a series of penetration curves of macro-sized spheres impact into 20wt% gelatin by experiments and the Poncelet equation. The experimental data are extracted from [163] and the parameters in the Poncelet equation[1] are C_d = 0.33 and R = 3.5 MPa from [164]. It can be noticed that for macro-scale impacts, a same combination of parameters (C_d = 0.33, R = 3.5 MPa) in Poncelet equation demonstrates important discrepancies in the case of d = 2.38 mm projectile and v=2229 m/s initial velocity. An important error emerges in this case compared with the other penetrations involving larger projectile and lower impact velocities. On the contrary, an increase for the drag and resistance terms in Poncelet equation [2] with C_d = 0.35 and R = 5 MPa can acquire a better agreement between experimental result and Poncelet curve. The high velocity such as 2229 m/s in the above example leads to a sufficiently high strain rate. Therefore, this test justifies the tendency to have R increase with strain rate. According

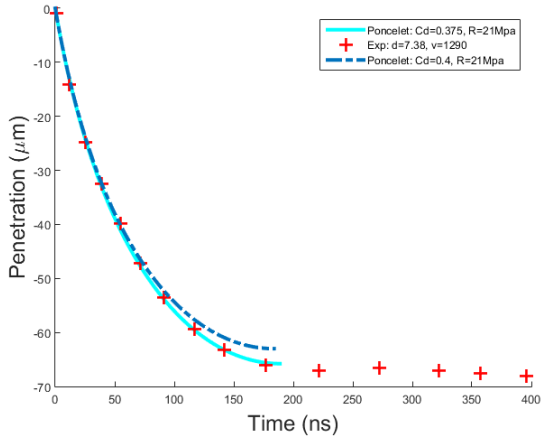

Figure 4.1: The curves of silica particle $d = 7.38\mu$m impact with 1290 m/s in 10wt% gealtin, compared between experimenal data and the Poncelet model with two combinations of parameters C_d and R.

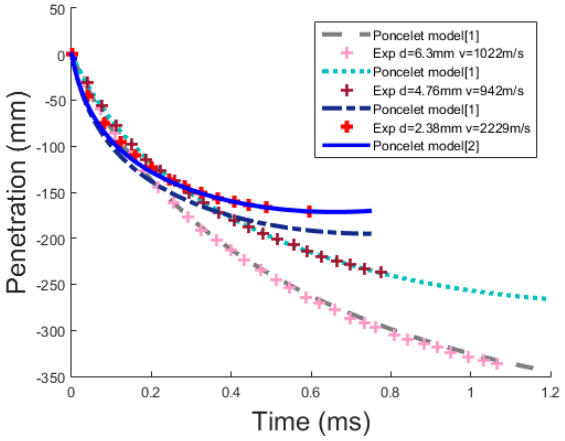

Figure 4.2: The curves of steel spheres impact 20wt% gealtin: the experimental data is from [163] ; the Poncelet equation [1] with C_d = 0.33 and R = 3.5 MPa [164], and the Poncelet equation [2] with C_d = 0.35 and R = 5.0 MPa.

to [210], both the decrease in dimension scale and the increase in impact velocity can achieve high strain rates, even beyond $10^6 s^{-1}$, and the high-velocity impact of microparticles typically belongs to this phenomenon. Hence, the applicability and generalization of the Poncelet model should be further researched, particularly in micro-sized penetration with high velocity.

4.2.2/ A COMPARISON ON THREE MODELS

Generally, the suitability of analytical models depends on the physical conditions, experimental fitting, as well as empirical data. Considering the uncertainty of the analytical models in micro-penetrations, an investigation on the performance of three analytical models is performed in this section.

4.2.2.1/ THE FORMULATIONS OF LIU AND MODIFIED-CG MODELS

By the above discussion, it can be seen that the impact strain rate seems a key to the applications of the Poncelet model. A few analytical models considered the effects of impact strain rate such as [166, 168]. Liu et al. [168] developed an analytical model involving the dependent-strain-rate resistance and a viscous term to investigate the trajectory of

a projectile in 20 wt % gelatin. In the recent study of Veysset et al. [2], a Modified-CG model was developed to model the penetration trajectories in SEBS gel material in the micro-scale. It considers the viscosity term involved in the drag coefficient and was proven to have a better performance than the Poncelet model. Firstly, their formulations are represented here.

- Liu's model

This total force to projectile is decomposed into three parts: an inertial component from the traget material including a constant frag coefficient C_d; a viscous component representing the friction on the surface of the fragment, including a constant coefficient C_v; a resistance owing to the inherent structural characteristics of the target material. It follows the form as,

$$-M\dot{V} = F_I + F_v + F_T \tag{4.8}$$

where, every component can be expressed as,

$$\begin{aligned} F_I &= \frac{1}{2}C_d A_0 v^2 \\ F_v &= C_v A_0 v \\ F_T &= A_0\sigma_0[1 + (\frac{\dot{\epsilon}}{\dot{\epsilon}_0})^2] \end{aligned} \tag{4.9}$$

where, the resistance part is depending on a strain-rate. The analytical expression on time history and maximum penetration depth can be acquired, seen in [168].

- Modified-CG model

The Modified Clift-Gauvin model is based on an assumption that the Reynolds number $Re < 10^5$ during the experimental penetrations, combined with a empirical form for C_d from the work of [212]. The total force is expressed as,

$$-M\dot{V} = \frac{1}{2}C_d^{C-G}\rho_s A v^2 + AR \tag{4.10}$$

Where, the drag coefficient is followed by,

$$C_d^{C-G} = \frac{24}{Re}(1 + 0.15Re^{0}.687) + \frac{0.42}{1 + 4.25e^4 Re^{-1.16}} \tag{4.11}$$

Where, $Re = \rho_s v D/\eta$ involves the dynamic viscosity η. Therefore, viscosity η and resistance R are coefficients required to be fitted from experimental data. Additional, in return, the fitted value of η should satisfy the precondition of $Re < 10^5$ in this model.

4.2.2.2/ EMPLOYMENTS OF THESE MODELS

The Poncelet and Liu formulas can obtain the analytical solutions for penetration history $P(t)$ and maximum penetration depth P_{max}. Numerical iteration in the Modified-CG model is required to get the penetration trajectory. Tab.4.1 lists these three models including their coefficients required fitting, physical meanings of terms, as well as practical application. Two kinds of fitting approaches $*a)$ and $*b)$ through experimental data are introduced:

1. $*a)$: fitting time-penetration

By fitting a whole trajectory (Time-penetration curve) to acquire the constant parameters in analytical models, then using these fitted parameters to simulate other trajectories or maximum penetration depths.

2. $*b)$: fitting maximum-penetration depths

By fitting a large number of maximum penetration depths from impacts involving various diameters and velocities to acquire the constant parameters in analytical models, then using these fitted parameters to simulate other trajectories or maximum penetration depths.

Table 4.1: The list for three analytical models to penetrations.

	Poncelet [163]	Liu [168]	Modified-CG [2]
Resistance	R	$\sigma_0 f(\dot{\epsilon})$	R
Drag coefficient	C_d	C_d	C_d^{C-G}
Viscosity	no	C_v	η in C_d^{C-G}
Analytical solution	$P(t)$, P_{max}	$P(t)$, P_{max}	No
Applied scale	macro/micro	macro	micro
Fitting parameters	R, C_d	σ_0,C_d,C_v	R,η

The coefficients in analytical models are extracted via fitting with experimental data. Fig.4.3 and Tab.4.2 include the experiments about impact SEBS gel material by the mi-

Table 4.2: The list for three experimental trajectories Curve1-3 from [2], used to fit the analytical models.

Experimental trajectory	diameter D	impact velocity v_0
Curve1	20 μm	215 m/s
Curve2	16 μm	440 m/s
Curve3	13 μm	630 m/s

croprojectiles with the diameters from 10um-25um at a range of velocities [2]. These experimental results are used to fit the analytical models in the Tab.4.1.

The Fig.4.4 shows the fitting results for three analytical models via the $*a)$ approach. In every subfigure, the curve2 with red solid style is acquired by fitting with experimental data, and then values of coefficients in the analytical model are obtained. Next, the other two analytical curves using these fitted coefficients are compared with experimental trajectories as the validations. The values of fitted coefficients for three models are (C_d=0.8708, R=36.3 MPa) in Poncelet, (C_d=0.3966, C_v=6.8112e-6, σ_0=23.2 MPa) in Liu's model, (η=7.8911e-2, R=16 MPa) in Modified-CG, all of them locating in the reasonable range. It can be seen that the Poncelet equation performs badly in modeling the curve1 with a lower velocity and bigger projectile, and both Liu and Modified-CG models can not fit well to the curve3 with a higher velocity and smaller size of projectile. Therefore, it has to be admitted that using only one experimental trajectory to fit the analytical model can not get universal coefficients to keep the accuracy for modeling other penetration trajectories. All of these three analytical models illustrate a similar situation.

The analytical models are fitted via the $*b)$ approach using the experimental data in Fig.4.3 (b). Fig.4.5 shows the fitting results on the normalized maximum penetration depth as a function of impact velocity. The values of (C_d=0.8, R=33.7MPa) in Poncelet, (C_d=0.8, C_v=5.31e-7, σ_0=15MPa) in Liu's model, and (η =4.5e-2, R=25MPa) in Modified-CG are obtained in the reasonable ranges. Fig.4.6 shows the results using these fitted coefficients to model the penetration trajectories. It can be seen that a general agreement compared to different experimental trajectories is acquired for every model. It implies that the $*b)$ fitting approach can get more stable and universal fitting coefficients for analytical models than the $*a)$ approach. This is because that the $*b)$ fitting approach uses more experimental data including a large diversity on projectile size and impact velocity, while the $*a)$ approach uses the information only from one penetration trajectory.

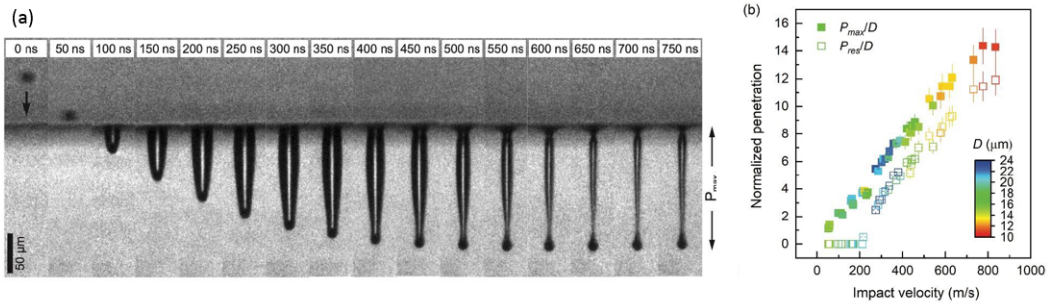

Figure 4.3: The experiments performed on the penetration SEBS gel by steel microparticles in [2]: (a) The experimental images showing the projectile trajectory of Curve3 with particle diameter 13 μm penetration into 40-vol% SEBS gel. (b) Normalized penetration depths as a function of impact velocity, involving various diameter particles marked by colors.

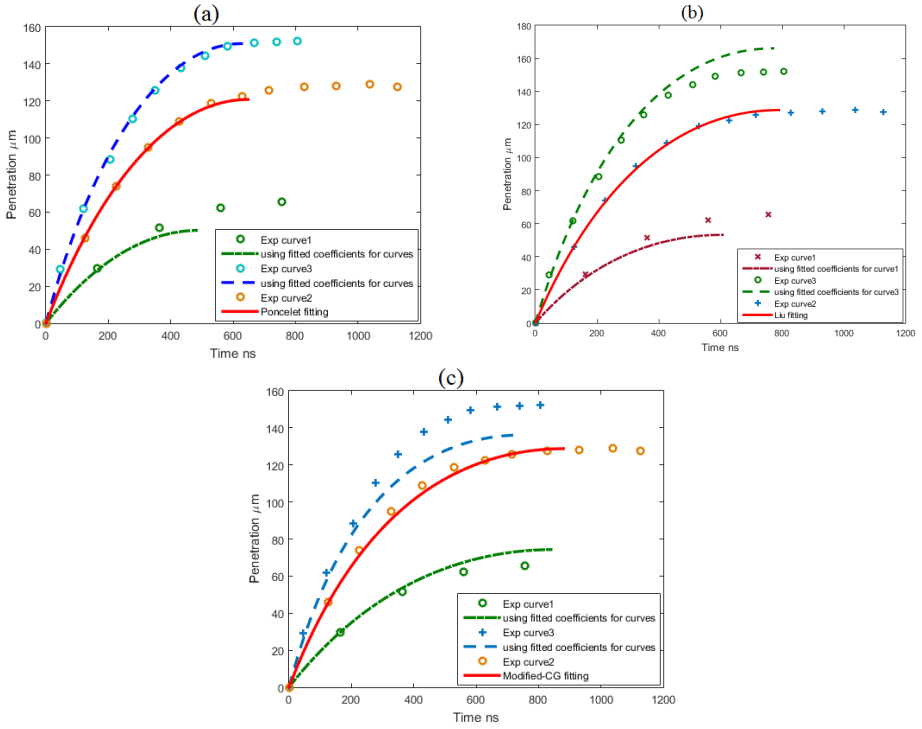

Figure 4.4: Fitting results via $*a)$ approach: (a) Poncelet model (b) Liu's model (c) Modified-CG model. The configurations of curves: Curve1 (v_0=215 m/s, D=20 μm), Curve2 (v_0=440 m/s, D=16 μm), Curve3 (v_0=630 m/s, D=13 μm).

Worthy to be noticed that in Fig.4.5, the fitting curve by the Modified-CG model traverses the other two fitting lines by Poncelet and Liu. Besides, the fitting result by the Modified-CG model is closer to the trend of experimental results than the other two. It suggests that Poncelet and Liu models tend to underestimate the penetration at low velocity and overestimate it at high velocity. Comparatively, for the penetrations with a wider range

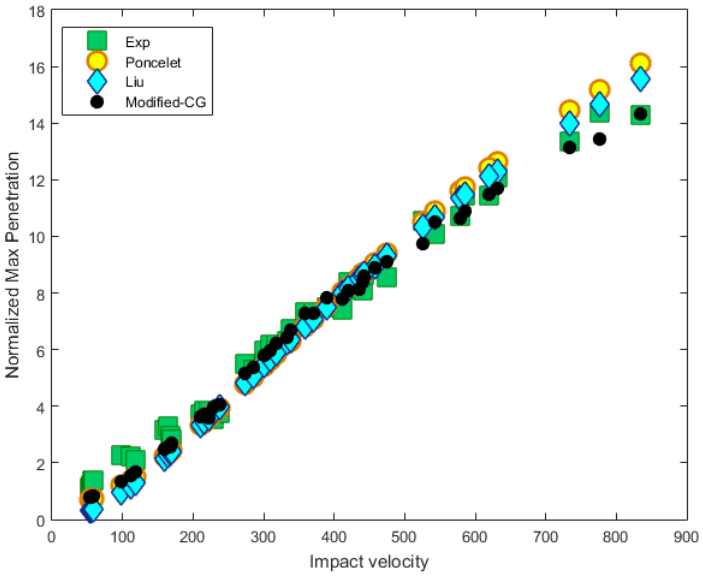

Figure 4.5: Fitting results via $*b$) approach.

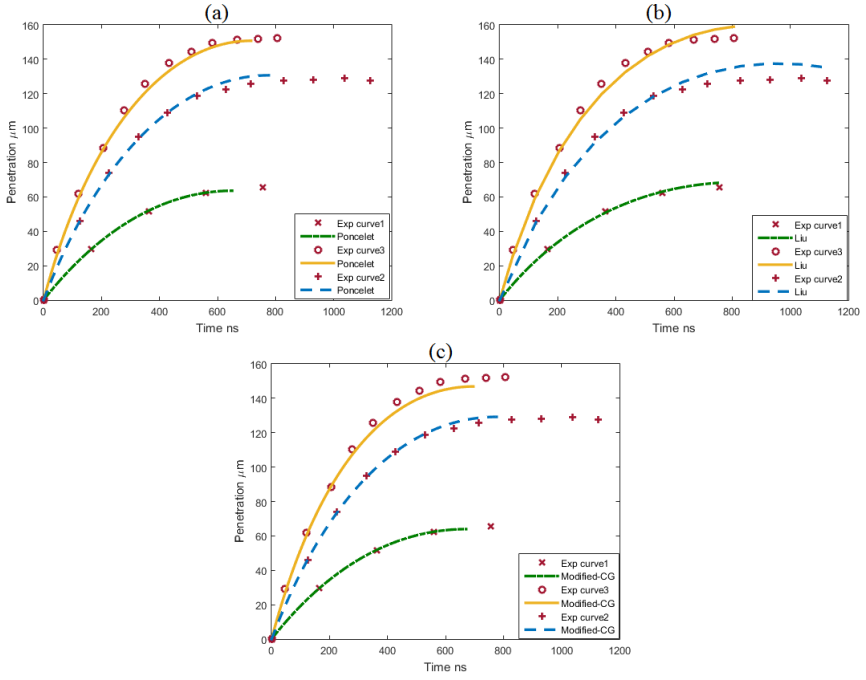

Figure 4.6: Validating the fitted coefficeints from Fig.4.5: (a) Poncelet model (b) Liu's model (c) Modified-CG model. The configurations of curves: Curve1 (v_0=215 m/s, D=20 μm), Curve2 (v_0=440 m/s, D=16 μm), Curve3 (v_0=630 m/s, D=13 μm).

of impact velocities, the Modified-CG model has a more stable prediction to penetration depth. However, the performance of Modified-CG still depends on the work with a large number of experiments, which seems to lost the initial objective of the analytical models that avoid the experimental costs. Therefore, the development of the numerical method

is highly required.

4.3/ THE NUMERICAL MODEL FOR MICRO-PENETRATIONS

4.3.1/ DESCRIPTION OF NUMERICAL MODEL

A 3D SPH model combined with FEM elements is created to investigate the impact behavior of soft materials, as shown in Fig.4.7. Considering the efficiency of time-consuming in the SPH model, the area located far from the impact center where involves small deformations is discretized by finite elements while SPH particles are distributed in the dominant penetrating part. The projectile is regarded as a rigid sphere and also modeled by finite elements. The contact is based on master surface-slave nodes approach between projectile elements and particles in impact center (TYPE7 which is widely used for HVI problems in the commercial software Radioss.) Interface Type2 in Radioss is used for the modeling of the interaction between the SPH domain and the FEM domain of the target. So, the link between the FEM elements and SPH particles constructed with a kinematic interface is well defined and provide a correct extension of the gelatin sample. More details of Type7 and Type2 contact algorithms can be seen in [213]. L_{sph} defines the size of the whole SPH domain in the whole model. dx_i is the discretization length of the SPH components, and it is increased gradually with the distance to penetrating center (the same strategy was adopted for macroscale simulation in [133]).

4.3.2/ MATERIAL CONSTITUTIVE LAW

The hyper-elastic or visco-elastic properties of soft materials like gelatin and gels have been recognized, but the motion of the projectile in a soft tissue target can be described by yield-stress fluids according to several studies such as [157, 2]. That means the deformations of soft tissues involve both solid-like behavior and Newtonian fluid-like behavior during the penetrations. The target material represents an elastic-plastic deformation like solids under law-velocity impact and then transition to hydrodynamic movements like fluids when its mechanical stresses exceed a yield strength under higher velocity. Therefore, an elastic-plastic hydrodynamic constitutive law is employed for the target materials. In terms of modeling the solid-like behavior, the linear-elastic plasticity model is used, and

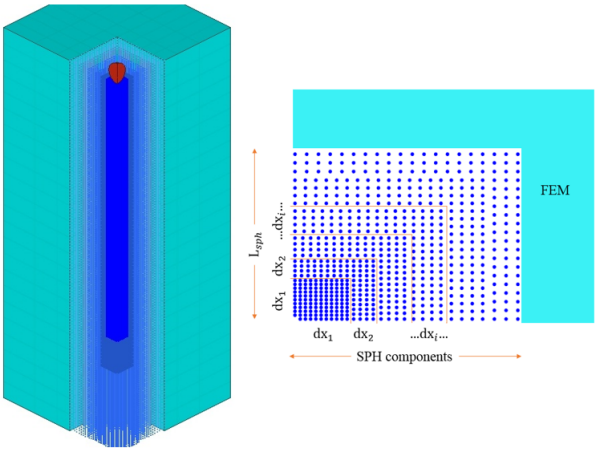

Figure 4.7: Numerical model combining SPH and finite elements is built in the commercial software Hypermesh: L_{sph} defines the width of SPH colume; SPH part consists of several SPH components with different discretization lengths dx_i, and the values of dx_i increase with the distance between SPH component and impact center ($dx_1 < dx_2 < ... < dx_i < ...$).

the yield-stress in soft materials follows the form,

$$\sigma_y = A + B\varepsilon_p^n \tag{4.12}$$

where σ_y and ε_p^n are, respectively, the yield stress and the effective plastic strain. The apparent yield stress A, the hardening parameter B, and the hardening exponent n are the constant values related to the plastic property of materials. About failure, working on ballistic gelatin, Moy et al.in [214] showed a very small plasticity domain : There is a notable lack of plastic deformation in the gelatin. The specimens were subjected to large strains and after failure, the ballistic gelatin exhibited little to no plastic deformation. Knowing that the SEBS gel has a similar behavior, it is assumed that SEBS gel breaks after reaching maximum stress which is close to the yield-stress value.

Besides, the Mie-Gruneisen EOS is applied to describe the non-linear pressure evolution, considering that the hydrodynamic effect becomes predominant upon the impacts into soft tissues at high impact velocities . The equation has the following form:

$$P = \begin{cases} \sum_{k=0}^{3} C_k \varrho^k & \varrho > 0, \\ C_0 + C_1 \varrho & \varrho < 0. \end{cases} \tag{4.13}$$

$$\varrho = \frac{\rho}{\rho_0} - 1 \tag{4.14}$$

$$\begin{cases} C_0 = P_0 \\ C_1 = \rho_0 c_0^2 - 0.5\Gamma_0 P_0 \\ C_2 = (2S - 1)C_1 \\ C_3 = (S - 1)(3S - 1)C_1 \end{cases} \tag{4.15}$$

According to [179], the C_k coefficients depend on the parameters ρ_0, c_0, S, E_0 and Γ_0, which are, respectively, the target materials density, the sound of speed, the slope of the linear Shock Hugoniot function, the initial volumetric internal energy, and the Gruneisen parameter.

The physical problems simulated by this model are based on a series of experiments on 10 wt% gelatin conducted in [167] and 40 vol% SEBS gel conducted in [2]. The parameters about these two kinds of soft materials as simulant of soft tissues used in this constitutive law are represented in Tab.4.3. In the numerical model, the projectile is considered as a non-deformable body and modeled with a linear elastic constitutive law and a high value for the Young modulus. The material parameters of the projectiles are shown in Tab.4.4.

Table 4.3: Material parameters of the target materials. The value of Young's modulus underlined will be investigated combined with numerical simulations. The value of apparent yield stress A is equal to the ballistic resistance which is extracted from the study in [167] for gelatin and [2] for SEBE gel.

Parmeters	10 wt% gelatin	40 vol% SEBS gel
Density	1030 kg/m^3	875 kg/m^3
Poisson's ratio	0.499	0.495
Young's modulus	1 - 100 MPa	1 - 100 MPa
A	21 MPa	25 MPa
B	0.01	0.01
n	0.1	0.1
c_0	1520 m/s	1520 m/s
S	1.8	1.87

It should be noticed that, in Tab.4.3, two material parameters are underlined. One is Young's modulus E which is given a value in a range, and an further investigation about the influence on penetration process from this value is provided in simulation results. Both

Table 4.4: Material parameters of the projectiles.

Material	Diameter	Density	Poisson's ratio	Young's modulus
Silica	7.38 μm	1850 kg/m^3	0.3	70 GPa
Steel	10-25 μm	7800 kg/m^3	0.3	210 GPa

Young's modulus E and apparent yield stress A can represent the material resistance to some degree, but there is no direct correlation between them. The value 21 MPa of apparent yield stress A in Tab.4.3 is extracted from the literature [167]. Based on this investigation, the target's resistance in micro-particle penetration is raised to 21 MPa compared with the value of 0.52 MPa obtained in macro-scale experiments using the same target. Therefore, the Young's modulus is predicted to a range of 1-100Mpa in the micro-scale, considering an increase on the strength of target materials. For the target of SEBS gel, the similar range for the values of Young's modulus is predicted taking into account a value of 0.12 MPa used as constant Young's modulus in the study of [132], as well as a resistance value in the Modified-CG analytical model [2].

4.4/ SIMULATIONS ON BALLISTIC GELATIN

The simulation results are obtained with the commercial software RADIOSS, and validated by the experimental data derived from the laser-induced particle impact test (LIPIT) by Veysset et al. in [167]. In these experiments, silica spheres (micro-scale diameter) were accelerated from 200 to 1500 m/s and penetrated into gelatin sample. Fig.4.8 shows a typical image sequence of a silica particle (d=7.38 μm) impact on a 10wt% gelatin sample at a velocity of 1290 m/s and its experimental trajectory is extracted from [167], as a validation for the following simulations.

4.4.1/ NUMERICAL PARAMETERS IN SPH MODEL

4.4.1.1/ CONFIGURATION OF SPH DOMAIN

Firstly, this model is built with SPH particles and FEM elements. Since SPH is more time-consuming than FEM, we optimize the distributions of SPH and FEM parts to ensure simulation efficiency. The width of the SPH column in Fig.4.7 is defined as L_{sph} and its

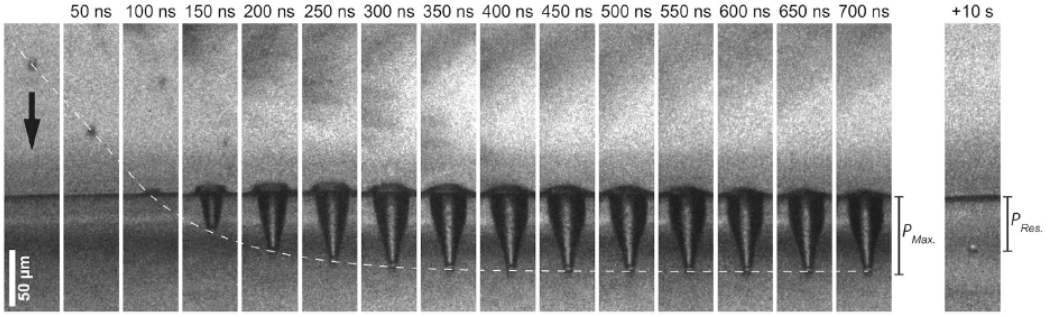

Figure 4.8: Multi–frame sequence showing a high-velocity impact on 10 wt% gelatin at 1290 m/s and a maximum penetration depth reaching around 200-250 ns after impact, provided in [167].

value is set as the multiple of the projectile diameter d. Fig.4.9 illustrates the numerical results on impact trajectory with 1290 m/s velocity by giving different values of L_{sph}. It can be noticed that the radial size of the SPH domain does not have much influence if only investigating the penetrating trajectory of the projectile. Thus, to reduce simulation time, we set the width of the SPH domain to be twice of the projectile diameter in this model.

In addition, the SPH part in this model consists of several components with different discretization length dx_i and the total number of particles is a key factor in model performance. Taddei et al.in 2015 [133] suggested a relation between the average brick element length of the master surface and dx_1 in the first SPH component (see the scheme of model in Fig.4.7). The first SPH component is one which interacts with the projectile directly and thereby predominantly affects the impact trajectory in this simulation. Results in term of penetrating trajectory of 1290 m/s impact are presented in Fig.4.10 to show a suitable value of dx_1 ranging from 0.4 μm to 0.5 μm.

4.4.1.2/ ARTIFICIAL VISCOSITY AND XSPH

Artificial viscosity and XSPH (also called Conservative Smoothing) were developed in order to ensure numerical stability of the SPH method, but both of them can generate unavoidable and unphysical energy dissipation. Shaw et al.[103] showed that it easily makes the system over-dissipative if unsuitable artificial viscosity parameters (qa, qb) are used. Studies in the literature also indicate that artificial viscosity has an important influence on the penetration history [133, 41].

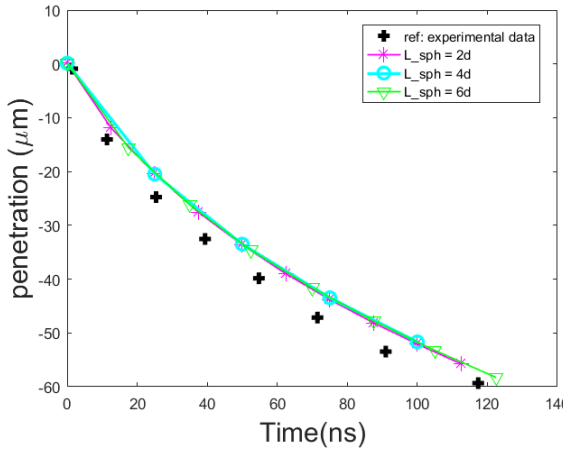

Figure 4.9: The numerical trajectories with different width L_{sph} of SPH column, compared to experimental result.

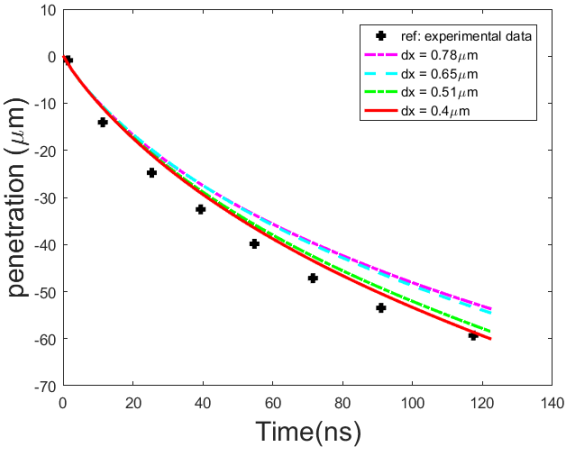

Figure 4.10: The numerical trajectories with different discretization length dx_1 of SPH particles, compared to experimental result.

Fig.4.11 illustrates the numerical curves of silica particle penetration with different series of artificial viscosity coefficients $(\mathrm{qa}, \mathrm{qb})$. It can be noticed that the different sets of values $(\mathrm{qa}, \mathrm{qb})$ yield no large difference in micro-particle impact to gelatin. In general, the larger values of $(\mathrm{qa}, \mathrm{qb})$ can produce more energy dissipation in the system while keep the smoothness more easily during particles movement. Considering the correlation between the numerical and experimental trajectories, (0.5,0.2) is better for the values of $(\mathrm{qa}, \mathrm{qb})$ (see Fig. 4.11), which is in accordance with previous studies on macro-scale particles impacts in gelatin [133].

Likewise, we investigate the effects of the XSPH coefficient α_{cs} on penetration trajectories(see the Fig.4.12). A larger value of α_{cs} leads to a smaller final penetration compared to the experimental result because of more kinetic energy loss among particles. The XSPH term is regarded as an approach to mitigate the tensile instability in solids. What can be noticed in Fig.4.12 is XSPH coefficient which seems to affect more at the end than at the beginning of impact. It can be explained by the fact that at the end of impact, when the penetration velocity is small, the elastic-plastic behavior is more important and tensile instability happens, which may be the cause of poor accuracy. Then, a value of $\alpha_{cs} = 0.015$ is chosen as a suitable value for the microparticle penetration problem.

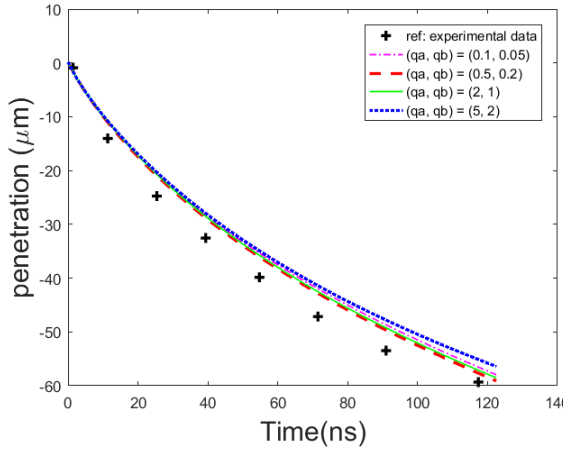

Figure 4.11: Comparison between experimental result and numerical curves using different values of artificial viscocity coefficients (qa, qb).

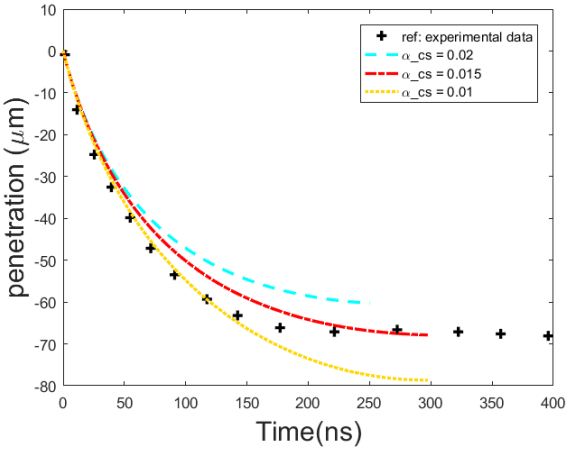

Figure 4.12: Comparison between experimental result and numerical curves using different values of conservative smoothing α_{cs}.

4.4.2/ GENERAL VALIDATION

To understand the process of microparticle impact into gelatin using the numerical model, determining and validating material parameters in constitutive laws is an important task, especially for gelatin material whose elastic modulus is complex and defined in a wide range. A series of simulations are conducted using a 7.38 micrometer diameter silica spheres impact into 10 wt% gelatin, and the effect of the young modulus value is investigated. The Tab. 4.5 shows four cases in which the value of E is changed from 1 MPa to 40 MPa, and all the other SPH settings are kept the same and shown in the left of the table.

4.4.2.1/ PENETRATION TRAJECTORY

In Fig.4.13 (a), the trajectory curves for a 1290 m/s impact velocity are presented, showing the effects of E on the trajectory and the final penetration. Particularly, the penetration depth in case 4 is still increasing after 300 ns. The results in other three cases are more reasonable, in which the penetration curves tend to constant after 300 ns, the velocity reaching at 0 m/s. The experimental value of around 67 μm of maximum penetration length within 200 to 250 ns is extracted from the experiment in [**?**]. By contrast, the errors on maximum penetration length obtained by the simulations of four cases with

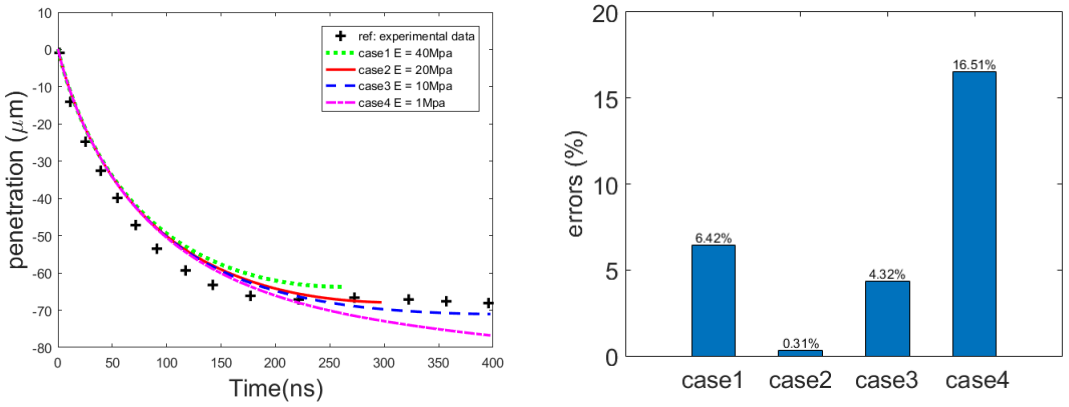

Figure 4.13: (a) Comparison between experimental result and numerical curves of four cases simulations in Tab. 4.5. (b) The errors on maximum penetration length of simulation results in four cases compared to experimental result.

Table 4.5: Simulation cases to investigate the effects of Young's modulus.

SPH parameters	Young's modulus (MPa)			
-	case 1	case 2	case 3	case 4
L_{sph} = 2d, dx_1 = 0.48 μm (qa, qb) = (0.5, 0.2), α_{cs} = 0.015	40	20	10	1

different Young's modulus E are displayed in Fig.4.13 (b). The result achieved in the case 2 with E =20 MPa is the closest to experimental data.

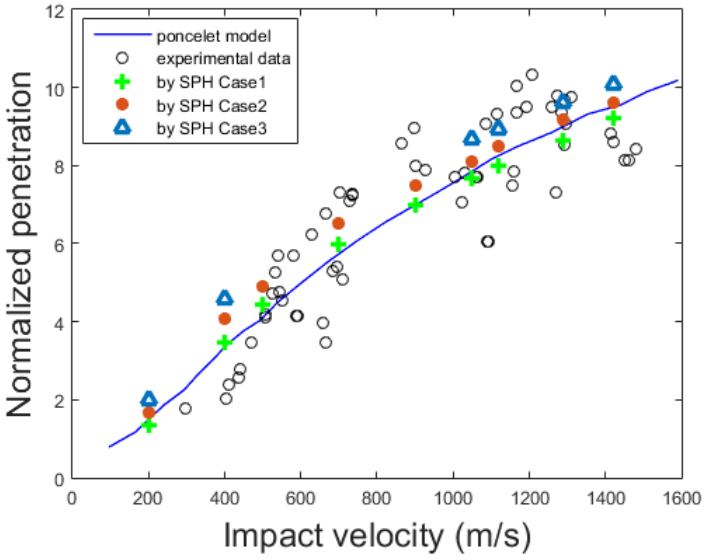

Figure 4.14: Normalized maximum as a function of impact velocity for impacts on 10 wt% gelatin with a same projectile (silica sphere with d=7.38 μm). The maximum penetration data obtained by simulations and experiments are fitted with the Poncelet model in [167].

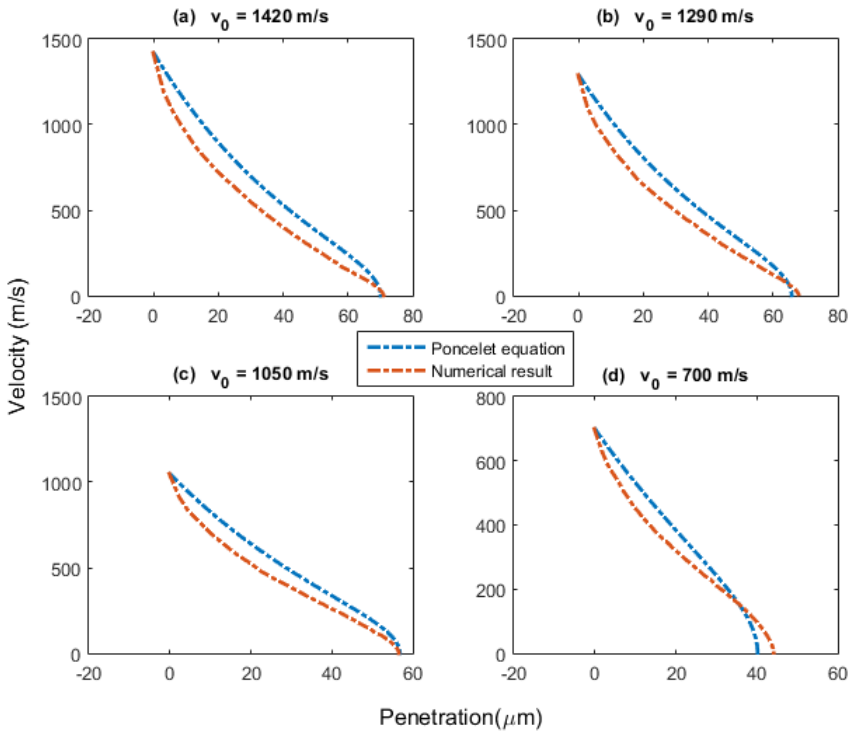

Figure 4.15: Penetration velocity vs penetration depth fitting between the Poncelet equation and simulation curves in case 2 at different impact velocities v_0.

Fig.4.14 shows the normalized penetrations (defined as P_{max}/d) of a 7.38 micrometer diameter silica particle impact the gelatin target with different impact velocities. The black circles in Fig.4.14 are experimental results by laser-induced particle impact test (LIPIT) provided by Veysset et al. [167]. The blue solid line in Fig.4.14 represents the Poncelet equation with the recommended strength resistance R = 21 MPa [167]. For the drag coefficient C_d used in Poncelet model, a value of 0.375 is applied in this work instead of 0.4 in [**?**]. This is because that a value of C_d = 0.375 can keep a consistency between maximum penetration length Eq.(4.6) and the whole time history of penetration Eq.(4.2). It can be seen that the experimental normalized penetrations are located well around the curve of the Poncelet model, which confirms the choice of the parameters C_d = 0.375 and R = 21 MPa.

The numerical results were compared to the experimental data and the Poncelet analytical model in Fig.4.14 involving cases 1 to 3, ignoring case 4 whose results where much farther from the experimental data. It can be observed that the numerical results match relatively well the experimental data, as well as the Poncelet equation. Therefore, the results demonstrate that this numerical model is a promising approach to simulate penetra-

tion of microparticles into 10wt% gelatin. Based on these numerical results, the Young's modulus values between 10 MPa to 40 MPa are applicable when using elastic-plastic hydrodynamic behavior law to model 10wt% gelatin. Fig.4.15 illustrates the penetration velocity as a function of the penetration depth in simulations with E = 20 MPa for silica particle impact with 1420 m/s, 1290 m/s, 1050 m/s, and 700 m/s, respectively. From these figures, it can be seen that the numerical curves are also in agreement with the Poncelet equation.

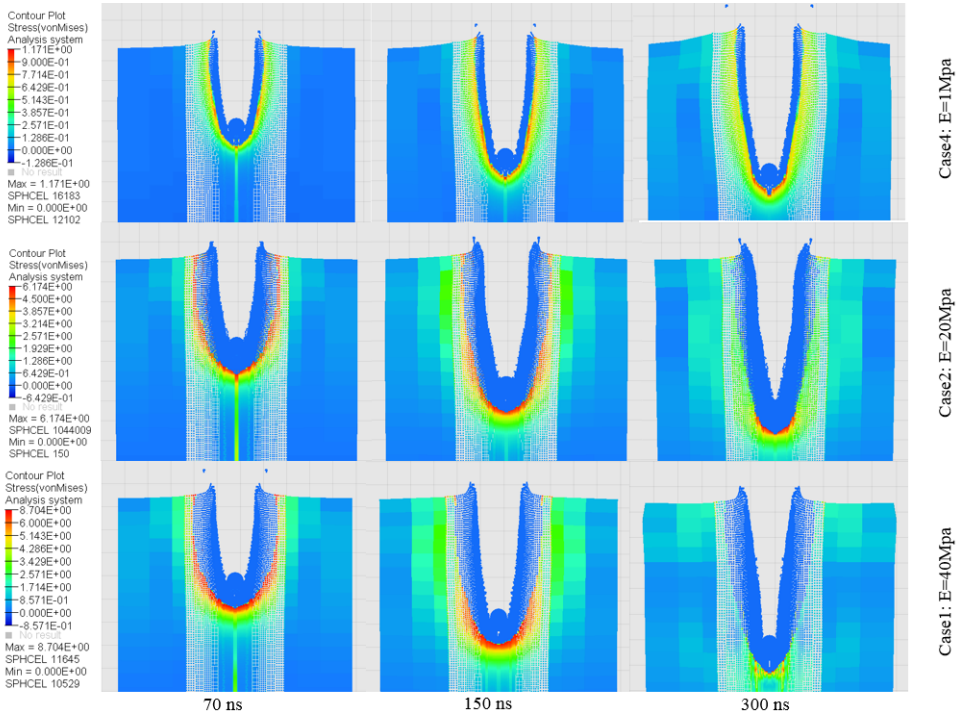

Figure 4.16: The dynamic process of cavity in gelatin sample impact with 1290 m/s; Contours of stress in the gelatin around the temporary cavity and a comparison in three cases of simulations with different Young's modulus E are presented. The result of case 3 ignored involves the similar shape with that in the case 2.

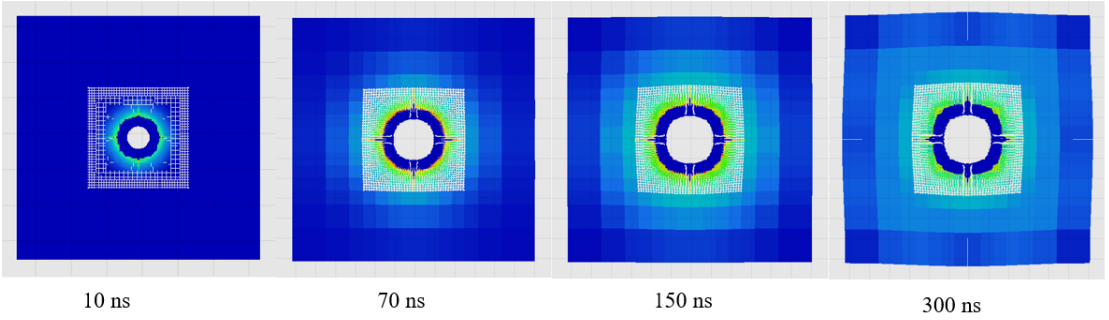

Figure 4.17: The diameter of temporary cavity in gelatin sample in the case 2 simulation with E = 20 MPa at 10 ns, 70 ns, 150 ns, and 300 ns after impact.

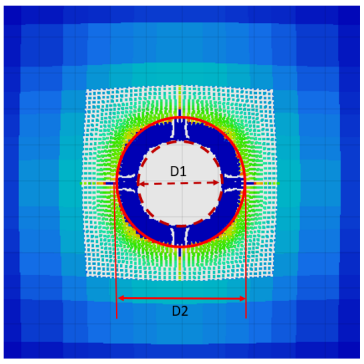

Figure 4.18: The measure of cavity diameter in in the numerical simulation from Fig.4.17; the blue area between D1 and D2 means the damaged SPH particles with zero stress.

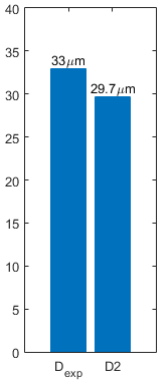

Figure 4.19: The maximum cavity diameters obtaind by experiment (D_{exp}) and simulation (D2).

4.4.2.2/ CAVITY EVALUATION AND DISCUSSION

Another important point in the phenomenon of gelatin perforation by a projectile is the size of the cavity. Although the penetration is a very important parameter to investigate, the size of the cavity in the radial dimension is also of interest. As it can inform, for instance, about the extent of tissue damage following projectile penetration. Fig.4.16 shows the shapes of the cavity obtained using the different elastic modulis considering the same silica particle impacting the target at 1290 m/s. The shape is exhibited like a slender cone that with the tunnel of time expands in both radial and longitudinal directions. It also can be observed that the cavity tends to collapse more quickly after expanding to the maximum size in the case the target sample with a larger Young's modulus (more intuitively by the contrast between case 1 and case 4). The behavior of collapse in the temporary cavity is derived from the recovery of elastic deformations of target gelatin.

Fig.4.17 shows the cavity diameters positioned at 15 μm to the impact face at different time points in the case 2 simulation with E = 20 MPa. Fig.4.18 presents the approach to measure the cavity diameter in simulation result, denoting that D1 is the size of real empty cavity and D2 is the diameter of cavity including damaged particles area. The values of maximum cavity size obtained by the experiment and simulation (Fig.4.19) are observed and we note that the maximum diameter D2 of the numerical cavity is very close to the experimental data if the cavity considering the damaged particles (the error less than 10%).

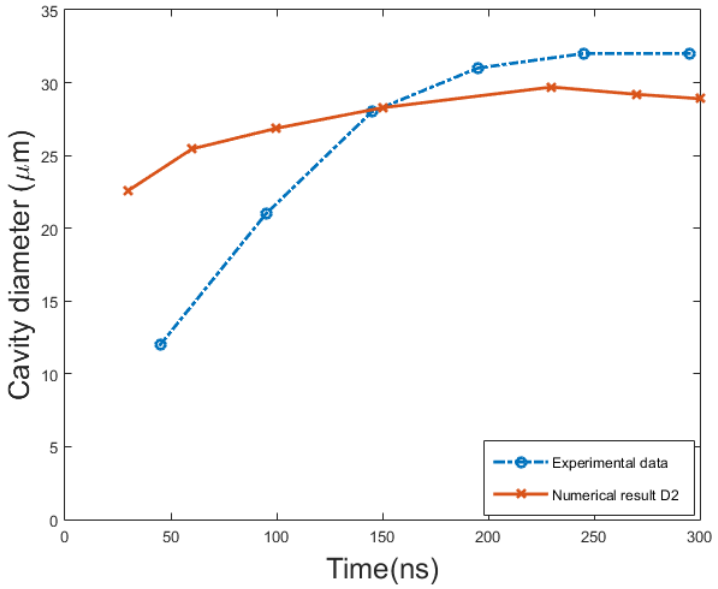

Figure 4.20: The time history of cavity diameter in gelatin for the experiment and numerical simulation. The experimental data is provided by Veysset et al.[167].

Fig.4.20 displays the time history of cavity diameter in gelatin for the experimental and simulation results. It can be noticed that the cavity in simulation expands very rapidly at the primary stage after impact. After 150 ns, nevertheless, the expanding trend of the numerical cavity is close to the experimental result. The discrepancy may be attributed to the predominantly hydrodynamic behavior at initial penetration, or reasonably no considering the hyperelastic property of the gelatin material in the numerical model. Although the value of the maximum cavity diameter obtained by SPH simulation is in the same order of amplitude with experimental results, the dynamic process of the cavity in gelatin should be more investigated in further research.

4.5/ SIMULATIONS ON BALLISTIC SEBS GEL

4.5.1/ THE PARAMETERS IN NUMERICAL AND MATERIAL MODELS

The same numerical model in Fig.4.7 is used to investigate the ballistic response of 40 vol% SEBS gel impacted by micro steel spheres. The numerical results are validated against experimental data provided by [2]. The numerical parameters including the size of SPH domain L_{sph}, artificial viscosity coefficients (qa, qb), the smallest particle distance

dx_1, and XSPH coefficient α_{cs}, are firstly managed.

The projectile is non-deformable and discretized by FEM elements. The element size on the projectile is controlled as $L_{av}/12$, L_{av} and D being the average element size and diameter of the projectile, respectively. Then, the target domain (SEBS gel block) is discretized by SPH particles according to the principle that L_{av}/dx_1 larger than 1.4 based on previous research [133]. L_{sph} is also set twice of diameter D, the same with simulations on gelatin impact. Next, about the coefficients of artificial viscosity and XSPH, a series of simulations are performed to validate them.

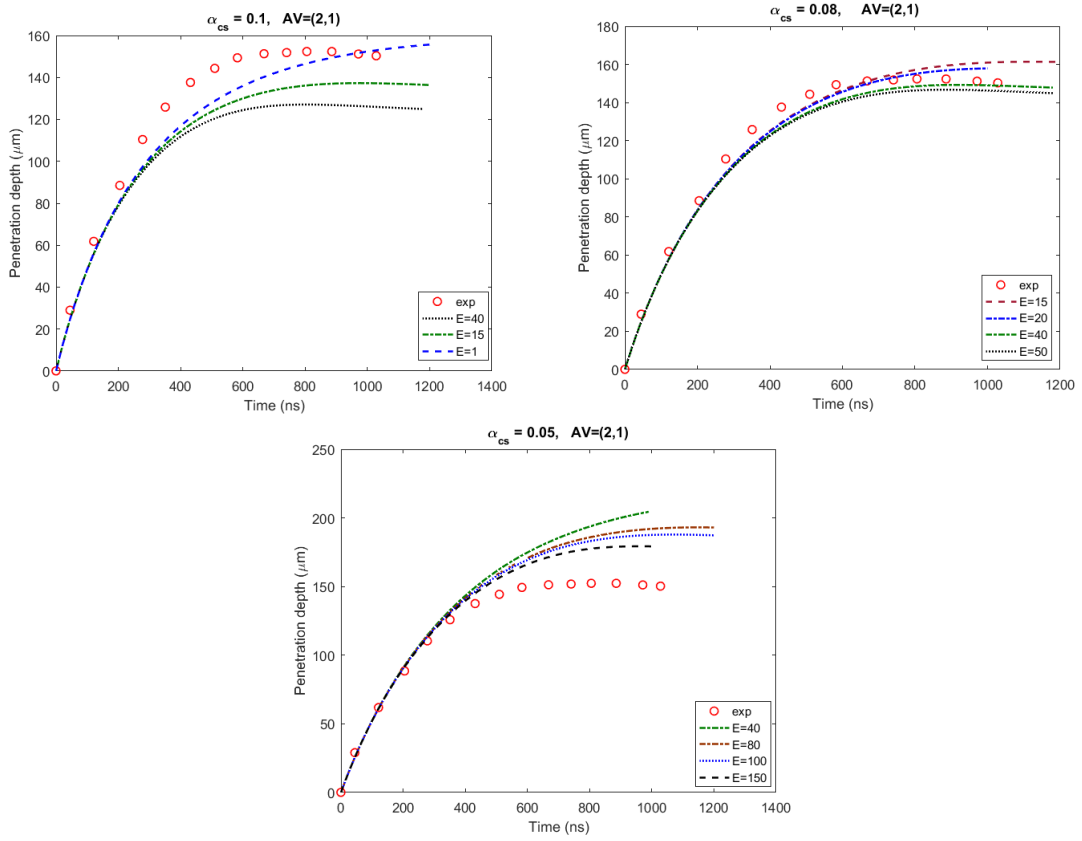

Figure 4.21: The numerical results for simulating the penetration in 40 vol% SEBS gel by D=13μm at 630 m/s: (a) α_{cs}=0.1 (b) α_{cs}=0.08 (c) α_{cs}=0.05; the value of Young's modulus is in the range of 1-150 MPa.

A series of simulations are carried out on the penetrations involving a D=13 μm steel impacting into SEBS gel with 630 m/s using different values of XSPH coefficient α_{cs} (0.1, 0.08, and 0.05). In this case, the coefficients of (qa, qb) are set as (2,1) as used previously for SPH simulations [215]. Because there is no experience with the value of Young's model for SEBS gel material in the micro-scale case, a range of values is applied for each case with a fixed α_{cs}. Fig.4.21 shows the numerical results compared with the

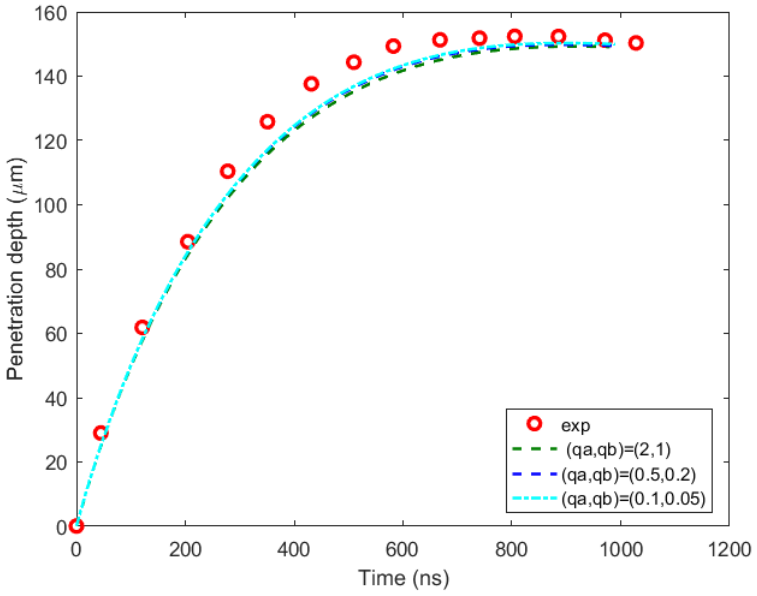

Figure 4.22: The curves of steel particle $D = 13$ impact with 630 m/s are obtained by SPH model with different values of artificial viscosity coefficients $(\mathrm{qa}, \mathrm{qb})$.

experimental data. It can be seen that the numerical curves with a small range of Young's modulus are closer to the experimental trajectory in Fig.4.21 (b) compared to Fig.4.21 (a) using α_{cs}=0.1 and (c) using α_{cs}=0.05. Besides, the values of Young's modulus from 15 MPa to 50 MPa used in the Fig.4.21 (b) are located in the predicable range of 1-100MPa. On the contrary, in the other two cases of α_{cs}=0.1 and 0.05, numerical curves still can not match with experimental trajectory even the Young modulus decreases to 1 MPa or increases to 150 MPa, respectively. Therefore, a specific value of α_{cs}=0.08 is employed in this numerical model.

With the specific values of XSPH α_{cs}=0.08 and Young's modulus 50 MPa, Fig.4.22 also illustrates the performances of this SPH model with several different artificial viscosity coefficients by simulating the same penetration case with Fig.4.21. Obviously, the artificial viscosity does not lead to much difference of the numerical results, so the recommended value of (2,1) is used in this model.

Subsequently, the value of Young's modulus E is further validated by conducting the simulations on the various penetrations involving the different size projectiles and impact velocities. Fig.4.23 and 4.24 show the numerical results for the penetrations with the projectile of D=20 μm at 215 m/s and D=22 μm at 300 m/s using a range of 15-50 MPa of the Young's modulus. It can be found that the simulations with E = 40-50 MPa illustrate better

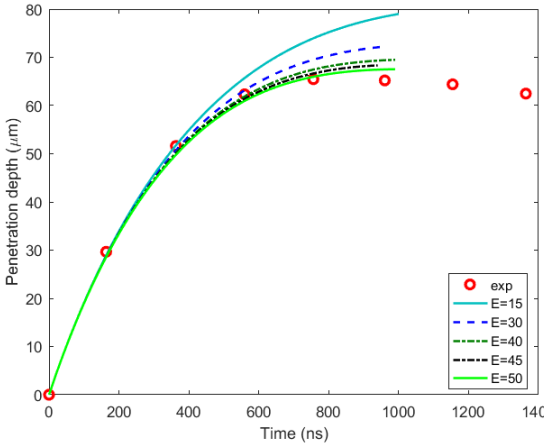

Figure 4.23: The curves of steel particle $D = 20$ impact with 215 m/s are obtained by SPH model with the coefficients $\alpha_{cs} = 0.08$, (qa, qb)=(2,1), compared to the experimental data.

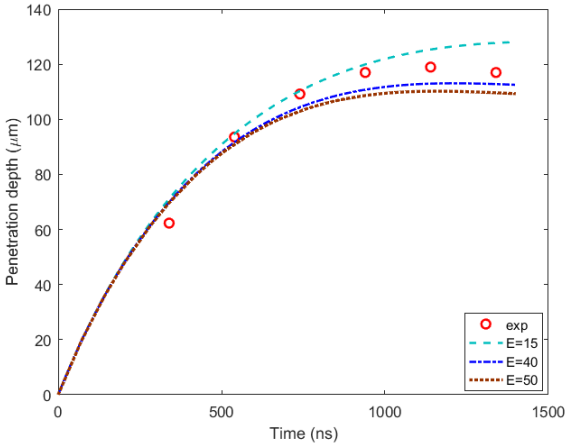

Figure 4.24: The curves of steel particle $D = 22$ impact with 300 m/s are obtained by SPH model with the coefficients $\alpha_{cs} = 0.08$, (qa, qb)=(2,1), compared to the experimental data.

agreements with experimental results. From comparisons between the simulations and experiments in the Fig.4.21,4.23, and 4.24, when using a linear-elastic hydrodynamic law for the SEBS gel as target material, Young's modulus can be set to 40-50 MPa.

4.5.2/ THE GENERAL VALIDATION

As a general validation, more simulations involving different diameter projectiles are carried out using this SPH model with the above numerical parameters and two values of Young's modulus. Fig.4.25 demonstrates the normalized maximum penetration depth as a function of impact velocities by various projectiles with the diameters from 11-22 μm. It can be seen that for both E=40 and 50 MPa, the agreement between numerical simulations and experimental results can be acceptable on the maximum penetration depths.

In addition, the time histories of penetrations acquired by numerical simulations are compared with the results of the experimental results in the cases the projectiles of two diameters (D=12 and 16 μm) from Fig.4.25. Good agreements are obtained in Fig.4.26 and 4.27. Moreover, the numerical simulations are also compared with the results of the Modified-CG model with the fitting coefficients (R=25MPa, η=4.5e-2). Fig.4.28 represents four penetration trajectories by the projectiles D = 19, 15, 13 and 11μm with various impact velocities. This comparison provides a further evidence to the reasonability of

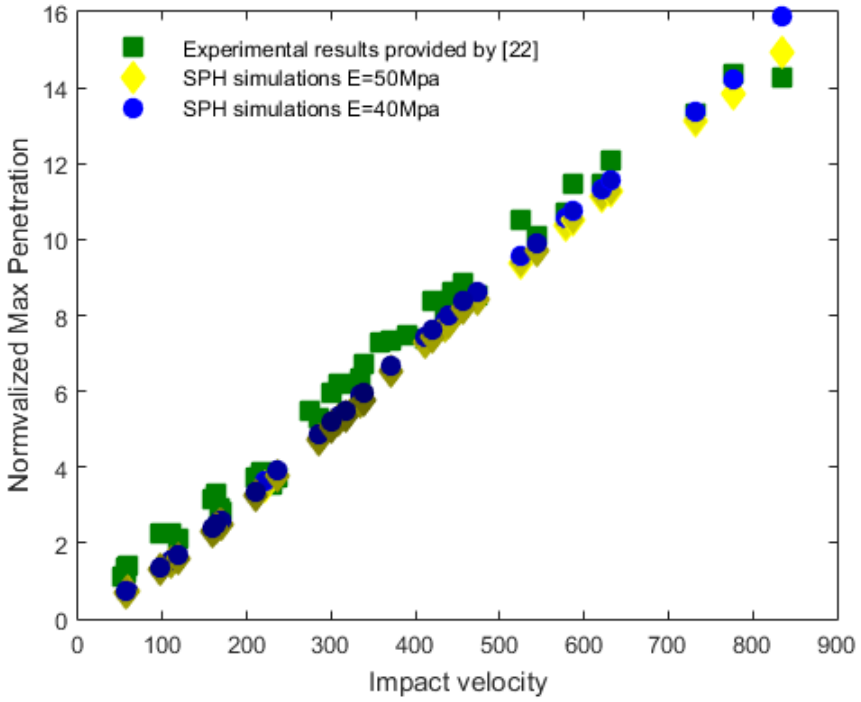

Figure 4.25: The normalized maximum penetration depths is the function of the impact velocity, involving a various projectile diameters from 10-22 μm and impact velocities from 50-900 m/s. The darker color is associated with a larger diameter of the projectile in the simulation results. A comparison is represented between numerical and experimental results.

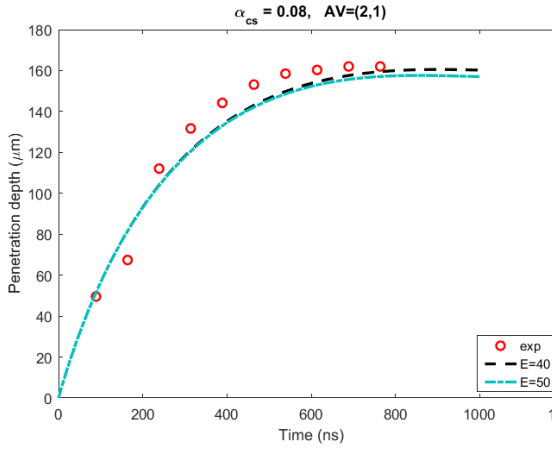

Figure 4.26: The curves of steel particle $D = 12$ impact with 735 m/s are obtained by SPH model with the coefficients $\alpha_{cs} = 0.08$, (qa, qb)=(2,1), compared to the experimental data.

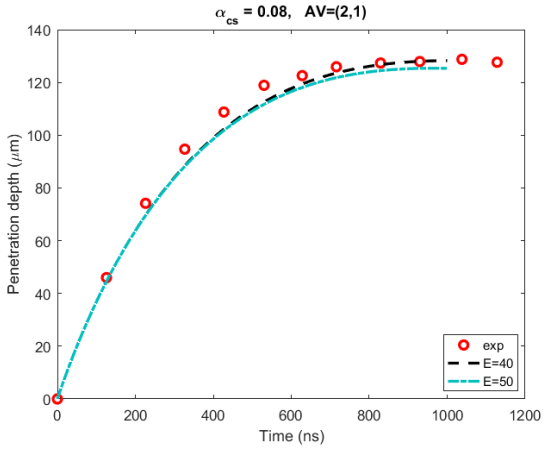

Figure 4.27: The curves of steel particle $D = 16$ impact with 440 m/s are obtained by SPH model with the coefficients $\alpha_{cs} = 0.08$, (qa, qb)=(2,1), compared to the experimental data.

this numerical model: a linear-elastic hydrodynamic behavior for SEBS gel target in the penetration simulations. The value of Young's modulus can be set as 40-50 MPa.

In addition, Fig.4.29 illustrates the shapes of the temporary cavity in the SEBS gel target at 100, 200 and 300 ns after impact during the penetration by the D=13 projectile with 630 m/s. Firstly, it can be observed that the strain distribution demonstrates an extreme deformation located around the projectile. Then, the revolution of the cavity shape can be discovered like a slender cone expanding and then shrinking with the tunnel of time in the longitudinal direction, which shows a similar trend between experimental and numerical results, compared to Fig.4.3.

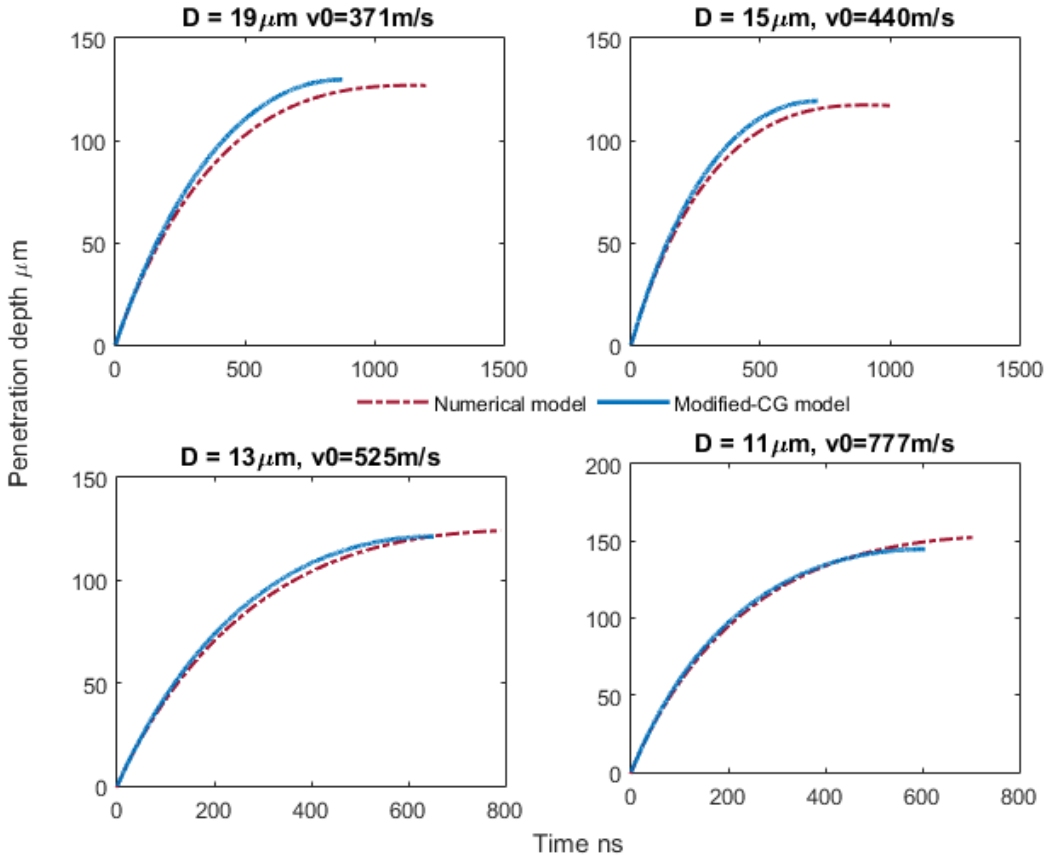

Figure 4.28: The comparisons between the analytical results by Modified-CG and numerical simulations in various penetrations.

4.6/ DISCUSSION

4.6.1/ NUMERICAL PARAMETERS

The numerical model consisting of SPH particles and FEM elements has been employed several times in the application of macro-penetrations such as [133, 57]. In this thesis,

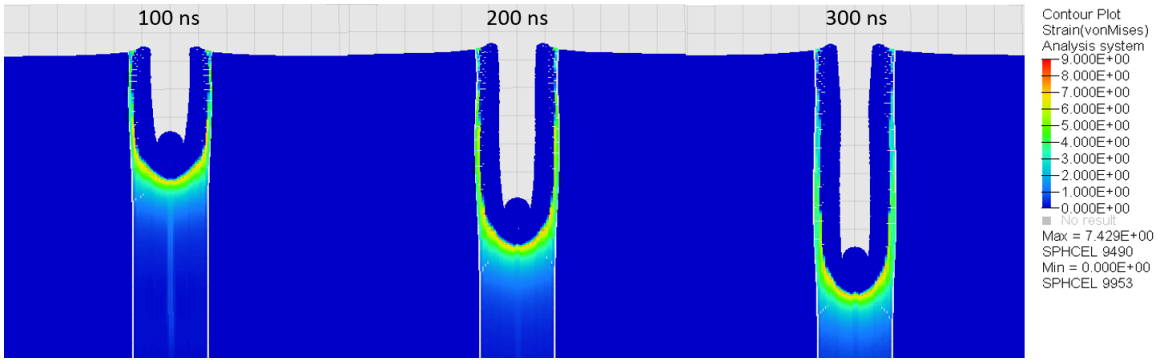

Figure 4.29: The temporary cavity in the SEBS gel during the penetration by D=13μm at 630 m/s: the strain distributions at three time points from the longitudinal direction; the value of Young's model used in this case is 50 MPa.

the employment of this numerical model is expanded to the ballistic behavior of soft materials in the micro-scale. A number of validations in 4.4.2 and 4.5.2 demonstrate that this numerical model is capable to acquire a general prediction for the trajectories of projectiles penetrating simulant of soft tissues including gelatin and SEBS gel, but it has to be admitted that all the validations for the simulation results are under the conditions of fixed and specific numerical settings (a fixed SPH particles discretization and a fixed coefficient of XSPH).

Fig.4.12 and Fig.4.21 illustrate that the usage of XSPH produces a substantial influence for the numerical trajectories, especially at the end of penetrations. This result in the micro-scale was not observed before since the standard employment of this corrective procedure does not have such influence in the classical macro-scale [24]. It is worthy to notice that the values of the XSPH coefficient and Young's modulus seem to represent a uniform effect on the trends of numerical penetrations at the half-section. It can be explained that an increase in Young's modulus leads to the harder target material and then more resistance stops the projectile more quickly. At the same time, an increase in the XSPH coefficient also makes a faster stop of the projectile during the penetrations, which can be surmised from multiple factors.

Firstly, at the end of penetrations, the velocity of the projectile decreases, and the target materials behaves predominately as elastic-plastic deformation, which can lead to particles clumping, and finally lead to tensile instability. Tensile instability is recognized as a severe problem when the solid materials are stretched simulated by the SPH method [23]. The XSPH also called smoothing conservative can mitigate the tensile instability by

smoothing the velocity field of the particles in the influence domains controlled by the SPH kernel function, but it produces energy dissipation in the system [96]. That is the reason why XSPH coefficient produce larger discrepancies between experimental and numerical results at the end of the penetration than at the beginning. Secondly, the function of the XSPH also can be regarded as adding a kind of friction to the interface between projectile and target material. The retardation force to the projectile coming from the target material consists of inertia force, resistance force, as well as friction part according to the analytical study for penetrations [168]. Therefore, it is perhaps also a factor that the higher values of the XSPH coefficient provide more friction to make the projectile stop quickly.

4.6.2/ MATERIALS PARAMETERS

The linear-elastic hydrodynamic law is attempted to study the ballistic behavior of gelatin and SEBS gel. The first consideration to use this is that the movement of soft material under high-velocity impact has a fluid hydrodynamic behavior especially at the beginning of penetration, which has been reported in various research like [216, 178]. The second concern is that a macro-scale investigation to SEBS gel by [132] demonstrated a small difference between using a linear-elasticity and nonlinear-elasticity depending on the strain rate. Moreover, the experimental and analytical observation for gelatin under micro-impacts [2, 210] discovered a multiplier increase on the strength of target materials when the penetrations involve a higher strain rate, especially the dimension transitions from macro-scale to micro-scale.

Therefore, during the simulations, the initial Young's modulus of ballistic gelatin was predicted in the range of 1-100 MPa referring the value of E = 1 Mpa used for the macro penetrations [57]. Subsequently, the range of Young's modulus was narrowed down to a more suitable value to predict the general trajectories of penetrations. The final values of Young's modulus for 10 % gelatin are 20-40 MPa, which is matched with this trend. The same range of 1-100 MPa was for ballistic SEBS gel under micro-impacts compared to 0.12 MPa used in the macro cases [132]. The final values of Young's modulus for 40 vol% SEBS gel are 40-50 MPa. According to the investigation of the relation between mechanic properties and penetrations for SEBS gel in the macro-scale [161], the authors described the penetration depths in SEBS gel using the elastic Froude number involving Young's modulus ranging from 60 to 630 kPa on the macro-scale. Therefore, a range of

40-50 MPa extracted for the value of Young's modulus for the SEBS gel under the micro penetrations in this study can be reasonable.

As mentioned that this numerical model is capable to predict the trajectory of micro-penetrations, but the results are depending on a fixed set of numerical parameters including the discretization density and coefficients of the XSPH. Because the numerical validations are based on these numerical parameters, the extracted values of Young's modulus for both ballistic gelatin and SEBS gel are limited to the exact physic. As known that the mechanical properties of soft tissues become questionable when they are under the micro-impact loading. Although the non-linear elastic or hyper-elastic properties are identified widely in the literature, there is no much study to extract the quantitative values of elasticity (Young's modulus or shear modulus) for soft materials like ballistic gelatin and SEBS gel. Gelatin has become the most common simulant to be investigated to understand the penetrating process in the macro-scale, but the behavior shows a considerable different in the micro-scale. The SEBS gel is recognized as involving a better performance as a simulant of soft tissues compared to the gelatin, unfortunately, its mechanical properties are less investigated in the literature. To the authors' knowledge, there is no failure model developed for SEBS gel up to now, particularly, for the micro-scale condition. In this numerical model, the simplest failure model was attempted for both of gelatin and SEBS gel, which maybe should be further improved to model the breaking process of soft materials during the impacts. The size of temporary cavity is strongly linked to failure criterion in the penetration, as shown in the Fig.4.17 for gelatin and Fig.4.29 for SEBS gel, which also limits the quantitative investigation on the cavity size in this model. The other concern is the high strain rate which is identified in the cases involving the micro-scale and the high-velocity impact. It also can be noticed that in the Fig.4.25, the accuracy of numerical result decreases at the case with a higher impact velocity (close to 900 m/s), while the modified-CG model demonstrates a better fit in this point, as seen in the Fig.4.5. It can be explained that the viscosity becomes more important in the micro-penetration with a higher strain rate, which is taken into account into the modified-CG model [2]. Therefore, a more accurate constitutive law for ballistic gelatin and SEBS gel including the strain rate, viscosity, and even failure criterion should be further developed.

4.7/ CONCLUSION

This chapter provided the investigations on ballistic behavior of soft materials including 10 % gelatin and 40 vol% by analytical and numerical approaches. Firstly, the performances and fitting coefficients for three analytical models were discussed to model the penetrating trajectories in the micro-scale. Analytical models such as Poncelet, Liu, and Modified-CG models are practical tools to obtain the trajectory thanks to their simple formulations by deducting the retardation force from different parts including inertia, resistance, and viscosity or friction. But, for the penetrations in the micro-scale involving more complex mechanics, especially, the strain rate higher than $10^6 s^{-1}$, the robustness of their coefficients highly depends on the fitting procedure requiring tremendous experimental data, which weaken the value of avoiding high experimental costs as analytical models.

The main contribution in this chapter is to develop a numerical model based on SPH method to the micro-impacts with high velocities. A large number of simulations were performed for penetrations into two kinds of soft materials involving a variety of projectile sizes from 7-22 μm with velocities from 50-1300 m/s. The numerical trajectories and maximum penetrating depths were predicted well and agreed with the experimental and analytical models. The ranges of Young's modulus for both ballistic gelatin and SEBS gel were extracted based on the agreement between numerical and experimental results. Then, a discussion about numerical results was provided, including the numerical parameters, physical parameters, as well as the limitations of this model.

5

CONCLUSIONS, LIMITS, AND PERSPECTIVES

5.1/ CONCLUSIONS

Transdermal drug delivery is one of the most significant technologies in the pharmaceutical industry. This kind of techniques such as a needle-free drug delivery device typically include the process of micro-particles travelling through the soft tissues. The micro-particles size of the drug powders generally is on the range of 1-20 μm, and they penetrate into soft tissues at a high velocity and finally integrate into the soft tissues at some depths. A good understanding on several factors in this process involving the particle diameters, trajectories, and momentum or velocities of projectile, as well as the deformation of soft tissues is required in order to develop this technique and design the relevant device. At the same time, numerical simulation become one of the important approaches to study the engineering problems thanks to the large advance of computer science. Therefore, this thesis developed a numerical model based on a particle method to investigate the ballistic behavior of two kinds of simulant of soft tissues during the micro-penetrations.

Firstly, this thesis provided a state of the art on the advances in ballistic perforation impact on structures. The advantages of SPH method are convinced during this review. The property of particle discretizations of SPH method makes it naturally suitable for modeling the structures involving large deformations, particularly for the debris clouds and fragmentation phenomenons during HVIs. The appendix table lists a large number of examples on SPH simulating HVI process. However, in terms of penetrations on

thick structures, typically happened in soft materials, there are only a few studies by SPH method. Particularly, for high-velocity impacts into soft materials in the micro-scale, there is no investigations concerning numerical simulations in the literature. Taking into account this vacancy in the applications of SPH simulations, this thesis developed an SPH model to investigate the ballistic process in the soft materials including 10% gelatin and 40 vol% SEBS gel under micro impacts.

After confirmed the target and method of this research, the first part in the chapter 2 is to develop a SPH code to study the dynamic solids, aiming to understand the algorithm and procedure of SPH method and its performances in some benchmark problems. This code is implemented for elastic-plastic formulations based on the standard SPH combined with artificial viscosity, artificial stress, XSPH terms , as well as a correction on kernel calculation (CSPH). The role of SPH kernel was paid attentions during programming this code. The relationship between the inhered shortcoming called tensile instability happened in the SPH simulation for solid problems and its kernel function types was studied. This code involves six kinds of kernel functions like traditional ones (Gaussian function, B-spline functions, Wendland function), and new types constructed for some specific problems (Double cosine function and Hyperbolic shaped). These kernel functions demonstrate a different accuracy and stability for SPH algorithm because of their mathematical properties on shapes, derivatives, smoothness, and influence domains. A series of common examples including elastic beam vibration and Taylor rod impacts were simulated with this code. By comparisons, the most suitable function called Wendland is confirmed to achieve a stable and accurate simulations for elastic-plastic solids. This code also provides an useful preparation including the kernel function and numerical parameters to develop the SPH model to complex ballistic process.

Ballistic gelatin is one of the main simulant of soft tissues, which has been investigated experimentally and numerically in the literature in the macro-scale. The synthetic polymer SEBS gel (styrene-ethylene-butylene-styrene) is recognized recently as a better simulant because of its several benefits like environmental stability, reproducibility, mechanical consistency, transparency, and biofidelic ability to reproduce human soft tissues behavior. The second contribution of this thesis in the chapter 4 is the development of a numerical model based on SPH particles and FE elements using the commercial software Hyperworks to investigate the ballistic behavior of 10% gelatin and 40 vol% SEBS gel under

micro impacts with high velocities. One of the challenges in this study is to determine the material constitutive law and related material parameters because of the complex mechanical properties of soft materials such as hyper-elasticity, viscous-elasticity, high sensitivity on strain rate, as well as the hydrodynamic process. A elasto-hydrodynamic law using a constant elastic modulus and EOS is employed for both gelatin and SEBS gel. According to the validations of the model against experimental results, the ranges of young's modulus were determined, being 20-40 MPa for 10% ballistic gelatin and 40-50 MPa for 40 vol% SEBS gel, respectively. This result matches with the observations from other experiments and analytical models that the resistance and strength of soft material increase when the penetrations transform from macro-scale to micro-scale. The numerical parameters including artificial viscosity and XSPH coefficients, as well as particle density were studied to achieve a stable numerical model. Then, a series of simulations for gelatin impacted by a silica particle with 7.38 μm with initial velocities ranging from 200 to 1290 m/s were carried out and good agreements were obtained between numerical and experimental results in terms of trajectories of projectiles. This model also successfully simulated the trajectories of steel spheres with various sizes penetrating 40 vol% SEBS gel by different velocities.

To sum up, the main contribution of this thesis is further expanding the application of SPH method to complex dynamic solids. One part focus on the SPH algorithm itself to study the relation between the SPH kernel types and the instability in simulating elastic-plastic solids. The other part is to develop a SPH model for the penetrations of micro-particles into soft materials (gelatin and SEBS gel), and a good investigation is achieved by SPH simulations.

5.2/ LIMITS

This thesis mainly provided an investigation on the ballistic behavior of the two soft materials (gelatin and SEBS gel) under micro-scale impacts via the numerical approaches. The aim is to improve and develop the transdermal drug delivery techniques which involve the process of the micro-particles penetrating soft tissues. Although the predictions of penetrating parameters like trajectories and maximum depths of the projectiles are obtained by a series of simulations by an SPH model, the investigation is still limited to

several points.

Soft materials like gelatin and SEBS gel are regarded as the simulant of living soft tissues to investigate the penetrating process because they have similar behavior. However, the complex environment of living soft tissues is difficult to be defined on artificial materials like gelatin and SEBS gel. The behavior model of soft tissues involves viscosity, hyper-elasticity, temperature sensitivity, hydrodynamic behavior, thermodynamic behavior, phase changes (liquid-solid). Besides, the mechanical properties of these soft tissues under high-velocity impact have been recognized as highly-sensitive to the strain rate in the literature. Unfortunately, there is no existence of an accurate constitutive law for this kind of material including so many complex properties.

Therefore, the employment of behavior law in this numerical simulation is the most challenging work. An elastohydrodynamic law was attempted to model the behavior of the gelatin and SEBS gel, and a simple failure criterion was employed to model their breaking process. Firstly, it is not enough accurate to model real physics, which leads to a limited investigation. Another difficulty is that the quantitative values of materials parameters, particularly, in the micro-scale cases are not confirmed in the literature. There is no much study on the mechanical properties of gelatin and SEBS gel in the micro-scale. The limited knowledge on the soft materials leads to the limited investigation in this numerical work:

It only can acquire a satisfying prediction to the trajectories and maximum penetration depths of projectiles, but the specific deformation of target materials can not be captured accurately. The temporary cavity is another important phenomenon during the penetrations into soft materials, and its evolution with time is strongly linked to the hyper-elasticity and viscosity properties. As an initial attempt in chapter 4, the maximum cavity size in ballistic gelatin is simulated closely to the experimental result, but the time-evolution is hard to model correctly. This limit also leads to the validations of numerical results depending on a fixed set of numerical parameters such as the SPH particle discretization and XSPH coefficient, as shown in the discussion part of chapter 4.

In addition, this numerical model also has some limitations by itself. By developing an SPH code to study the instability of the SPH algorithm, the main discovery in chapter 2 is that the types of kernel functions have considerable influences on the SPH simulation. A more suitable kernel called Wendland function is found to the solid dynamics, a better al-

ternative than the conventional kernels like B-spline functions. But the numerical model to the micro-penetration into soft materials is built with the commercial software Hyperworks, and the solving processor is the Radioss which is based on a standard SPH algorithm involving the B-spline kernel. Therefore, the tensile instability should be removed by extra corrective terms like XSPH. That is also one of the factors why the coefficient of XSPH produces a large difference at the end of penetration when the target material behaves predominately as elastic-plastic deformation and more possibly includes particles clumping. Therefore, a more stable and accurate SPH algorithm is required to get a better understanding of the penetrating process in the micro-scale.

5.3/ FUTURE WORKS

The ballistic behavior of soft tissues under high-velocity impact by micro-particles is investigated via numerical approaches at the first time. Taking into account the conclusion and limitations, several interesting points can be further researched:

1. The first and also the most important study on the development of the behavior laws for soft materials should be paid more attention. Especially for the simulant of soft materials including ballistic gelatin and SEBS gel, the hyper-elasticity, viscosity and dependence on strain-rate should be considered. The hydrodynamic behavior, therm-dynamic behavior, phase changes (liquid-solid) as well as failure model of soft materials under the high-velocity impact loading should be further investigated. There are a few constitutive law involving hyper-elastic or viscous-elastic properties developed for some soft materials in the literature, such as a static hyperelastic constitutive for rubber [217], Visco-hyperelastic model for skeletal muscle [218], Neo-Hookean model, Ogden model, and Mooney-Rivlin model for soft materials like ballitic gelatin and SEBS gel [219, 162, 220]. Especially, an elastohydrodynamic constitutive law depending on impact strain rate for SEBS gel was proposed in a recent work [132], which is a very promising behavior to improve the numerical investigation on the ballistic soft tissues in the micro-penetrations.

2. In terms of the SPH algorithm, the tensile instability is still an important barrier, particularly, when it simulates the impact problems involving large deformations of solid

materials. Based on the work of chapter 2, a 3D SPH code including a more suitable kernel can be developed to model the impact problem. Of course, considering the high accuracy and effectiveness, the more creative SPH formulations like Total Lagrangian SPH should be implemented for the penetration problems, instead of standard SPH algorithm [30, 31]. In addition, the interface between the projectile and target should be modeled accurately maybe considering the surface tension, which is predicted as a key factor to capture the evolution of temporary cavity in the soft materials during penetrations [171].

3. To investigate the evolution of the temporary cavity in the gelatin or SEBS gel during penetrations is important to understand the deformations of soft-tissue, which is highly based on a more accurate constitutive law for target materials as mentioned. Chapter 4.4.2 studied the temporary cavity in the ballistic gelatin, and the numerical results show that the SPH method is a very promising way to model this process, but still requires a more suitable constitutive law involving the hyper-elastic or viscous-elastic properties of soft tissues. In the drug delivery techniques, the human body penetrated by drug particles generally consists of several different soft tissues such as skin, muscle, water, inner organs, etc. The multi-layered target structure demonstrates various behaviors and then influence the trajectory of drug particles. Therefore, to investigate the penetrating parameters into the multi-layered gelatin, or multi-layered SBES gels, or even mix-layered gelatin and SEBS gels is an important study, which is also under-researched in my group [57]. In real applications like transdermal drug delivery, the drug particles integrate to the soft tissues gradually during the penetrations, which means the large deformations should also be considered on the projectiles. This is another interesting research in the future. In addition, as experimental observations [188], the micro-particles have the rebounding process after arriving at the maximum penetration depths. This phenomenon is never investigated via both analytical and numerical methods, therefore, this point will be possibly studied in the future, or based on an improved numerical model.

BIBLIOGRAPHY

[1] Guang Zhang, Ik In Lee, Tokitada Hashimoto, Toshiaki Setoguchi, and Heuy Dong Kim. Experimental studies on shock wave and particle dynamics in a needle-free drug delivery device. *Journal of Drug Delivery Science and Technology*, 41:390–400, 2017.

[2] D Veysset, Y Sun, J Lem, SE Kooi, AA Maznev, ST Cole, RA Mrozek, JL Lenhart, and KA Nelson. High-strain-rate behavior of a viscoelastic gel under high-velocity microparticle impact. *Experimental Mechanics*, pages 1–8, 2020.

[3] Jonas A. Zukas. *Introduction to hydrocodes*. Elsevier, 2004.

[4] Predrag M. Elek, Slobodan S. Jaramaz, Dejan M. Micković, and Nenad M. Miloradović. Experimental and numerical investigation of perforation of thin steel plates by deformable steel penetrators. *Thin-Walled Structures*, 102:58–67, may 2016.

[5] A. Arias, J.A. Rodríguez-Martínez, and A. Rusinek. Numerical simulations of impact behaviour of thin steel plates subjected to cylindrical, conical and hemispherical non-deformable projectiles. *Engineering Fracture Mechanics*, 75(6):1635–1656, apr 2008.

[6] Andrea Manes, Davide Lumassi, Lorenzo Giudici, and Marco Giglio. An experimental-numerical investigation on aluminium tubes subjected to ballistic impact with soft core 7.62 ball projectiles. *Thin-Walled Structures*, 73:68–80, 2013.

[7] Milan Žmindák, Zoran Pelagić, Peter Pastorek, Martin Močilan, and Martin Vybošťok. Finite Element Modelling of High Velocity Impact on Plate Structures. *Procedia Engineering*, 136:162–168, jan 2016.

[8] R. A. Gingold and J. J. Monaghan. Smoothed particle hydrodynamics - Theory and application to non-spherical stars. *Monthly Notices of the Royal Astronomical Society*, 181:375–389, 1977.

[9] L. B. Lucy. A numerical approach to the testing of the fission hypothesis. *The Astronomical Journal*, 82(12):1013–1024, 1977.

[10] Sophie Adélaıde Magnier and Frédéric-Victor Donzé. Numerical simulations of impacts using a discrete element method. *Mechanics of Cohesive-frictional Materials: An International Journal on Experiments, Modelling and Computation of Materials and Structures*, 3(3):257–276, 1998.

[11] Antonio A Munjiza. *The combined finite-discrete element method*. John Wiley & Sons, 2004.

[12] Ting Ye and Yu Li. A Comparative Review of Smoothed Particle Hydrodynamics, Dissipative Particle Dynamics and Smoothed Dissipative Particle Dynamics. *International Journal of Computational Methods*, 15(8):1–19, 2018.

[13] S. Ma, X. Zhang, and X.M. Qiu. Comparison study of MPM and SPH in modeling hypervelocity impact problems. *International Journal of Impact Engineering*, 36:272–282, 2009.

[14] Matthias Röthlin, Hagen Klippel, and Konrad Wegener. Meshless methods for large deformation elastodynamics. *arXiv preprint arXiv:1807.01117*, 2018.

[15] Ted Belytschko, Yury Krongauz, Daniel Organ, Mark Fleming, and Petr Krysl. Meshless methods: an overview and recent developments. *Computer methods in applied mechanics and engineering*, 139(1):3–47, 1996.

[16] Shaofan Li and Wing Kam Liu. Meshfree and particle methods and their applications. *Appl. Mech. Rev.*, 55(1):1–34, 2002.

[17] P.W. W Randles and L.D. D Libersky. Smoothed Particle Hydrodynamics: Some recent improvements and applications. *Computer Methods in Applied Mechanics and Engineering*, 139(1-4):375–408, dec 1996.

[18] Larry D. Libersky, Albert G. Petschek, Theodore C. Carney, Jim R. Hipp, and Firooz A. Allahdadi. High Strain Lagrangian Hydrodynamics. *Journal of Computational Physics*, 109(1):67–75, nov 1993.

[19] Rade Vignjevic, Juan R Reveles, and James Campbell. Sph in a total lagrangian formalism. *CMC-Tech Science Press-*, 4(3):181, 2006.

[20] Joe J Monaghan. Smoothed particle hydrodynamics. *Annual review of astronomy and astrophysics*, 30(1):543–574, 1992.

[21] Joseph J Monaghan and Robert A Gingold. Shock simulation by the particle method sph. *Journal of computational physics*, 52(2):374–389, 1983.

[22] JJ Monaghan. On the problem of penetration in particle methods. *Journal of Computational physics*, 82(1):1–15, 1989.

[23] Joseph J Monaghan. Sph without a tensile instability. *Journal of computational physics*, 159(2):290–311, 2000.

[24] James P Gray, Joseph J Monaghan, and RP Swift. Sph elastic dynamics. *Computer methods in applied mechanics and engineering*, 190(49-50):6641–6662, 2001.

[25] Larry D Libersky, Phil W Randles, Ted C Carney, and David L Dickinson. Recent improvements in sph modeling of hypervelocity impact. *International Journal of Impact Engineering*, 20(6-10):525–532, 1997.

[26] JK Chen, JE Beraun, and CJ Jih. An improvement for tensile instability in smoothed particle hydrodynamics. *Computational Mechanics*, 23(4):279–287, 1999.

[27] Keisuke Sugiura and Shu-ichiro Inutsuka. An extension of godunov sph: Application to negative pressure media. *Journal of Computational Physics*, 308:171–197, 2016.

[28] Shu-ichiro Inutsuka. Reformulation of smoothed particle hydrodynamics with riemann solver. *arXiv preprint astro-ph/0206401*, 2002.

[29] Timon Rabczuk, T Belytschko, and SP Xiao. Stable particle methods based on lagrangian kernels. *Computer methods in applied mechanics and engineering*, 193(12-14):1035–1063, 2004.

[30] Juan R Reveles. Development of a total lagrangian sph code for the simulation of solids under dynamioc loading. 2007.

[31] Georg C Ganzenmüller. An hourglass control algorithm for lagrangian smooth particle hydrodynamics. *Computer Methods in Applied Mechanics and Engineering*, 286:87–106, 2015.

[32] Sukanta Chakraborty and Amit Shaw. A pseudo-spring based fracture model for sph simulation of impact dynamics. *International Journal of Impact Engineering*, 58:84–95, 2013.

[33] Md Rushdie Ibne Islam, Sukanta Chakraborty, Amit Shaw, and Stephen Reid. A computational model for failure of ductile material under impact. *International Journal of Impact Engineering*, 108:334–347, 2017.

[34] Md Rushdie Ibne Islam and Amit Shaw. Pseudo-spring sph simulations on the perforation of metal targets with different damage models. *Engineering Analysis with Boundary Elements*, 111:55–77, 2020.

[35] Gary A Dilts. Moving-least-squares-particle hydrodynamics—i. consistency and stability. *International Journal for Numerical Methods in Engineering*, 44(8):1115–1155, 1999.

[36] Gary A Dilts. Moving least-squares particle hydrodynamics ii: conservation and boundaries. *International Journal for Numerical Methods in Engineering*, 48(10):1503–1524, 2000.

[37] Diego Molteni and Andrea Colagrossi. A simple procedure to improve the pressure evaluation in hydrodynamic context using the sph. *Computer Physics Communications*, 180(6):861–872, 2009.

[38] Jérôme Limido, Mohamed Trabia, Shawoon Roy, Brendan O'Toole, Richard Jennings, Wayne L Mindle, Michael Pena, Edward Daykin, Robert Hixson, and Melissa Matthes. Modeling of hypervelocity impact experiments using gamma-sph technique. In *ASME 2017 Pressure Vessels and Piping Conference*. American Society of Mechanical Engineers Digital Collection, 2017.

[39] MB Liu and GR Liu. Smoothed particle hydrodynamics (sph): an overview and recent developments. *Archives of computational methods in engineering*, 17(1):25–76, 2010.

[40] Joseph J Monaghan. Smoothed particle hydrodynamics and its diverse applications. *Annual Review of Fluid Mechanics*, 44:323–346, 2012.

[41] Gordon R Johnson. Artificial viscosity effects for sph impact computations. *International Journal of Impact Engineering*, 18(5):477–488, 1996.

[42] Gordon R Johnson and Stephen R Beissel. Normalized smoothing functions for sph impact computations. *International Journal for Numerical Methods in Engineering*, 39(16):2725–2741, 1996.

[43] JK Chen, JE Beraun, and TC Carney. A corrective smoothed particle method for boundary value problems in heat conduction. *International Journal for Numerical Methods in Engineering*, 46(2):231–252, 1999.

[44] JK Chen and JE Beraun. A generalized smoothed particle hydrodynamics method for nonlinear dynamic problems. *Computer Methods in Applied Mechanics and Engineering*, 190(1-2):225–239, 2000.

[45] RC Batra and GM Zhang. Analysis of adiabatic shear bands in elasto-thermo-viscoplastic materials by modified smoothed-particle hydrodynamics (msph) method. *Journal of computational physics*, 201(1):172–190, 2004.

[46] MB Liu and Gui-Rong Liu. Restoring particle consistency in smoothed particle hydrodynamics. *Applied numerical mathematics*, 56(1):19–36, 2006.

[47] Chun Hean Lee, Antonio J Gil, Giorgio Greto, Sivakumar Kulasegaram, and Javier Bonet. A new jameson–schmidt–turkel smooth particle hydrodynamics algorithm for large strain explicit fast dynamics. *Computer Methods in Applied Mechanics and Engineering*, 311:71–111, 2016.

[48] Marvin E Backman and Werner Goldsmith. The mechanics of penetration of projectiles into targets. *International Journal of Engineering Science*, 16(1):1–99, 1978.

[49] T Børvik, M Langseth, OS Hopperstad, and KA Malo. Ballistic penetration of steel plates. *International journal of impact engineering*, 22(9-10):855–886, 1999.

[50] Andrea Manes, Davide Lumassi, Lorenzo Giudici, and Marco Giglio. An experimental–numerical investigation on aluminium tubes subjected to ballistic impact with soft core 7.62 ball projectiles. *Thin-Walled Structures*, 73:68–80, 2013.

[51] Y. Michel, J.-M. J.M. Chevalier, C. Durin, C. Espinosa, F. Malaise, and J.-J. J.J. Barrau. Hypervelocity impacts on thin brittle targets: Experimental data and SPH simulations. *International Journal of Impact Engineering*, 33(1-12):441—-451, dec 2006.

[52] Andrew J Piekutowski. Characteristics of debris clouds produced by hypervelocity impact of aluminum spheres with thin aluminum plates. *International Journal of Impact Engineering*, 14(1-4):573–586, 1993.

[53] J.K. Chen, F.A. Allahdadia, and T.C. Carney. High-velocity impact of graphite/epoxy composite laminates. *Composites Science and Technology*, 57(9-10):1369–1379, 1997.

[54] K Shintate and H Sekine. Numerical simulation of hypervelocity impacts of a projectile on laminated composite plate targets by means of improved sph method. *Composites Part A: Applied Science and Manufacturing*, 35(6):683–692, 2004.

[55] S. Yashiro, K. Ogi, A. Yoshimura, and Y. Sakaida. Characterization of high-velocity impact damage in CFRP laminates: Part II – prediction by smoothed particle hydrodynamics. *Composites Part A: Applied Science and Manufacturing*, 56:308–318, 2014.

[56] Nikolas A Nordendale, William F Heard, Jesse A Sherburn, and Prodyot K Basu. A comparison of finite element analysis to smooth particle hydrodynamics for application to projectile impact on cementitious material. *Computational Particle Mechanics*, 3(1):53–68, 2016.

[57] Monzer Al Khalil, Hassan Frissane, Lorenzo Taddei, Shuangshuang Meng, Nadhir Lebaal, Frederic Demoly, Cynthia Bir, and Sébastien Roth. Sph-based method to simulate penetrating impact mechanics into ballistic gelatin: Toward an understanding of the perforation of human tissue. *Extreme Mechanics Letters*, 29:100479, 2019.

[58] H Frissane, L Taddei, N Lebaal, and S Roth. Sph modeling of high velocity impact into ballistic gelatin. development of an axis-symmetrical formulation. *Mechanics of Advanced Materials and Structures*, 26(22):1881–1888, 2019.

[59] Yihua Xiao, Hecheng Wu, and Xuecheng Ping. On the simulation of fragmentation during the process of ceramic tile impacted by blunt projectile with sph method. *Computer Modeling in Engineering & Sciences*, 122(3):923–954, 2020.

[60] Yihui Zhu, GR Liu, Yaoke Wen, Cheng Xu, Weilong Niu, and Guangyu Wang. Back-

spalling process of an al2o3 ceramic plate subjected to an impact of steel ball. *International Journal of Impact Engineering*, 122:451–471, 2018.

[61] Md Rushdie Ibne Islam, JQ Zheng, and Romesh C Batra. Ballistic performance of ceramic and ceramic-metal composite plates with jh1, jh2 and jhb material models. *International Journal of Impact Engineering*, 137:103469, 2020.

[62] Riccardo Scazzosi, Marco Giglio, and Andrea Manes. Fe coupled to sph numerical model for the simulation of high-velocity impact on ceramic based ballistic shields. *Ceramics International*, 2020.

[63] Robert F. Stellingwerf. Smooth particle hydrodynamics. In *Advances in the Free-Lagrange Method Including Contributions on Adaptive Gridding and the Smooth Particle Hydrodynamics Method*, pages 239–247. Springer Berlin Heidelberg, Berlin, Heidelberg, 1991.

[64] Lawrence D. Cloutman. An evaluation of smoothed particle hydrodynamics. In *Advances in the Free-Lagrange Method Including Contributions on Adaptive Gridding and the Smooth Particle Hydrodynamics Method*, pages 227–238. Springer Berlin Heidelberg, Berlin, Heidelberg, 1991.

[65] Gordon R. Johnson, Robert A. Stryk, and Jack G. Dodd. Dynamic Lagrangian computations for solids, with variable nodal connectivity for severe distortions. *International Journal for Numerical Methods in Engineering*, 23(3):509–522, mar 1986.

[66] Joseph J Monaghan. An introduction to sph. *Comput. Phys. Comm.*, 48:89–96, 1988.

[67] A.G. Petschek and L.D. Libersky. Cylindrical Smoothed Particle Hydrodynamics. *Journal of Computational Physics*, 109(1):76–83, nov 1993.

[68] R.F. Stellingwerf and C.A. Wingate. Impact modeling with smooth particle hydrodynamics. *International Journal of Impact Engineering*, 14(1-4):707–718, jan 1993.

[69] CA Wingate, RF Stellingwerf, RF Davidson, and MW Burkett. Models of high velocity impact phenomena. *International Journal of Impact Engineering*, 14(1-4):819–830, 1993.

[70] Gordon R. Johnson, Eric H. Petersen, and Robert A. Stryk. Incorporation of an SPH option into the EPIC code for a wide range of high velocity impact computations, jan 1993.

[71] Colin J Hayhurst and Richard A Clegg. Cylindrically symmetric sph simulations of hypervelocity impacts on thin plates. *International Journal of Impact Engineering*, 20(1-5):337–348, 1997.

[72] Moreno Faraud, Roberto Destefanis, David Palmieri, and Mario Marchetti. SPH simulations of debris impacts using two different computer codes. *International Journal of Impact Engineering*, 23(1):249–260, dec 1999.

[73] S Hiermaier, D Könke, AJ Stilp, and K Thoma. Computational simulation of the hypervelocity impact of al-spheres on thin plates of different materials. *International Journal of Impact Engineering*, 20(1-5):363–374, 1997.

[74] Paul H.L. Groenenboom. Numerical simulation of 2D and 3D hypervelocity impact using the SPH option in PAM-SHOCK™. *International Journal of Impact Engineering*, 20(1-5):309–323, jan 1997.

[75] Namık Kılıç and Bülent Ekici. Ballistic resistance of high hardness armor steels against 7.62 mm armor piercing ammunition. *Materials & Design*, 44:35–48, 2013.

[76] Brendan O'Toole, Mohamed Trabia, Robert Hixson, Shawoon K. S.K. Roy, Michael Pena, Steven Becker, Edward Daykin, Eric Machorro, Richard Jennings, Melissa Matthes, B. O'Toole, Mohamed Trabia, Robert Hixson, Shawoon K. S.K. Roy, Michael Pena, Steven Becker, Edward Daykin, Eric Machorro, and Richard Jennings. Modeling Plastic Deformation of Steel Plates in Hypervelocity Impact Experiments. *Procedia Engineering*, 103:458–465, jan 2015.

[77] Shawoon K Roy, Mohamed Trabia, Brendan O'Toole, Robert Hixson, Steven Becker, Michael Pena, Richard Jennings, Deepak Somasoundaram, Melissa Matthes, Edward Daykin, et al. Study of hypervelocity projectile impact on thick metal plates. *Shock and Vibration*, 2016, 2016.

[78] Yihua Xiao, Huanghuang Dong, Jianmin Zhou, and Jungang Wang. Studying normal perforation of monolithic and layered steel targets by conical projectiles with sph

simulation and analytical method. *Engineering Analysis with Boundary Elements*, 75:12–20, 2017.

[79] T Børvik, OS Hopperstad, T Berstad, and M Langseth. A computational model of viscoplasticity and ductile damage for impact and penetration. *European Journal of Mechanics-A/Solids*, 20(5):685–712, 2001.

[80] Andrew Thurber and Javid Bayandor. On the Fluidic Response of Structures in Hypervelocity Impacts. *Journal of fluide engineering*, 137(4):041101, apr 2015.

[81] Jae Sakong, Sung-Choong Woo, and Tae-Won Kim. Determination of impact fragments from particle analysis via smoothed particle hydrodynamics and k-means clustering. *International Journal of Impact Engineering*, 134:103387, 2019.

[82] Sukanta Chakraborty and Amit Shaw. Crack propagation in bi-material system via pseudo-spring smoothed particle hydrodynamics. *International Journal for Computational Methods in Engineering Science and Mechanics*, 15(3):294–301, 2014.

[83] Sukanta Chakraborty and Amit Shaw. Prognosis for ballistic sensitivity of pre-notch in metallic beam through mesh-less computation reflecting material damage. *International Journal of Solids and Structures*, 67:192–204, 2015.

[84] Sukanta Chakraborty, Md Rushdie Ibne Islam, Amit Shaw, LS Ramachandra, and SR Reid. A computational framework for modelling impact induced damage in ceramic and ceramic-metal composite structures. *Composite Structures*, 164:263–276, 2017.

[85] Md Rushdie Ibne Islam and Chong Peng. A total lagrangian sph method for modelling damage and failure in solids. *International Journal of Mechanical Sciences*, 157:498–511, 2019.

[86] ZL Zhang and MB Liu. Smoothed particle hydrodynamics with kernel gradient correction for modeling high velocity impact in two-and three-dimensional spaces. *Engineering Analysis with Boundary Elements*, 83:141–157, 2017.

[87] JR Shao, HQ Li, GR Liu, and MB Liu. An improved sph method for modeling liquid sloshing dynamics. *Computers & Structures*, 100:18–26, 2012.

[88] ZL Zhang, T Ma, DL Feng, and MB Liu. A new formula for predicting the crater size of a target plate produced by hypervelocity impact. *International Journal of Computational Methods*, 17(01):1844004, 2020.

[89] Anthony Collé, Jérôme Limido, and Jean-Paul Vila. An accurate sph scheme for dynamic fragmentation modelling. In *EPJ Web of Conferences*, volume 183, page 01030. EDP Sciences, 2018.

[90] JP Vila. On particle weighted methods and smooth particle hydrodynamics. *Mathematical models and methods in applied sciences*, 9(02):161–209, 1999.

[91] Gianluca Lavalle, J-P Vila, G Blanchard, Claire Laurent, and François Charru. A numerical reduced model for thin liquid films sheared by a gas flow. *Journal of Computational Physics*, 301:119–140, 2015.

[92] ZL Zhang, DL Feng, T Ma, and MB Liu. Predicting the damage on a target plate produced by hypervelocity impact using a decoupled finite particle method. *Engineering Analysis with Boundary Elements*, 98:110–125, 2019.

[93] ZL Zhang, K Walayat, C Huang, JZ Chang, and MB Liu. A finite particle method with particle shifting technique for modeling particulate flows with thermal convection. *International Journal of Heat and Mass Transfer*, 128:1245–1262, 2019.

[94] Shigeki Yashiro, Keiji Ogi, Tsukasa Nakamura, and Akinori Yoshimura. Characterization of high-velocity impact damage in cfrp laminates: Part i–experiment. *Composites Part A: Applied Science and Manufacturing*, 48:93–100, 2013.

[95] E Giannaros, A Kotzakolios, V Kostopoulos, and G Campoli. Hypervelocity impact response of cfrp laminates using smoothed particle hydrodynamics method: Implementation and validation. *International Journal of Impact Engineering*, 123:56–69, 2019.

[96] Y Wen, DL Hicks, and JW Swegle. Stabilizing sph with conservative smoothing. Technical report, Sandia National Labs., Albuquerque, NM (United States), 1994.

[97] Gordon R Johnson, Robert A Stryk, and Stephen R Beissel. Sph for high velocity impact computations. *Computer methods in applied mechanics and engineering*, 139(1-4):347–373, 1996.

[98] Phil M Campbell. Some new algorithms for boundary value problems in smooth particle hydrodynamics. Technical report, MISSION RESEARCH CORP ALBUQUERQUE NM, 1989.

[99] Hidenori Takeda, Shoken M Miyama, and Minoru Sekiya. Numerical simulation of viscous flow by smoothed particle hydrodynamics. *Progress of theoretical physics*, 92(5):939–960, 1994.

[100] Larry D. Libersky, Phil W. Randles, Ted C. Carney, and David L. Dickinson. Recent improvements in SPH modeling of hypervelocity impact. *International Journal of Impact Engineering*, 20(6-10):525–532, jan 1997.

[101] T Belytschko and Shaoping Xiao. Stability analysis of particle methods with corrected derivatives. *Computers & Mathematics with Applications*, 43(3-5):329–350, 2002.

[102] Ted Belytschko, Yong Guo, Wing Kam Liu, and Shao Ping Xiao. A unified stability analysis of meshless particle methods. *International Journal for Numerical Methods in Engineering*, 48(9):1359–1400, 2000.

[103] Amit Shaw and Stephen R Reid. Heuristic acceleration correction algorithm for use in sph computations in impact mechanics. *Computer methods in applied mechanics and engineering*, 198(49-52):3962–3974, 2009.

[104] Dinshaw S Balsara. Von neumann stability analysis of smoothed particle hydrodynamics—suggestions for optimal algorithms. *Journal of Computational Physics*, 121(2):357–372, 1995.

[105] John VonNeumann and Robert D Richtmyer. A method for the numerical calculation of hydrodynamic shocks. *Journal of applied physics*, 21(3):232–237, 1950.

[106] Joseph P Morris and Joseph J Monaghan. A switch to reduce sph viscosity. *Journal of Computational Physics*, 136(1):41–50, 1997.

[107] Vishal Mehra and Shashank Chaturvedi. High velocity impact of metal sphere on thin metallic plates: A comparative smooth particle hydrodynamics study. *Journal of Computational Physics*, 212(1):318–337, feb 2006.

[108] ZS Liu, S Swaddiwudhipong, and MJ Islam. Perforation of steel and aluminum targets using a modified johnson–cook material model. *Nuclear Engineering and Design*, 250:108–115, 2012.

[109] Vishal Mehra, C D Sijoy, Vinayak Mishra, and Shashank Chaturvedi. Tensile Instability and Artificial Stresses in Impact Problems in SPH. *Journal of Physics: Conference Series*, 377(1):012102, jul 2012.

[110] Keisuke Sugiura and Shu-ichiro Inutsuka. An extension of godunov sph ii: Application to elastic dynamics. *Journal of Computational Physics*, 333:78–103, 2017.

[111] Anatoly N. Parshikov, Stanislav A. Medin, Igor I. Loukashenko, and Valery A. Milekhin. Improvements in SPH method by means of interparticle contact algorithm and analysis of perforation tests at moderate projectile velocities. *International Journal of Impact Engineering*, 24(8):779–796, sep 2000.

[112] Anatoly N. Parshikov and Stanislav A. Medin. Smoothed Particle Hydrodynamics Using Interparticle Contact Algorithms. *Journal of Computational Physics*, 180(1):358–382, jul 2002.

[113] Alejandro C Crespo, Jose M Dominguez, Anxo Barreiro, Moncho Gómez-Gesteira, and Benedict D Rogers. Gpus, a new tool of acceleration in cfd: efficiency and reliability on smoothed particle hydrodynamics methods. *PloS one*, 6(6):e20685, 2011.

[114] Alexis Hérault, Giuseppe Bilotta, and Robert A Dalrymple. Sph on gpu with cuda. *Journal of Hydraulic Research*, 48(S1):74–79, 2010.

[115] H Frissane, L Taddei, N Lebaal, and S Roth. 3d smooth particle hydrodynamics modeling for high velocity penetrating impact using gpu: Application to a blunt projectile penetrating thin steel plates. *Computer Methods in Applied Mechanics and Engineering*, 357:112590, 2019.

[116] Songwon Seo, Oakkey Min, and Jaehoon Lee. Application of an improved contact algorithm for penetration analysis in SPH. *International Journal of Impact Engineering*, 35(6):578–588, jun 2008.

[117] SW Attaway, MW Heinstein, and JW Swegle. Coupling of smooth particle hydrodynamics with the finite element method. *Nuclear engineering and design*, 150(2-3):199–205, 1994.

[118] Martin Sauer. *Adaptive Kopplung des netzfreien SPH-Verfahrens mit finiten Elementen zur Berechnung von Impaktvorgaengen*. Universität der Bundeswehr München, 2000.

[119] J Campbell, R Vignjevic, and L Libersky. A contact algorithm for smoothed particle hydrodynamics. *Computer methods in applied mechanics and engineering*, 184(1):49–65, 2000.

[120] GR Johnson, SR Beissel, and CA Gerlach. A combined particle-element method for high-velocity impact computations. *Procedia Engineering*, 58:269–278, 2013.

[121] S Swaddiwudhipong, MJ Islam, and ZS Liu. High velocity penetration/perforation using coupled smooth particle hydrodynamics-finite element method. *International Journal of Protective Structures*, 1(4):489–506, 2010.

[122] Gordon R. Johnson. Linking of Lagrangian particle methods to standard finite element methods for high velocity impact computations. *Nuclear Engineering and Design*, 150(2-3):265–274, sep 1994.

[123] Gordon R Johnson and Robert A Stryk. Conversion of 3d distorted elements into meshless particles during dynamic deformation. *International Journal of Impact Engineering*, 28(9):947–966, 2003.

[124] M Rodriguez-Millan, D Garcia-Gonzalez, A Rusinek, F Abed, and A Arias. Perforation mechanics of 2024 aluminium protective plates subjected to impact by different nose shapes of projectiles. *Thin-Walled Structures*, 123:1–10, 2018.

[125] T De Vuyst, R Vignjevic, and JC Campbell. Coupling between meshless and finite element methods. *International Journal of Impact Engineering*, 31(8):1054–1064, 2005.

[126] Zhichun Zhang, Hongfu Qiang, and Weiran Gao. Coupling of smoothed particle hydrodynamics and finite element method for impact dynamics simulation. *Engineering Structures*, 33(1):255–264, 2011.

[127] Leonard E Schwer, Kurt Hacker, and Kenneth Poe. Perforation of metal plates: laboratory experiments and numerical simulations. In *Proceedings to the 9th Annual LS DYNA users conference*, 2006.

[128] Xiaotian Zhang, JIA Guanghui, and Hai Huang. Fragment identification and statistics method of hypervelocity impact sph simulation. *Chinese Journal of Aeronautics*, 24(1):18–24, 2011.

[129] Z. Zhang, L. Wang, V.V. Silberschmidt, and S. Wang. SPH-FEM simulation of shaped-charge jet penetration into double hull: A comparison study for steel and SPS. *Composite Structures*, 155:135–144, 2016.

[130] Margaret Wilson and Young-Hoo Kwon. The role of biomechanics in understanding dance movement: a review. *Journal of Dance Medicine & Science*, 12(3):109–116, 2008.

[131] John D Finan. Biomechanical simulation of traumatic brain injury in the rat. *Clinical Biomechanics*, 64:114–121, 2019.

[132] Jianbo Shen, Lorenzo Taddei, and Sebastien Roth. Numerical modeling of a human tissue surrogate sebs gel under high velocity impacts: investigation of the effect of the strain rate in an elasto-hydrodynamic law. *Mechanics of Advanced Materials and Structures*, pages 1–9, 2020.

[133] Lorenzo Taddei, A Awoukeng Goumtcha, and Sébastien Roth. Smoothed particle hydrodynamics formulation for penetrating impacts on ballistic gelatine. *Mechanics research communications*, 70:94–101, 2015.

[134] Beat P Kneubuehl. *Wound ballistics: basics and applications*. Springer Science & Business Media, 2011.

[135] John Russell Bond and Brian William Barry. Limitations of hairless mouse skin as a model for in vitro permeation studies through human skin: hydration damage. *Journal of investigative dermatology*, 90(4):486–489, 1988.

[136] Nick Maiden. Historical overview of wound ballistics research. *Forensic science, medicine, and pathology*, 5(2):85–89, 2009.

[137] Cynthia A Bir. *The evaluation of blunt ballistic impacts of the thorax*. PhD thesis, Wayne State University Detroit, MI, 2000.

[138] Nicholas R Maiden and Roger W Byard. Unpredictable tensile strength biomechanics may limit thawed cadaver use for simulant research. *Australian Journal of Forensic Sciences*, 48(1):54–58, 2016.

[139] Birger Schantz. Aspects on the choice of experimental animals when reproducing missile trauma. *Acta chirurgica Scandinavica. Supplementum*, 489:121–130, 1979.

[140] John Nicholson. Reflections on the ethics of biomaterials science. *The New Bioethics*, 19(1):54–63, 2013.

[141] AK Dabrowska, G-M Rotaru, S Derler, F Spano, M Camenzind, S Annaheim, R Stämpfli, M Schmid, and RM Rossi. Materials used to simulate physical properties of human skin. *Skin Research and Technology*, 22(1):3–14, 2016.

[142] A Bracq, G Haugou, R Delille, F Lauro, S Roth, and O Mauzac. Experimental study of the strain rate dependence of a synthetic gel for ballistic blunt trauma assessment. *Journal of the Mechanical Behavior of Biomedical Materials*, 72:138–147, 2017.

[143] Martin L Fackler and John A Malinowski. The wound profile: a visual method for quantifying gunshot wound components. *The Journal of trauma*, 25(6):522–529, 1985.

[144] DS Cronin. Ballistic gelatin characterization and constitutive modeling. In *Dynamic Behavior of Materials, Volume 1*, pages 51–55. Springer, 2011.

[145] E Newton Harvey, JH McMillen, Elmer G Butler, and William O Puckett. Mechanism of wounding. *Wound ballistics*, pages 143–235, 1962.

[146] Martin L Fackler and John A Malinowski. Ordnance gelatin for ballistic studies. detrimental effect of excess heat used in gelatin preparation. *The American journal of forensic medicine and pathology*, 9(3):218–219, 1988.

[147] Gareth J Appleby-Thomas, PJ Hazell, JM Wilgeroth, CJ Shepherd, DC Wood, and A Roberts. On the dynamic behavior of three readily available soft tissue simulants. *Journal of Applied Physics*, 109(8):084701, 2011.

[148] JM Wilgeroth, PJ Hazell, and Gareth J Appleby-Thomas. The shock response of a rendered porcine fat. *Journal of Applied Physics*, 108(9):093527, 2010.

[149] GJ Appleby-Thomas, PJ Hazell, RP Sheldon, C Stennett, A Hameed, and JM Wilgeroth. The high strain-rate behaviour of selected tissue analogues. *Journal of the mechanical behavior of biomedical materials*, 33:124–135, 2014.

[150] DS Cronin, CP Salisbury, and CR Horst. High rate characterization of low impedance materials using a polymeric split hopkinson pressure bar. In *Proceedings of the 2006 Society for Experimental Mechanics (SEM) Annual Conference and Exposition on Experimental and Applied Mechanics*, pages 314–322, 2006.

[151] DS Cronin and C Falzon. Characterization of 10% ballistic gelatin to evaluate temperature, aging and strain rate effects. *Experimental mechanics*, 51(7):1197–1206, 2011.

[152] Nishant Ravikumar, Christopher Noble, Edward Cramphorn, and Zeike A Taylor. A constitutive model for ballistic gelatin at surgical strain rates. *Journal of the Mechanical Behavior of Biomedical Materials*, 47:87–94, 2015.

[153] DS Cronin and C Falzon. Dynamic characterization and simulation of ballistic gelatin. In *2009 SEM Conference & Exposition on Experimental & Applied Mechanics, June*, pages 1–4, 2009.

[154] Qunli Liu, Ghatu Subhash, and Harold A Evensen. Behavior of a novel iterative deconvolution algorithm for system identification. *Journal of Vibration and Control*, 11(7):985–1003, 2005.

[155] Srinivasan S Naarayan and Ghatu Subhash. Wave propagation in ballistic gelatine. *Journal of the mechanical behavior of biomedical materials*, 68:32–41, 2017.

[156] Jiwoon Kwon and Ghatu Subhash. Compressive strain rate sensitivity of ballistic gelatin. *Journal of biomechanics*, 43(3):420–425, 2010.

[157] Ralph W Ansley and Terence N Smith. Motion of spherical particles in a bingham plastic. *AIChE Journal*, 13(6):1193–1196, 1967.

[158] Caitlin Humphrey and Jaliya Kumaratilake. Ballistics and anatomical modelling–a review. *Legal Medicine*, 23:21–29, 2016.

[159] Ali İhsan Uzar, Mehmet Dakak, Tahir Ozer, G Oğünç, Taner Yiğit, Cengiz Kayahan, Köksal Oner, and Dervis Sen. A new ballistic simulant" transparent gel candle"(experimental study). *Ulusal travma ve acil cerrahi dergisi= Turkish journal of trauma & emergency surgery: TJTES*, 9(2):104–106, 2003.

[160] Paul Moy, Tusit Weerasooriya, Thomas F Juliano, Mark R VanLandingham, and Wayne Chen. Dynamic response of an alternative tissue simulant, physically associating gels (pag). Technical report, ARMY RESEARCH LAB ABERDEEN PROVING GROUND MD, 2006.

[161] Randy A Mrozek, Brad Leighliter, Christopher S Gold, Ian R Beringer, H Yu Jian, Mark R VanLandingham, Paul Moy, Mark H Foster, and Joseph L Lenhart. The relationship between mechanical properties and ballistic penetration depth in a viscoelastic gel. *Journal of the mechanical behavior of biomedical materials*, 44:109–120, 2015.

[162] A Bracq, G Haugou, B Bourel, C Maréchal, F Lauro, S Roth, and O Mauzac. On the modeling of a visco-hyperelastic polymer gel under blunt ballistic impacts. *International Journal of Impact Engineering*, 118:78–90, 2018.

[163] Larry M Sturdivan. A mathematical model of penetration of chunky projectiles in a gelatin tissue simulant. Technical report, ARMY ARMAMENT RESEARCH AND DEVELOPMENT COMMAND ABERDEEN PROVING GROUND MD . . . , 1978.

[164] G Wijk, Collin, and R Amiree. Sphere penetration into gelatine and board. In *19th International Symposium of Ballistics*, volume 2, pages 1019–1027, 2001.

[165] MJ Lighthill. Boundary layer theory, 1963.

[166] Steven B Segletes. Modeling the penetration behavior of rigid into ballistic gelatin. Technical report, ARMY RESEARCH LAB ABERDEEN PROVING GROUND MD, 2008.

[167] David Veysset, Steven E Kooi, AA aznev, Shengchang Tang, Aleksandar S Mijailovic, Yun Jung Yang, Kyle Geiser, Krystyn J Van Vliet, Bradley D Olsen, and Keith A Nelson. High-velocity micro-particle impact on gelatin and synthetic hydrogel. *Journal of the mechanical behavior of biomedical materials*, 86:71–76, 2018.

[168] Li Liu, Zhen Jia, Xiaolin Ma, Yurun Fan, Wei Li, and Hongwei Liu. A spherical cavity expansion model of large elastic deformation and its application to ballistic gelatin penetration problems. *International Journal of Impact Engineering*, 71:106–116, 2014.

[169] William A Allen, Earle B Mayfield, and Harvey L Morrison. Dynamics of a projectile penetrating sand. *Journal of Applied Physics*, 28(3):370–376, 1957.

[170] Liu Susu, Xu Cheng, Wen Yaoke, and Zhang Xiaoyun. A new motion model of rifle bullet penetration into ballistic gelatin. *International Journal of Impact Engineering*, 93:1–10, 2016.

[171] Li Liu, Zhen Jia, Xiaolin Ma, Yurun Fan, Wei Li, and Hongwei Liu. A spherical cavity expansion model of large elastic deformation and its application to ballistic gelatin penetration problems. *International Journal of Impact Engineering*, 71:106–116, 2014.

[172] Wanis Nafo. Experimental and analytical investigation of the cavity expansion method for mechanical characterization of soft materials. Master's thesis, University of Waterloo, 2016.

[173] Susu Liu, Cheng Xu, Yaoke Wen, Shu Wang, Jingling Zhou, and Xinkai Zhou. Cavity dynamics in 10 wt% gelatin penetration of rifle bullet. *International Journal of Impact Engineering*, 122:296–304, 2018.

[174] B An, J Jiang, and H Jiang. The numerical simulation of the temporary-cavity forming during the high-velocity steel-ball penetrating into water medium. *Explosion and Shock Waves*, 18:245–250, 1998.

[175] Gunther Dyckmans, N Ndompetelo, and André Chabotier. Numerical and experimental study of the impact of small caliber projectiles on ballistic soap. In *Journal de Physique IV (Proceedings)*, volume 110, pages 627–632. EDP sciences, 2003.

[176] L Koene and A Papy. Experimental and numerical study of the impact of spherical projectiles on ballistic gelatin at velocities up to 160m/s. In *25th international symposium on ballistics*, page 1573e9, 2010.

[177] MD Minisi. Gelatin impact modeling. pm-mas es-1a-9000, 2006.

[178] Yaoke Wen, Cheng Xu, Haosheng Wang, Aijun Chen, and RC Batra. Impact of steel spheres on ballistic gelatin at moderate velocities. *International Journal of Impact Engineering*, 62:142–151, 2013.

[179] Aristide Awoukeng-Goumtcha, Lorenzo Taddei, Floran Tostain, and Sébastien Roth. Investigations of impact biomechanics for penetrating ballistic cases. *Biomedical materials and engineering*, 24(6):2331–2339, 2014.

[180] Yaoke Wen, Cheng Xu, Yongxi Jin, and RC Batra. Rifle bullet penetration into ballistic gelatin. *Journal of the mechanical behavior of biomedical materials*, 67:40–50, 2017.

[181] Xiaoyun Zhang, Cheng Xu, Yaoke Wen, and Shaomin Luo. The experimental and numerical study of indirect effect of a rifle bullet on the bone. *Forensic science international*, 257:473–480, 2015.

[182] Feng Chen, Rong Chen, and Banghai Jiang. The adaptive finite element material point method for simulation of projectiles penetrating into ballistic gelatin at high velocities. *Engineering Analysis with Boundary Elements*, 117:143–156, 2020.

[183] Hiren J Patel, Darshan G Trivedi, Anand K Bhandari, and Dushyant A Shah. Penetration enhancers for transdermal drug delivery system: A review. *Journal of Pharmaceutics and Cosmetology*, 1(2):67–80, 2011.

[184] Shital H Bariya, Mukesh C Gohel, Tejal A Mehta, and Om Prakash Sharma. Microneedles: an emerging transdermal drug delivery system. *Journal of Pharmacy and Pharmacology*, 64(1):11–29, 2012.

[185] Thomas J Mitchell, Mark AF Kendall, and Brian J Bellhouse. A ballistic study of micro-particle penetration to the oral mucosa. *International journal of impact engineering*, 28(6):581–599, 2003.

[186] JH Lee, D Veysset, JP Singer, M Retsch, G Saini, T Pezeril, KA Nelson, and EL Thomas. High strain rate deformation of layered nanocomposites nat, 2012.

[187] Jae-Hwang Lee, Phillip E Loya, Jun Lou, and Edwin L Thomas. Dynamic mechanical behavior of multilayer graphene via supersonic projectile penetration. *Science*, 346(6213):1092–1096, 2014.

[188] David Veysset, Alex J Hsieh, Steven Kooi, Alexei A Maznev, Kevin A Masser, and Keith A Nelson. Dynamics of supersonic microparticle impact on elastomers revealed by real–time multi–frame imaging. *Scientific reports*, 6:25577, 2016.

[189] David Veysset, Alex J Hsieh, Steven E Kooi, and Keith A Nelson. Molecular influence in high-strain-rate microparticle impact response of poly (urethane urea) elastomers. *Polymer*, 123:30–38, 2017.

[190] RA Guha, NH Shear, and M Papini. Ballistic impact of single particles into gelatin: experiments and modeling with application to transdermal pharmaceutical delivery. *Journal of biomechanical engineering*, 132(10), 2010.

[191] Zhuo Zhang, Liang Li, and Dingguo Zhang. Effect of arbitrary yaw/pitch angle in bird strike numerical simulation using sph method. *Aerospace Science and Technology*, 81:284–293, 2018.

[192] Yadong Zhou, Youchao Sun, and Wenchao Cai. Bird-striking damage of rotating laminates using sph-cdm method. *Aerospace Science and Technology*, 84:265–272, 2019.

[193] J Zhou, J Liu, X Zhang, Y Yan, L Jiang, I Mohagheghian, JP Dear, and MN Charalambides. Experimental and numerical investigation of high velocity soft impact loading on aircraft materials. *Aerospace Science and Technology*, 90:44–58, 2019.

[194] R Vignjevic, J Campbell, and L Libersky. A treatment of zero-energy modes in the smoothed particle hydrodynamics method. *Computer methods in Applied mechanics and Engineering*, 184(1):67–85, 2000.

[195] Gui-Rong Liu and Moubin B Liu. *Smoothed particle hydrodynamics: a meshfree particle method*. World scientific, 2003.

[196] MB Liu, GR Liu, and KY Lam. Constructing smoothing functions in smoothed particle hydrodynamics with applications. *Journal of Computational and applied Mathematics*, 155(2):263–284, 2003.

[197] XF Yang, SL Peng, and MB Liu. A new kernel function for sph with applications to free surface flows. *Applied Mathematical Modelling*, 38(15-16):3822–3833, 2014.

[198] Xiufeng Yang, Moubin Liu, and Shiliu Peng. Smoothed particle hydrodynamics modeling of viscous liquid drop without tensile instability. *Computers & Fluids*, 92:199–208, 2014.

[199] JW Swegle, DL Hicks, and SW Attaway. Smoothed particle hydrodynamics stability analysis. *Journal of computational physics*, 116(1):123–134, 1995.

[200] Walter Dehnen and Hossam Aly. Improving convergence in smoothed particle hydrodynamics simulations without pairing instability. *Monthly Notices of the Royal Astronomical Society*, 425(2):1068–1082, 2012.

[201] Leonardo Di G Sigalotti, Otto Rendón, Jaime Klapp, Carlos A Vargas, and Fidel Cruz. A new insight into the consistency of the sph interpolation formula. *Applied Mathematics and Computation*, 356:50–73, 2019.

[202] Jun Lin. *Nonlinear transient analysis of isotropic and composite shell structures under dynamic loading by SPH method*. PhD thesis, 2014.

[203] SP Timoshenko and JM Gere. Mechanics of materials. van nordstrand reinhold company. *New York*, 1972.

[204] Larry D Libersky and Albert G Petschek. Smooth particle hydrodynamics with strength of materials. In *Advances in the free-Lagrange method including contributions on adaptive gridding and the smooth particle hydrodynamics method*, pages 248–257. Springer, 1991.

[205] Joel W House, John C Lewis, Peter P Gillis, and LL Wilson. Estimation of flow stress under high rate plastic deformation. *International journal of impact engineering*, 16(2):189–200, 1995.

[206] Romesh C Batra and GM2450980 Zhang. Modified smoothed particle hydrodynamics (msph) basis functions for meshless methods, and their application to axisymmetric taylor impact test. *Journal of Computational Physics*, 227(3):1962–1981, 2008.

[207] S Marrone, Andrea Colagrossi, A Di Mascio, and David Le Touzé. Prediction of energy losses in water impacts using incompressible and weakly compressible models. *Journal of Fluids and Structures*, 54:802–822, 2015.

[208] B Fontenier, A Hault-Dubrulle, P Drazetic, C Fontaine, and H Naceur. On the mechanical characterization and modeling of polymer gel brain substitute under dynamic rotational loading. *Journal of the mechanical behavior of biomedical materials*, 63:44–55, 2016.

[209] Hermann Schlichting and Klaus Gersten. *Boundary-layer theory*. Springer, 2016.

[210] Mostafa Hassani, David Veysset, Keith A Nelson, and Christopher A Schuh. Material hardness at strain rates beyond 106 s- 1 via high velocity microparticle impact indentation. *Scripta Materialia*, 177:198–202, 2020.

[211] Charles E Anderson Jr. Analytical models for penetration mechanics: a review. *International Journal of Impact Engineering*, 108:3–26, 2017.

[212] R Clift. The motion of particles in turbulent gas-streams. *Proc. Chemeca'70*, 1:14, 1970.

[213] Altair Hyperworks. Hypermesh user's manual, 2009.

[214] Paul Moy, C Allan Gunnarsson, and Tusit Weerasooriya. Tensile deformation and fracture of ballistic gelatin as a function of loading rate. In *Proceedings of the SEM Annual Conference*. Society for Experimental Mechanics Inc. Albuquerque, New Mexico, USA, 2009.

[215] Shuangshuang Meng, Lorenzo Taddei, Nadhir Lebaal, David Veysset, and Sebastien Roth. Modeling micro-particles impacts into ballistic gelatine using smoothed particles hydrodynamics method. *Extreme Mechanics Letters*, 39:100852, 2020.

[216] Alastair F Johnson and Martin Holzapfel. Numerical prediction of damage in composite structures from soft body impacts. *Journal of materials science*, 41(20):6622–6630, 2006.

[217] LM Yang, VPW Shim, and CT Lim. A visco-hyperelastic approach to modelling the constitutive behaviour of rubber. *International Journal of Impact Engineering*, 24(6-7):545–560, 2000.

[218] YT Lu, Hanxing X Zhu, Stephen Richmond, and John Middleton. A visco-hyperelastic model for skeletal muscle tissue under high strain rates. *Journal of biomechanics*, 43(13):2629–2632, 2010.

[219] Beomkeun Kim, Seong Beom Lee, Jayone Lee, Sehyun Cho, Hyungmin Park, Sanghoon Yeom, and Sung Han Park. A comparison among neo-hookean model, mooney-rivlin model, and ogden model for chloroprene rubber. *International Journal of Precision Engineering and Manufacturing*, 13(5):759–764, 2012.

[220] Muhammad Azeem Aslam, Saiaf Bin Rayhan, Wang Jing Yu, et al. Ballistic gelatin lagrange mooney-rivlin material model as a substitute of bird in finite element bird strike case studies. *Latin American Journal of Solids and Structures*, 17(6), 2020.

[221] Hossein Asadi Kalameh, Arash Karamali, Cosmin Anitescu, and Timon Rabczuk. High velocity impact of metal sphere on thin metallic plate using smooth particle hydrodynamics (sph) method. *Frontiers of Structural and Civil Engineering*, 6(2):101–110, 2012.

[222] K.A. Alhussan, V.A. Babenko, I.M. Kozlov, and A.S. Smetannikov. Development of modified SPH approach for modeling of high-velocity impact. *International Journal of Heat and Mass Transfer*, 55:6340–6348, 2012.

[223] S.A. Poniaev, R.O. Kurakin, A.I. Sedov, S.V. Bobashev, B.G. Zhukov, and A.F. Nechunaev. Hypervelocity impact of mm-size plastic projectile on thin aluminum plate. *Acta Astronautica*, 135:26–33, jun 2017.

LIST OF FIGURES

List of Tables

5

APPENDIX

Table 5.1: List the SPH simulations for Projectile-Target systems in the literature.

Model & techniques	Impact condition	Projectile-Target system			Physical problem
		projectile	target	behavior law	
3D standard SPH [67]	• normal impact • v0 = 5.55 km/s	copper disk	• Al bumber plate • 2.87 mm thick	• elastic-perfectly-plastic law • Mie-Gruneisen	size of debris clouds
standard SPH in EPIC code [70]	• normal impact • v0 = 2.0-5.0 km/s	copper rod	• steel plate • 2.6/12.7 cm thick	• Johson-Cook (1983) • Mie-Gruneisen	debris cloud, penetration craters, spall cases
SPHC code [68]	• normal impact • hull impact • oblique impact • 6.0-10 km/s	Al sphere/disk	• Al plate • mm-scale	• elastic-perfectly-plastic law • Johson-Cook strength model • Mie-Gruneisen	debris fragments secondary impacts
SPH, MESA, EPIC, CALE codes[69]	• normal impact • 6.0-24.5 km/s	copper sphere	• copper plate • 3.0/4.0 cm	• elastic-perfectly-plastic law • Johson-Cook strength model • Mie-Gruneisen	crater volume effects of yield strength
Coupled FE-SPH [122]	• normal impact • 0.3-3 km/s	tungsten rod, rigid	• Al • Steel	• Johnson-Cook model	coupled algorithm, the SPH generation algorithm
SPH code [73]	• normal impact • 5-7 km/s	Al sphere	• thin plates • different materials	• Johson-Cook strength model • Tillotson equation	debris clouds diameters of the craters
SPH code in AUTODYN-2D [71]	• normal impact • 6-8 km/s	Al sphere	• thin whipple shield plates • Al	• Steinberg-Guinan strength model • Mie-Gruneisen	debris cloud velocity and shape
SPH code in PAM-SHOCK [74]	• normal impact • oblique impact • 6-10 km/s	Al sphere	• thin Al plates • a triple shield • a 'stuffed' Whipple shield	• Johnson-Cook yield model • Sesame eos • Polynomial eos	debris cloud damage to backwall of shield shapes of craters ejecta trajectories
3D SPH code [53]	• normal impact • 0.6-2 km/s	steel cube, deformed	• fiber composite • eight-layer laminate • 0.09648 cm	• anisotropic elastic plasticity • Mie-Gruneisen Eos • failure criterion	debris clouds and crater and spall

Model & techniques	Impact condition	Projectile-Target system			Physical problem
		projectile	target	behavior law	
SPH in PAM-SHOCK 3D and AUTODYN 2D hydrocodes [72]	• normal impact • 7 km/s	Al sphere	• thin Al plates • triple wall system	• Johnson-Cook model • Steinberg-Guinan • Sesame, Shock, Tillotson	SPH limitations to debris shielding system
2D-SPH code [111]	• normal impact • 820-840 m/s	Lead/steel rod, deformed	• steel plate • 6 mm	• elasto-plastic model	contact algorithm, numerical fractures
3D-SPH code [112]	• normal impact • oblique impact • 2000 m/s	steel cube, deformed	• steel plate • 3 mm	• elasto-perfectly-plastic model	contact algorithm, numerical fractures
Improved SPH (new particle generation and merger techniques) [54]	• normal impact • oblique impact • 4.0 km/s	aluminum sphere, deformed	• Gr/Ep laminate • 1 - 8 layers • 1mm	• Elastic–plastic of single layer	damage and debris clouds
Coupled FE-SPH [125]	• oblique impact • 400 m/s	steel rod with ogive–nose, rigid	• Al plate • 2.63 cm	• elastic perfectly plastic model • Gruneisen EOS	the contact potential algorithm
FE-SPH-FE in LS-DYNA [128]	• normal impact • 6.64 m/s	Al, deformed	• Al plates • 2 mm	• Johnson-Cook model with EOS	fragment identification and statistics method,debris clouds
2D SPH [221]	• normal impact • 0.3-3.1 km/s	Al/Lead/Steel spheres	• 2 mm plates • Al/Lead/Steel	• elastic-perfectly plastic law	the effects of impact velocity and target thickness on penetration depth and crater size
SPH in LS-Dyna [75]	• normal impact • 7 km/s	54R B32 API hardened steel core ammunition	• 500 HB armor steel • 9-20mm	• Johnson-Cook model • Mie-Gruneisen	ballistic limit, spall and fragmentation
Combined Particle-Element Method (CPEM) [120]	• oblique impact • 2 km/s	Steel, deformed	• Steel plate • mm-scale	• elastic-plastic law	element-partile convert and contact algorithms
3D SPH code [55]	• normal impact • 200-1200 m/s	steel ball, deformed	• CRFP laminate • 1.6 mm	• Elastic–plastic of single layer • Chang-Chang critera	damage pattern, fiber breaks, cracks

Model & techniques	Impact condition	Projectile-Target system			Physical problem
		projectile	target	behavior law	
SPH in LS-Dyna and Eulerian-based hydrocode CTH, [76] ,[77]	• normal impact • 4.5-6 km/s	Lexan cylinder	• A36 steel target plates • 12.7 mm	• Johnson-Cook model • Mie-Gruneisen	Crater diameter, Penetration Bulge, numerical settings
SPH in Abaqus [56]	• normal impact • 1067-1097 m/s	FSP, Steel, rigid and deformed	• single plate • stacked double-plate • cementitious • 11.9 mm	• Advanced Fundamental Concrete (AFC) model • user-defined material model	ballistic limit, spalling, crack propogation
SPH in LS-Dyna Eulerian-based hydrocode CTH [78]	• normal impact • 80-405.7 m/s	Arne tool steel cone	• monolithic and layered plates • Weldox 460 E steel • 2-12 mm	• modified Johnson-Cook model • viscoplasticity and damage	effects of target thickness and number of layers for ballistic resistance
pseudo-spring SPH [33]	• normal impact • 100-300 m/s	Weldox 460 E steel cylinder	• monolithic and layered plates • Weldox 460 E steel • 8-10 mm	• Johnson-Cook plasticity • perfectly plasticity	crack propogation
pseudo-spring SPH [34]	• normal impact • 70-500 m/s	Weldox 460 E steel cylinder	• monolithic and layered plates • Weldox 460 E steel • 2024-T351 Al alloy • 6-16 mm	• Johnson-Cook model • six damage models	perforations
pseudo-spring SPH [61]	• normal impact • 700-2259 m/s	cylindesr with nose shapes (blunt, hemispherical and conical)	• ceramic plates • ceramic-metal composite plates • 9-30 mm	• Johnson-Holmquist I and II • Johnson-Holmquist-Bissel	spall plane, cracks, numerical parameters sensitivitiy
γ-SPH-ALE [89]	• normal impact • oblique impact • 4 -7 km/s	Al sphere	• Al plates • mm-scale	• Elastic perfectly Plastic • Mie-Grüneisen	debris clouds
GAMMA-SPH [38]	• normal impact • oblique impact • 4-7 km/s	Al sphere, Lexan cylinder	• Al plates with 0.8-4mm • steel plates with 12.7mm	• linear elastic- plastic model • Mie-Grüneisen	debris clouds and crater and spall

Model & techniques	Impact condition	Projectile-Target system			Physical problem
		projectile	target	behavior law	
SPH code [107]	• normal impact • 3.1 km/s	Al/Steel spheres, deformed	• Al/Steel plate • 0.2 cm	• Elastic–perfectly plastic model • Steinberg-Guinan • Mie-Gruneisen EOS • HOM equation	shapes of debris clouds, effects of types of artificial viscosities
SPH in LS-DYNA [51]	• normal impact • 1-4 km/s	steel sphere, deformed	• fused silica plates • disposable debris shields (DDS) • 2-10 mm	• Johnson Holmquist model • pressure cut-off criteria	debris cloud, perforation hole and spallation zones
SPH in LS-DYNA [127]	• normal impact • 70-1050 m/s	Caliber/steel/Al, deformed	• Al/steel/brass plates • 3-12 mm	• Johnson-Cook model with EOS	residual velocities, ballistic limit, perforation
3D-SPH code [116]	• normal impact • 200 m/s	steel sphere, deformed	• steel plate • 1 mm	• elasto-plastic model • Mie-Gruneisen	contact algorithm, numerical fractures
SPH and MPM [13]	• normal impact • 6150 m/s	Al sphere, deformed	• Al plate • 0.8 mm	• Elastic-plastic model • Mie-Gruneisen equation	shapes of debris clouds
SPH in LS-DYNA [121]	• normal impact • 10-400 m/s	steel rod with various noses, rigid	• steel/Al plates • 6-30 mm	• Johnson-Cook model with EOS	residual and ballistic limit velocities, perforation
SPH–FEM coupled [126]	• normal impact • 180-300 m/s	steel cylinder, rigid	• Weldox 460 E steel • 12 mm	• Viscoplasticity and ductile damage model • Mie-Gruneisen equation	coupling algorithm, ballistic limit velocity.
modified SPH [222]	• normal impact • 6.18/6.7 km/s	Al sphere, deformed	• Al plate • mm-scale	• not introduced	boundary deficiencies, shapes of formed craters and apertures.
FE-SPH code [108]	• normal impact • 200-400 m/s	steel cylinder with blunt, conical, ogival noses, rigid	• Steel/Al plates • 6-20 mm	• modified Johnson–Cook (MJC) model	residual and ballistic limit velocities

Model & techniques	Impact condition	Projectile-Target system			Physical problem
		projectile	target	behavior law	
SPH with artifitial stress and Godunov scheme [109]	• normal impact • 3.1 km/s	Al/Steel spheres, deformed	• Al/Steel plate • 0.2 cm	• Elastic–perfectly plastic model • Steinberg-Guinan model • Mie-Gruneisen equation • HOM equation	tensile instability, shapes of debris clouds
FE-SPH code [129]	• normal impact • 200-400 m/s	Al sphere, mental jet	• double hull structure • copper/steel/SPS (Sandwich Plate System) • mm-scale	• Johnson-Cook model • Jones-Wilkins-Lee (JWL) • Mie-Grüneisen	the penetration process and the damage response
SPH in LY-DYNA [223]	• normal impact • oblique impact • 5-6 km/s	polycarbonate 2mm-cube, deformed	• Al plates • double-plate structure • 0.5-1.5 mm	• Johnson-Cook model • Mie-Grüneisen	debris cloud, secendary impact for witness plates, craters
SPH-FE in ABAQUS/Explicit. [124]	• normal impact • 5-200 m/s	rods with noses (conical, hemispherical, blunt), rigid	• Al plates • 4 mm	• Johnson-Cook model • Mie-Grüneisen	residual velocities, failure mechanisms and energy absorption
3D SPH-GPU code [115]	• normal impact • 130-400 m/s	steel cylinder, rigid	• Weldox 460 E steel • 8-12 mm	• Johnson–Cook model • Mie-Gruneisen equation	GPU technique, residual velocities.
SPH in LS-DYNA combined machine learning techniques [81]	• normal impact • 2.15 or 6.64 km/s	Al, Steel, cylinder, sphere, deformed	• Al plates • mm-scale	• Johnson–Cook model • Mie-Gruneisen	residual velocity, hole diameter, and spalling diameter, debris clouds
SPH in LS-DYNA [95]	• normal impact • 1.93-4.96 km/s	Al sphere, deformed	• carbon fiber reinforced polymer composites (CFRP) • 2.3 mm	• MAT_59 material model in LS-DYNA	crater diameters, the secondary debris cloud, ballistic limit
Improved SPH with KGC [86]	• normal impact • 4-7 km/s	Al sphere and cylinder	• Al plates • 0.4 cm	• Johnson–Cook model • Mie-Grüneisen	evolution of the debris cloud and particle distribution.
Improved SPH with KGC [88]	• normal impact • 2-11 km/s	Al sphere	• Al plates • 0.4 cm	• Johnson–Cook model • Tillotson EOS	the sizes of the craters

Model & techniques	Impact condition	Projectile-Target system			Physical problem
		projectile	target	behavior law	
Corrective SPH (DFPM) [92]	• normal impact • oblique impact • 2-12 km/s	Cu, Al, deformed	• Al plates • 2-4 mm	• Johnson–Cook model • Mie-Grüneisen • Tillotson equation	the craters size and debris clouds
SPH in LS-DYNA (contact model: PCM and PAM) [59]	• normal impact • 903 m/s	alloy, deformed	• AL2O3 ceramic • 12.7 mm	• JH-2 model	contact algorithm, fragmentation, residual velocity

5

PUBLICATIONS

1. Meng, Shuangshuang, et al. ”Advances in ballistic penetrating impact simulations on thin structures using Smooth Particles Hydrodynamics: A state of the art.” Thin-Walled Structures (2020): 107206.
2. Meng, Shuangshuang, et al. ”Modeling micro-particles impacts into ballistic gelatine using smoothed particles hydrodynamics method.” Extreme Mechanics Letters 39 (2020): 100852.
3. Meng, Shuangshuang, et al. ”The study on performances of kernel types in solid dynamic problems by smoothed particle hydrodynamics.” Computational Particle Mechanics (2020): 1-15.
4. Al Khalil, Monzer, Frissane, H., Taddei, L., Meng, S., et al. ”SPH-based method to simulate penetrating impact mechanics into ballistic gelatin: Toward an understanding of the perforation of human tissue.” Extreme Mechanics Letters 29 (2019): 100479.

Document generated with LaTeX and:
the LaTeX style for PhD Thesis created by S. Galland — http://www.multiagent.fr/ThesisStyle
the tex-upmethodology package suite — http://www.arakhne.org/tex-upmethodology/

Titre : **Modélisation numérique d'impacts à hautes vitesses par la méthode sans maillage Smoothed Particles Hydrodynamics. Application aux micro-impacts dans des tissus mous.**

Mots clés : SPH (Smoothed Particles Hydrodynamics), impact à hautes vitesse, tissus mous, pénétrations à micro-échelle.

Résumé : L'étude sur les impacts à hautes vitesses dans les tissus mous constituent un des pans de la recherche en biomécanique des chocs, et peuvent avoir des applications importantes en médecine, que ce soit à l'échelle microscopique ou macroscopique. La perforation d'un projectile dans les tissus mous doit être compris, à l'échelle macroscopique, pour analyser un impact ballistique perforant par exemple, mais également à plus petite échelle, avec l'administration de particules médicamenteuses à hautes vitesses au travers de différents tissus, comme la peau, en prenant en compte différents paramètres du phénomène, comme la vitesse d'impact ou la taille du projectile.
Un des moyens efficace pour comprendre ces phénomènes à très hautes vitesses est la simulation numérique. Les modèles numériques doivent être alors validés par rapport à des tests expérinentaux permettant de s'assurer de leurs biofidélités.Bien que les méthodes basées sur un maillage comme la méthode des éléments finis sont des outils puissante, les grandes distorsions des éléments tels qu'ils peuvent apparaître lors d'impacts pénétrant génèrent des erreurs numériques importantes. Ainsi, des méthodes sans maillage baséessur une modélisation particulaire s'affranchissant de toutes grillessont très adaptées pour simuler à hautes vitesses et grandes déformations. Un des plus anciennes méthode, la méthode SPH (Smoothed Particles Hydrodynamics) a été appliquée, dans cette thèse à la mécanique du solide en grandes vitesses et grandes déformations. Cette thèse s'attache à étudier la méthode SPH en développant un code "maison" pour ls impacts perforants ou non, puis propose un modèle numérique pour étudier le processus de pénétration de projectiles dans les tissus mous (la gélatine et le polymère synthétique gel SEBS sont considérés dans la litérature comme des substituts de tissus biofidèles) à échelle micrométrique.

Title : **Numerical modeling of impacts at high velocities by a meshfree method Smoothed particles Hydrodynamics. Application to micro-impacts in soft tissues.**

Keywords: Smoothed Particles Hydrodynamics, high-velocity impact, soft tissues, micro-impacts

Abstract: Investigations on the ballistic behaviours of soft tissue materials are significant research in a medical and pharmaceutical framework. They mainly focus on particles penetrating or traveling into the soft materials. For instance, in the needle-free drug delivery, the micro-scale particles as drug powders are injected into skin with high velocity, and several factors should be considered such as the particle diameters, trajectories, and momentum or velocities of projectile in this process. There have been investigated by some experiments, but there is still no study from the numerical insights.
The numerical methods are suitable to study these kinds of processes. Although grid-based methods like FEM have been powerful tools in engineering, the large distortions of elements exist when solid structures are extremely deformed. The methods based on the particle modelling are very suitable for simulating phenomena like the high velocity impacts. As the earliest meshless method, Smoothed Particles Hydrodynamics (SPH) has been applied in solid dynamics because of its great potentials in simulating extremely large deformation and perforation of targets by various projectiles at high velocities. This thesis mainly studies the SPH method by developing a SPH code for solid dynamics, and then propose a numerical model based on SPH method to investigate the penetration process into soft tissues (gelatin and synthetic polymer SEBS gel (styrene-ethylene-butylene-styrene) considered as biofidelic soft tissue simulants) at micro-scale.

Université Bourgogne Franche-Comté
32, avenue de l'Observatoire
25000 Besancon